

Aus dem Institut für Neuropathologie
(Zentrum für Neuropathologie und Prionforschung ZNP)
Institut der Ludwig-Maximilians-Universität München
Direktor: Prof. Dr. Jochen Herms

In Zusammenarbeit mit dem
Deutschen Zentrum für Neurodegenerative Erkrankungen, München
der Helmholtz-Gesellschaft



***Characterization of Synaptic and Epigenetic
Alterations in the Context of the Astrocytic Pathology
in Progressive Supranuclear Palsy and
Corticobasal Degeneration***

Dissertation

zum Erwerb des Doktorgrades der Medizin
an der Medizinischen Fakultät der
Ludwig-Maximilians-Universität zu München

vorgelegt von

Nils Briel

aus

Trier

Jahr

2024

Dedicated to Lorenz.

“Each thing we see hides something else we want to see.”

– René Magritte –

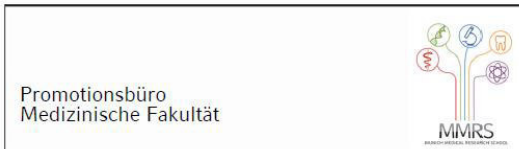
Mit Genehmigung der Medizinischen Fakultät der
Ludwig-Maximilians-Universität München

Erster Gutachter: *Prof. Dr. Jochen Herms*
Zweiter Gutachter: Prof. Dr. Johannes Levin
Dritter Gutachter: Prof. Dr. Matthias Brendel
ggf. weitere Gutachter: Prof. Dr. Magdalena Götz

Mitbetreuung durch den
promovierten Mitarbeiter: Dr. med. Felix L. Strübing
Dekan: Prof. Dr. med. Thomas Gudermann

Tag der mündlichen Prüfung: 25.01.2024

Affidavit



Affidavit

Briel, Nils

Surname, first name

Street

Zip code, town, country

I hereby declare, that the submitted thesis entitled:

Characterization of Synaptic and Epigenetic Alterations in the Context of the Astrocytic Pathology in Progressive Supranuclear Palsy and Corticobasal Degeneration

.....

is my own work. I have only used the sources indicated and have not made unauthorised use of services of a third party. Where the work of others has been quoted or reproduced, the source is always given.

I further declare that the submitted thesis or parts thereof have not been presented as part of an examination degree to any other university.

Zurich, 31.01.2024

place, date

Nils Briel

Signature doctoral candidate

Table of content

Affidavit	4
Table of content	5
List of abbreviations	7
List of publications	10
1. Contribution to the publications	11
1.1 Contribution to <i>Paper I: Contribution of the Astrocytic Tau Pathology to Synapse Loss in Progressive Supranuclear Palsy and Corticobasal Degeneration</i>	11
1.2 Contribution to <i>Paper II: Single-Nucleus Chromatin Accessibility Profiling Highlights Distinct Astrocyte Signatures in Progressive Supranuclear Palsy and Corticobasal Degeneration</i>	11
2. Introduction	12
2.1 Neuropathological Entities: Progressive Supranuclear Palsy and Corticobasal Degeneration	12
2.1.1 Epidemiology	12
2.1.2 Etiology and Genetics.....	13
2.1.3 Clinicopathological Correlations and Diagnostic Accuracy	14
2.1.4 Neuropathological Criteria and Their Utility in Differential Diagnosis	15
2.1.5 Clinical Criteria and Their Utility in Differential Diagnosis	16
2.2 Glial Involvement in the Pathophysiology of Tauopathies.....	17
2.2.1 Glial Functions in Synapse Maintenance	18
2.2.2 Astrocytes in Tau Degradation and Propagation.....	19
2.2.3 Pharmacological Strategies and Perspectives in Tauopathies	20
2.3 Motivation and Research Contributions.....	22
2.3.1 Contribution of This Thesis to Synapse Maintenance in 4R Tauopathies.....	22
2.3.2 Contribution of This Thesis to Degradation Pathways in 4R Tauopathies	23
2.3.3 Contribution of This Thesis to Pharmacological Targets in 4R Tauopathies	23
3. Summary	24
4. Zusammenfassung	25
5. Paper I	26
Contribution of the Astrocytic Tau Pathology to Synapse Loss in Progressive Supranuclear Palsy and Corticobasal Degeneration	26

6. Paper II	41
Single-Nucleus Chromatin Accessibility Profiling Highlights Distinct Astrocyte Signatures in Progressive Supranuclear Palsy and Corticobasal Degeneration	41
Bibliography	62
Appendix A:	73
Appendix B:	73
Acknowledgements	76
Curriculum vitae	77

List of abbreviations

Abbreviation	Term
(bv)FTD	(Behavioral variant) Frontotemporal Dementia
AD	Alzheimer's Disease
AGD	Argyrophilic grain disease
ALS	Amyotrophic Lateral Sclerosis
AMPA	α -amino-3-hydroxy-5-methyl-4-isoxazolepropionic acid receptor
ANOVA	Analysis of Variance
AP	Astrocytic plaque
APP	Amyloid precursor protein
AQP4	Aquaporin-4
ASO	Antisense oligonucleotide
Ast	Astrocytes
ATAC-seq	Assay for Transposase-Accessible Chromatin using sequencing
ATP/Ado	Adenosine tri-phosphate/adenosine
BG	Basal ganglia
BH	Benjamini-Hochberg
BMSC	Bone marrow stem cells
bp	Base pairs
BP	Biological process
CA	Control astrocyte(s)
CADRO	Common Alzheimer's and Related Dementias Research Ontology
CB	Coiled bodies
CBD	Corticobasal Degeneration
CC	Cellular compartment
CMA	Chaperon-mediated autophagy
CRE	<i>Cis</i> -regulatory element
CREB	cAMP response element-binding protein
Ctrl	Control
DAR	Differentially accessible region
DEG	Differentially expressed gene
DF	Degrees of freedom
DLN	Deep-layer neurons
DNA	Desoxyribonucleic acid
dpi	Dots per inch
EAAT2	Excitatory amino acid transporter 2
Exc.	Excitatory
fCtx	Frontal cortex of the middle frontal gyrus
FDR	False discovery rate

FTLD	Frontotemporal lobar degeneration
GA	Gene accessibility
GABA_{(A,B)R}	γ -aminobutyric acid (receptor)
GAT	GABA transporters
GEM	Gel-bead in emulsion
GFAP	Glial fibrillary acidic protein
GGT	Globular glial tauopathy
Gln/Glu	Glutamate/glutamine
GluT	Glucose transporter
GO	Gene ontology
GSEA	Gene-set enrichment analysis
GWAS	Genome-wide association study
IC	Internal capsule
Inh.	Inhibitory
Kb/Gb	Kilo bases /Giga bases
LB(D)	Lewy Body (Dementia)
Lime	Local interpretable model-agnostic explanations
LINE1	Long interspersed nuclear elements
LOCA	Late onset cerebellar ataxia
Log2-FC	Binary logarithm fold-change
LSM	Light sheet microscope
Lv/nfa/svPPA	Logopenic variant / non-fluent agrammatic / semantic variant primary progressive aphasia
MAPT	Microtubule-associated Protein Tau
MCT1	Monocarboxylate-transporter 1
Mes	Mesencephalon
MF	molecular function
MFG	Middle frontal gyrus
mGluR	Metabotropic glutamate receptor
Mic	Microglia
ML	Machine learning
MND	Motor neuron disease
MSA	Multiple System Atrophy
NA	Numerical aperture
NA(R)	Noradrenaline (receptor)
NFIA	Nuclear factor IA
NFT	Neurofibrillary tangles
NMDAR	N-methyl-D-aspartate-receptor
NT	Neuropil threads
Oli	Oligodendrocytes

OPC	Oligodendrocytic precursor cells
OR	Odds ratio
P2Y₁R	Purinergic-2-Y-receptor
PAGF	Progressive akinesia and gait freezing
PART	Primary age-related tauopathy
PBS	Phosphate buffered saline
PCA	Principal component analysis
PCAt	Posterior cerebral atrophy
PD	Parkinson Disease
PET	Positron emission tomography
PMI	<i>Postmortem</i> interval
PSP	Progressive Supranuclear Palsy
pTau	Hyperphosphorylated Tau
RAP	Regulon activity profile
RNA-seq	Ribonucleotide acid sequencing
ROI	Region of interest
RTN	Reconstruction of transcriptional regulatory networks
SB	Sudan Black
sn*	Single nucleus
SNP	Single nucleotide polymorphism
Str	Striatum
SV2A	Synaptic vesicle protein 2A
TA	Tufted astrocyte
TDP-43	Transactive response DNA binding protein 43 kDa
TF(M)(E)	Transcription factor (motif) (enrichment)
TGF-β1(R)	Transforming growth factor-beta-1 (receptor)
ThF	Thalamic fascicle
TSP	Thrombospondin
ULN	Upper-layer neurons
UMAP	Uniform Manifold Approximation and Projection
UPR	Unfolded protein response
UPS	Ubiquitin proteasome system
vGAT	Vesicular GABA transporter
vGLUT1	Vesicular glutamate transporter 1
WM	White matter
XGB	Extreme gradient boosting

List of publications

This dissertation is based on the work published in:

- **Paper I**

Briel N, Pratsch K, Roeber S, Arzberger T, Herms J (2020) Contribution of the astrocytic tau pathology to synapse loss in progressive supranuclear palsy and corticobasal degeneration. *Brain Pathology*. <https://doi.org/10.1111/bpa.12914>

- **Paper II**

Briel N, Ruf VC, Roeber S, Mielke J, Dorostkar MM, Windl O, Arzberger T, Herms J*, Struebing FL* (2022) Single-Nucleus Chromatin Accessibility Profiling Highlights Distinct Astrocyte Signatures in Progressive Supranuclear Palsy and Corticobasal Degeneration. *Acta Neuropathologica*. <https://doi.org/10.1007/s00401-022-02483-8>

* Denotes shared last authorship

Additional publications not included in this work:

- Eckenweber F, Medina-Luque J, Blume T, [...] **Briel N**, [...] Höglinger GU, Herms J, Brendel M (2020) Longitudinal TSPO expression in tau transgenic P301S mice predicts increased tau accumulation and deteriorated spatial learning. *Journal of Neuroinflammation*. doi: 10.1186/s12974-020-01883-5
- Xiang X, Wind K, Wiedemann T, [...] **Briel N**, [...] Herms J, Haass C, Brendel M (2021) Microglial activation states drive glucose uptake and FDG-PET alterations in neurodegenerative diseases. *Science Translational Medicine*. doi: 10.1126/scitranslmed.abe5640
- Shi Y, Cui M, Ochs K, [...] **Briel N**, [...] Rammes G, Herms J*, Dorostkar M* (2022) Long-term diazepam treatment enhances microglial spine engulfment and impairs cognitive performance via the mitochondrial translocator protein (TSPO). *Nature Neuroscience*. doi: 10.1038/s41593-022-01013-9

* Denotes shared last authorship

Additional preprint not included in this work:

- Bartos LM, Kirchleitner SV, Kolabas ZI, [...] **Briel N**, [...] von Baumgarten L, Albert NL, Brendel M (2023) Deciphering sources of PET signals in the tumor microenvironment of glioblastoma at cellular resolution. *bioRxiv*. doi: 10.1101/2023.01.26.522174

1. Contribution to the publications

1.1 Contribution to *Paper I: Contribution of the Astrocytic Tau Pathology to Synapse Loss in Progressive Supranuclear Palsy and Corticobasal Degeneration*

Briel is the only first author of this journal article. Herms, Roeber and Arzberger preselected possible tauopathy and control cases from the brain bank. Together with Roeber, Briel confined the cohorts to cases with high cortical Tau load. Briel worked on brain preparation from formalin-fixed brain samples to immunofluorescent labeling and confocal imaging, while Pratsch supervised the laboratory steps.

Data collection and analysis were performed by Briel under supervision of Pratsch, Arzberger and Herms. The first draft of the manuscript was written by Briel. All co-authors commented on the preliminary version of the manuscript. All authors read and approved the final manuscript.

1.2 Contribution to *Paper II: Single-Nucleus Chromatin Accessibility Profiling Highlights Distinct Astrocyte Signatures in Progressive Supranuclear Palsy and Corticobasal Degeneration*

Briel is the only first author of this publication. Herms, Strübing, Briel and Ruf conceived the project. Herms, Ruf, Roeber, Arzberger and Windl preselected possible tauopathy and control cases from the brain bank and matched cohorts together with Strübing and Briel.

Briel and Ruf worked on brain sample processing from cryo-frozen brain samples to snATAC-libraries. Ruf, Mielke and Briel performed quality control assessment of snATAC-libraries. Ruf and Mielke conducted quality control and sequencing of libraries in a commercial laboratory facility. Ruf supervised all library generation and sequencing steps. Briel performed all bioinformatic analyses under supervision of Strübing and additional input from Dorostkar.

Immunofluorescence stainings of dysregulated target proteins were conducted by Pratsch and Widmann and were supervised by Strübing and Briel. Strübing, Pratsch and Widmann performed confocal imaging, while Briel performed image readout and statistical analysis under supervision of Strübing.

The first draft of the manuscript was written by Briel and Strübing. All co-authors commented on the preliminary version of the manuscript. All authors read and approved the final manuscript.

2. Introduction

2.1 Neuropathological Entities: Progressive Supranuclear Palsy and Corticobasal Degeneration

Despite the growing prevalence of neurodegenerative diseases causal treatment strategies remain largely unavailable. Given Alzheimer's Disease (AD) and Parkinson's Disease (PD) as the most prevalent entities, one important unmodifiable risk factor is aging [40, 64]. Thus, incidence rates rise with improving life expectancy due to declines in cardiovascular and neoplasm-attributed mortality [111]. In high-income countries, such as the USA, the estimated health economic expenditure of Alzheimer's Disease and related dementias constitute the major share with \$243 billion (30.4 %) in 2014, \$259 billion in 2017, and a predicted \$1.1 trillion in 2050 (presumptions based on available data in 2017) [5, 51]. Moreover, disease-related burdens arise for affected patients, their relatives and their caregivers [5]. In this context, improved management options for neurodegenerative diseases are a desirable goal.

At present, genetic and environmental factors contributing to these diseases are incompletely understood. With the rise of a diversifying array of multi-layered molecular techniques such as (epi-)genomics, transcriptomics, and parallelized microscope imaging approaches, we can gather a more integrative understanding of these diseases. Besides highly prevalent and intensively researched neurodegenerative diseases AD and PD, Progressive Supranuclear Palsy (PSP) and Corticobasal Degeneration (CBD) represent rarer entities with typically earlier onset, fast progression and high rates of socio-cognitive impairment [40, 83]. While the neuropathological assessment poses the diagnostic gold standard to detect pathognomonic intracellular inclusions of the microtubule-associated protein Tau (*MAPT*/Tau), the clinical phenotypes comprise a broad spectrum between atypical parkinsonian syndromes, dementia syndromes and psychiatric disorders. To complicate clinical entity prediction, PSP patients might present with Corticobasal Syndrome (CBS) – the classical manifestation of CBD patients – and vice versa. The clinical workup usually includes cerebral imaging, cerebrospinal fluid (CSF) analyses, and neuropsychiatric testing, as well as additional methods as required [27, 60, 83]. However, a valid *in vivo* diagnosis does not yet imply access to established disease-modifying treatments, which are currently under investigation in several tauopathies [119, 126, 135]. Therefore, advances in theragnostic target identification and accuracy-refined diagnosis algorithms could empower future clinical trials. This underscores the importance of research that seeks to understand the underlying pathomechanisms and how translational evidence can support the implementation of novel diagnostic and therapeutic approaches.

2.1.1 Epidemiology

PSP and CBD are rather rare diseases with a crude prevalence reaching from 1-18.1/100 000 people for PSP (Appendix B Table 1; [29, 44, 50, 73, 83, 99, 100, 104, 128, 140, 150, 151]) and a varying registration rate for CBS/CBD of 0-9/100.000 included probands [29, 44, 104, 151]. A recent meta-analysis by Swallow et al. including 16 PSP and 9 CBS/CBD prevalence studies inferred rates of 7.1/100 000 and 2.3/100 000 in PSP and CBS/CBD, respectively [139]. Since a range of pathologies can mimic typical CBD manifestations and thus diagnostic accuracy via clinical criteria is suboptimal, the definite diagnosis is based on neuropathological assessment [1, 9, 68, 118]. Usually, first symptoms occur in the 6th or 7th decade in both diseases with a slightly earlier mean onset in CBD/CBS at 65 (definite CBD 63.6; Appendix B Table 1) and PSP at 68 years (definite PSP 67.7). Life expectancy

at the time of diagnosis is given at 4-8 years, depending on methodological approaches and clinical subtypes [68, 83]. Only a few studies investigated validated *postmortem* cohorts. Those publications providing data on the age at death report a range of 54-86 (weighted mean 69.94) for CBD and 49-106 (weighted mean 74.89) for PSP cases.

2.1.2 Etiology and Genetics

The etiology of PSP and CBD is unidentified. While understanding risk factors and underlying mechanisms is important, preventing and delaying them is an aspired goal. Although most cases are attributable to *unmodifiable* risk factors such as aging and complex non-mendelian genetics, a recent multi-ethnic meta-analysis suggests that up to 40% of dementia syndromes can be prevented or delayed through the adoption of modifiable lifestyle risk factors addressed by public health strategies [91]. Unfortunately, specific modifiable risk factors for primary tauopathies remain largely unknown, while age and some genetic factors (i.e., *APOE* genotype) increase the risk of developing co-pathologies (e.g., Amyloid-beta levels, TDP-43 pathology) [123]. Additionally, epidemiologic evidence suggests heart disease, hypercholesterolemia, lower educational attainment, history of traumatic brain injury, and family history of dementia or parkinsonism heighten the odds [33, 134].

Although the majority of PSP and CBD cases are sporadic, they seem to share a common genetic background, as genome wide-association studies (GWAS) from large *postmortem* validated cohorts suggest [59, 69, 79, 153]. Collectively, these studies have identified several risk variants associated with the *MAPT* locus, and further variants with effects on *STX6*, *EIF2AK3*, *MOBP*, *KIF13B-1*, *SOS1*, *NSF*, *CXCR4*, *EGFR*, and *GLDC* utilizing expression quantitative trait loci analyses. This gene network is enriched for synaptic, homeostatic, and immune pathways. Even earlier, a 900 kb inversion polymorphism in *MAPT* was described as characteristic in populations of European descent [26, 65]. Inheriting this H1 haplotype is the most significant risk factor for sporadic PSP (odds ratio [OR] 5.5 [59]) and CBD (OR 3.7 [79]), though it also increases odds in FTD and PD [110, 153].

Monogenetic forms of Frontotemporal Dementia and Parkinsonism Linked to Chromosome 17q21.31 (FTDP-17) harbor autosomal-dominantly inherited mutations in *MAPT*. These mutations (e.g., P301S or P301L, used in murine models of familial tauopathies) are *bona fide* sufficient to facilitate aggregation of Tau monomers into insoluble higher-order assemblies such as neurofibrillary tangles (NFT) [37, 46]. Over 50 exonic and intronic mutations have been described as of 2023. Most of these accumulate within the microtubule binding region (MTBR) indicating a significant location effect for quaternary molecule structure [48]. *MAPT* translation is regulated in a cell type- and tissue-specific manner, resulting in six different isoforms based on alternative mRNA splicing. Variability arises from in- or exclusion of exon 10 – which relates to repeat R2 of the MTBR – and defines the 4R or 3R Tau isoforms, respectively. Other second order isoforms involve E2/E3 differential splicing, together leading to final proteins of 352-441 amino acids.

Tau expression is mainly confined to the nervous system, herein especially in neuronal axons and to a lesser degree in astrocytes and oligodendrocytes [42]. Post-translational modifications (e.g., by phosphorylation, acetylation, methylation, or ubiquitination) alter its properties in the cytobiological context as microtubule (MT) transport protein. The locational logic of phosphorylation patterns primarily in proline-rich, and C-terminal regions not only determines the protein's affinity to MTs but could also premise Tau aggregation [4, 45, 54]. Nevertheless, that Tau found in *postmortem* brain tissue is abnormally (hyper-)phosphorylated might even be a consequence not the necessary cause of aggregation, particularly as the effects of strategic mutations are more significant and do not overlap with phosphorylation sites. Moreover, compounds of negative charge (e.g., RNA or glycosaminoglycans)

as well as RNA binding proteins strongly interact with both non- and hyperphosphorylated Tau and might prime Tau assembly with higher experimental confidence [48, 72].

Although differential aggregation mechanisms of proteinopathies remain incompletely understood, some evidence links H1 (sub-)haplotypes with altered *MAPT* mRNA splicing (exon 3, 2 and possibly 10; [143, 153]). Apparently, several partly unidentified paths lead to predominantly 4R Tau assemblies in the 4R tauopathies PSP, CBD, Glial Globular Tauopathy (GGT), Argyrophilic Grain Disease (AGD) and FTDP-17 with P301S mutation. Contrarily, 3R Tau is detected by isoform-specific antibodies in Pick Disease (PiD); likewise mixed 3R/4R Tau in AD, Amyotrophic Lateral Sclerosis (ALS)/parkinsonism-dementia complex, Anti-IgLON5-related Tauopathy and Chronic Traumatic Encephalopathy (CTE) among others [43, 48, 71]. Although this broad range of tauopathies shares the same proteinopathic agent, biochemical and neuropathological assessments aid to discriminate peculiarities in tertiary Tau structure or cellular distribution of aggregates. Ultrastructural analyses of PSP Tau report 15-18 nm straight filaments as correlates of NFTs in neurons and bulks in astrocytes. These astrocytic proximal inclusions with fine peripheral ramifications led to the designation of *tufted astrocytes* (TA). In contrast, 20-24 nm twisted tubular ribbons in astrocytes and twisted tubules in oligodendrocytes emerge in CBD brain tissue as *astrocytic plaques* (AP) and *coiled bodies* (CB), respectively [49].

Thus far, research on molecular pathogenesis of primary tauopathies has employed bulkRNA-seq, microarray and GWAS studies [2, 3, 59, 79]. Subsequently to the work included in this dissertational thesis, new datasets with cell type-resolved molecular profiling in induced pluripotent stem cells treated with oligomeric Tau from P301S transgenic mice [121] and peripheral blood mononuclear cells of familial *MAPT* mutation carriers were published [131] (preprint). These studies have identified potentially novel disease-relevant genes (synaptic proteins, chemokines, trans-membrane proteins), cell types (neurons, astrocytes, microglia, peripheral myeloid and natural killer lineages) and pathways (neuroinflammation and proteostasis). Furthermore, investigations of transcriptomic alterations in combination with neuropathological traits showed that differentially expressed [synaptic] genes (DEGs) were correlated with NFTs, and immune networks were linked with TA [3].

However, besides Yokoyama and colleagues' GWAS integration across the PSP-CBD-FTD spectrum [153], no integrative and particularly no single cell-resolved comparison between PSP and CBD has been published yet. Discoveries from such genetic studies provide a basis for an understanding of their underlying pathogenesis, for the development of new diagnostic techniques and eventually for more targeted treatments for PSP and CBD.

2.1.3 Clinicopathological Correlations and Diagnostic Accuracy

The first series of 4 PSP cases was published in 1963/64 [137], followed by the first 3 cases with "*Corticodentatonigral Degeneration with Neuronal Achromasia*" in 1967 [117]. J. Steel et al. described PSP (former eponym: Steel-Richardson-Olszewski syndrome or Richardson syndrome) as a syndrome encompassing "*Supranuclear ophthalmoplegia affecting chiefly vertical gaze, pseudobulbar palsy, dysarthria, dystonic rigidity of the neck and upper trunk, and other less constant cerebellar and pyramidal symptoms [and mild] Dementia*" that histologically depict NFT, neuronal loss and gliosis in various subcortical and brainstem nuclei. Conversely, Rebeiz et al. considered the "*Severe impairment in the control of muscular movements, by abnormalities in posture and by involuntary motor activity*" paired with asymmetric fronto-parietal cortical atrophy and microscopical signs of extensive neuronal loss, swollen achromatic neurons and astrogliosis as typical features of CBD. Notably, their work already emphasized the relevance of comparing differential pathological and clinical diagnoses.

This is of particular interest, as the varying and partly overlapping syndromes of both tauopathies still pose a challenge for clinical diagnosis and in trial recruitment. Owing to the low prevalence and complex symptomatology of these diseases, our understanding of clinicopathological correlations has since profited from studying comprehensive cohorts gathered through international collaboration efforts. These studies have added to the phenotypic heterogeneity and promoted neuropathological criteria [36, 57, 90, 124] as well as clinical criteria [9, 60, 88, 118].

2.1.4 Neuropathological Criteria and Their Utility in Differential Diagnosis

According to the 1994 *National Institute of Neurological Disorders and Stroke* (NINDS) PSP criteria, assessing presence and distribution of NFT in 13 neuroanatomical regions is required [57, 90]. However, inter-rater metrics attested only moderate agreement [118], anti-phosphorylated Tau antibodies were used unstandardized and highly distinctive astroglipathic features were not included. Thus, the *Rainwater Charitable Foundation* working group just recently developed more accurate and simplified criteria which include scoring of TAs (in peri-Rolandic cortices, putamen) besides NFT and pretangles (in Substantia nigra, subthalamic nucleus, and Globus pallidus) [124].

In 2002, the *Office of Rare Diseases* working group published criteria for the neuropathological diagnosis of CBD [36]. The diagnosis is syndrome-agnostic and requires histologic and immunohistochemical assessment of neuronal loss, ballooned neurons and APs across 15 brain regions. Differential diagnoses and co-pathologies, such as AD or Lewy body (LB) pathology, should additionally be evaluated. A validation study of the same group supported their criteria accuracy against other tauopathies (except against FTL-17) [36].

FEATURE	PSP	CBD
Gross Pathology (Atrophy Patterns)	Frontal, parasagittal, paracentral, more dorsal midbrain	Mesial frontal, frontal opercular, parietal
Symmetry	Rather symmetrical	Rather asymmetrical
Ballooned Neurons	Rare	Numerous, often achromatic
NFT	Globose & flame shaped (Str, Mes)	Mostly globose (corticobasal bodies, Mes)
Pick Body-Like Tau Inclusions	Dentate fascia	Cortex (layers II/III)
Neuropil Threads	Sparse to many (BG, IC, ThF)	Numerous (Cortex, WM, IC, ThF, Mes)
Glial Lesions	Tufted astrocytes, oligodendroglial coiled bodies	Astrocytic plaques, oligodendroglial coiled bodies
Miscellaneous	Grumose degeneration of cerebellar dentate nucleus	Corticospinal tract degeneration

Table 1. Comparison of the neuropathological entities PSP and CBD. Modified from Dickson et al. 1999 and Sha et al. 2006 [35, 129].

Abbreviations: IC, internal capsule; Mes, Mesencephalon; Str, Striatum; ThF, Thalamic fascicle; WM, white matter.

When contrasting PSP against CBD, earlier reports emphasized the predominantly subcortical atrophy (i.e., midbrain) and neuroglial features confined to extrapyramidal system nuclei (i.e., Globus pallidus, subthalamic nucleus, Substantia nigra, Cerebellum), while mostly sparing the cortex. And yet, in the wake of collecting comprehensive pathological cohorts, frequent involvement of (frontal) cortex – especially by TA and NFT – has been recognized in up to 96% of PSP cases [35, 67, 124, 154]. In CBD, atrophy patterns and clinical symptoms are mainly asymmetric, with symmetric CBD (S-CBD) being less common [56]. Typically affected by neuropathologic changes are fronto-parietal cortices, white

matter, basal ganglia and to a lesser extent brainstem regions including Substantia nigra and the corticospinal tract. Particularly, achromatic ballooned neurons, neuron loss and APs are considered the hallmarks of this tauopathy.

Astroglipathy itself is supported as one major distinguishing factor between PSP and CBD by diagnosis criteria [36, 124], machine learning-based approaches being trained on pre-processed phospho-tau immunohistochemistry scores [78] and deep learning applications directly on phospho-tau (pTau) immunohistochemistry images [77]. From a more gradual dimension view, neuronal pathology including a ballooned aspect, achromasia or tangle shapes can contribute to disease differentiation as well [35, 129, 156] (see also Figure 2B). A comprehensive comparison of the neuropathological entities is shown in Table 1.

2.1.5 Clinical Criteria and Their Utility in Differential Diagnosis

In addition to autopsy-based evidence, a variety of clinical criteria have been developed, mainly aiming to differentiate between PSP/CBD and other parkinsonian or dementia syndromes. Since 1996, the NINDS-sponsored PSP clinical criteria were broadly used [88]. Despite high diagnostic accuracy for manifested typical PSP (i.e., Richardson syndrome), early detection of atypical forms was suboptimal [89]. Therefore, the *Movement Disorders Society* criteria for the diagnosis of PSP (MDS-PSP) should account for the phenotypic heterogeneity and improve sensitivity at earlier disease stages [60, 118]. The MDS-PSP criteria, accepted as the gold standard of clinical diagnosis, require a three-level assessment of ocular motor dysfunction, postural instability, akinesia, and cognitive dysfunction, which can be complemented by supportive features (e.g., Levodopa-resistance, dysarthric symptoms or imaging findings).

In 2013, Armstrong et al. defined the most recent comprehensive criteria for the clinical diagnosis of CBD [9], that integrate biographic data (i.e., age at and dynamics of onset, family history and *MAPT* mutations status) with CBS symptoms (i.e., limb rigidity, akinesia, dystonia, myoclonus or apraxia, cortical sensory deficit, alien limb phenomenon, PSP-, FTD- or progressive aphasia syndromes). Validation cohort studies, however, attested very limited criteria specificity and a lack of symptom enrichment in CBD cases [1]. To counter the insufficient accuracy in *antemortem* CBD diagnosis, the MDS-PSP criteria also include the label “probable 4R tauopathy”, summarizing those patients with high probability of underlying PSP or CBD pathology. As per combinatorial diagnostic feature importance, diagnoses of “possible” and “probable” PSP/CBS can be made *in vivo*, while the definite diagnosis remains a neuropathological one.

Given the immense variety of clinicopathological links provided in the literature (reviewed in [103], Figure 1A), predicting underlying neuropathology solely from clinical syndromes is valid only in the minority of cases. This is supported by principal component analysis (PCA) of pathological versus clinical features: While discrimination of PSP/CBD is highly driven by astroglipathy (items in loadings 3&4; Figure 1B), clinical syndromes associated with neuropathological changes are substantially less distinguishable (Figure 1C).

This highlights the need for accurate biomarkers and thorough exclusion criteria to reduce false positive (CBD) diagnoses. Research on cerebrospinal fluid (CSF) markers with prospect of future diagnostic use comprise CSF synaptic protein signatures [24, 101, 109] and CSF MTBR-Tau fragments 275 and 282 [63]. Markers with high predictive values have advanced towards serum-based detection of AD and exclusion of non-AD dementia (e.g., NfL, p-Tau217, p-Tau181 [10, 12, 16]). Supervised machine learning algorithms fit to cerebral imaging atrophy patterns could enhance clinical prediction as

well, though these cohorts remain clinically defined [80, 81]. Furthermore, positron emission tomography (PET) studies leverage differential binding in synaptic targets (e.g., synaptic vesicle protein 2A, tracer: UCB [61]), neuroinflammatory protein targets (e.g., 18 kDa Translocator Protein [TSPO], tracer: ^{18}F -GE-180[105]), and 4R Tau aggregates (tracer: ^{18}F -PI-2620 [21, 47, 93]).

Presumably, as demonstrated in Hansson et al. for preclinical AD [106], a multimodal parsimonious approach (i.e., cost-benefit-driven selection of modalities) could bring most accurate and efficient *ante-mortem* diagnoses.

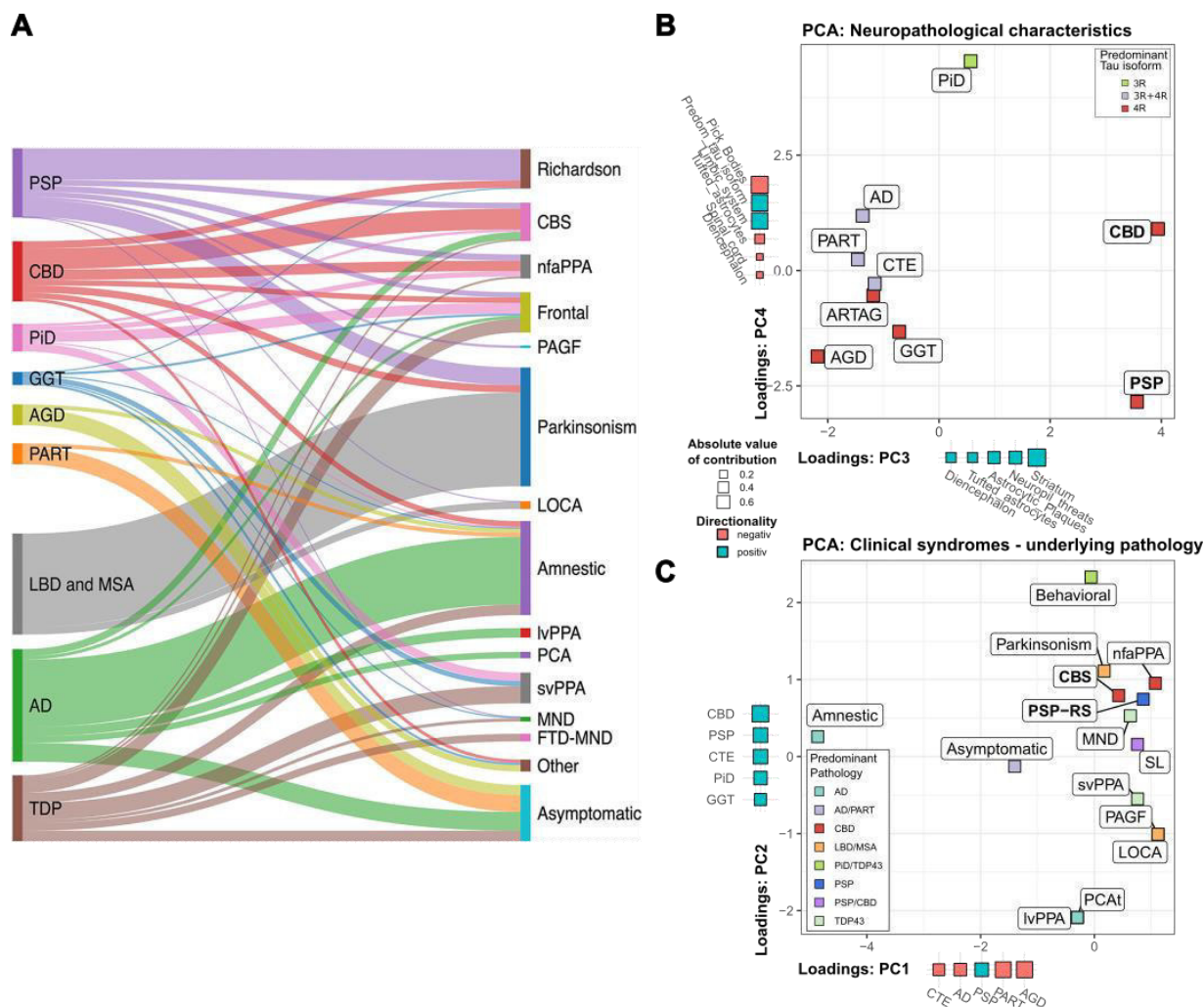


Figure 1. The spectrum of tauopathies and its clinicopathological correlations.

A. Clinicopathological correlations of major neurodegenerative diseases. Modified from Olfati et al. 2022 [103] (licensed under CC-BY). **B.** PCA of typical atrophy patterns + neuropathological features in major tauopathies (Briel, unpublished). Top loadings of PCs indicated as bubbles. Data from [60, 103, 156, 157]. **C.** PCA of atrophy patterns + clinical features. Structure and data source as in B.

Abbreviations: AD, Alzheimer disease; AGD, argyrophilic grain disease; GGT, globular glial tauopathy; LBD, Lewy body disease; LOCA, late onset cerebellar ataxia; IvPPA logopenic variant primary progressive aphasia; MND, motor neuron disease; nfaPPA, non-fluent agrammatic primary progressive aphasia; PAGF, progressive akinesia and gait freezing; PART, primary age-related tauopathy; PCAt, posterior cortical atrophy; svPPA, semantic variant primary progressive aphasia; TDP, transactive response DNAbinding protein 43 kDa pathology.

2.2 Glial Involvement in the Pathophysiology of Tauopathies

Basic and translational research in neurodegenerative diseases has been increasingly dedicated to glial cells in the last decade. Astrocytes are essential for guaranteeing proper CNS function, serving

multiple roles, such as maintenance of the blood–brain barrier, neurogenesis, modulation of immune responses, and of synaptic function (reviewed in [145]). Primary functions of microglia – the CNS division of the innate immune system – include phagocytosis, antigen presentation, and regulation of inflammation, as well as regulation of synaptic plasticity (reviewed in [23]). Both cell types respond to various external stimuli, such as infectious agents, injury, or cellular stress, by undergoing activation and releasing pro-inflammatory cytokines.

In tauopathies, besides Tau pathology itself, infiltration and inflammation of glial cells contribute significantly to pathogenesis and treatment responses [71, 74, 84, 113]. Especially, microglia and astrocytes seem to be involved in various aspects of tauopathies from susceptibility to Tau aggregation to Tau clearance and its spread [32, 94, 95, 98]. They can switch from a homeostatic state to a palette of inflammatory response states, consequently affecting synapse integrity and neuronal survival [42, 130, 155]. Dysregulated glia has been linked to exacerbated Tau pathology on the microscopic as well as to cognitive dysfunction on the behavior level *in vivo* [94, 120]. Studies in human *postmortem* brain samples have even emphasized their critical role in AD [133]. The proposed binarized concept of microglial and astrocytic polarization towards pro-inflammatory (i.e., M1/A1-like) or anti-inflammatory and reparative (i.e., M2/A2-like) states [23, 85, 141] does not entirely capture the functional cellular heterogeneity. Thus, it is widely overcome in favor of a more diversified organism- and context-dependent signature notion [41, 92, 96, 133].

In the advent of single-cell molecular biology technologies, high-dimensional profiling of disease cell states seems a more realistic comprehension. Understanding how and to which extent glia can modulate the pathophysiology of tauopathies is of high importance in the search for targeted therapies.

2.2.1 Glial Functions in Synapse Maintenance

Besides their role in the propagation of Tau pathology, glial cells also impact synaptic transmission in the brain. Microglia exert differential roles in phagocytosis of Tau-laden synapses and in the theory of synaptic Tau spread (reviewed in [147]). Activated and maintained via various biochemical stimuli (e.g., cyto-/chemokines), prolonged and/or aggravated microglia-driven neuroinflammation promotes tangle formation, astrogliosis and synapse pruning (e.g., via interleukins and C1q-mediated synapse opsonization).

Under physiological conditions, astroglia provide neuronal support structurally, trophically, and functionally within their spatial domain via the tripartite synapse – a three-dimensional architecture formed by astrocytic perisynaptic endfeet together with neuronal pre- and postsynapses [55, 97]. Within this formation, astrocytes respond to and secrete neurotransmitters like γ -aminobutyric acid (GABA), glutamate or norepinephrine [8, 55, 76]. Importantly, astrocytic glutamate and GABA transporters (EAAT2, GAT) control levels of extracellular neurotransmitters and thus are essential in preventing deleterious effects of hyperexcitability (reviewed in [6]). Trophic factors and transmitters are exchanged bi-directionally on the astrocyte-neuron-axis. This comprises pro-synaptic astrocytic-neuronal signals like TGF-beta and thrombospondins [38], as well as neuronal-astrocytic glutamate signaling that triggers intracellular Ca^{2+} oscillations in astrocytes (reviewed in [107]). From a systems biology perspective, the synaptogenic phenotype in astrocytes underlies context-dependent cAMP response element-binding protein (CREB) and nuclear factor I-A (NFIA) hub network regulation [66, 108]. As a conjoint endpoint, disruption of astrocytic pro-synaptic expression programs and of local tripartite communication might cause synaptic degeneration.

Intriguingly, synapse loss is a common and characteristic finding in murine models of monogenetic tauopathies [62, 114, 155], and is regarded as the microscopic correlate of motor and cognitive deficits in PSP and CBD [17, 87]. The exact cellular mechanisms leading to synapse loss in these disorders are incompletely understood. One hypothesis states that pTau-mediated synaptic dysfunction in primary tauopathies could result from joint malfunctioning of neurons *and* astrocytes. Accordingly, astrocytic pTau might impede synapse integrity via disruption of transmitter clearance, synaptotrophic factors, mitochondrial distribution mechanisms, and compartmentalized Ca^{2+} currents [31, 113, 120, 130].

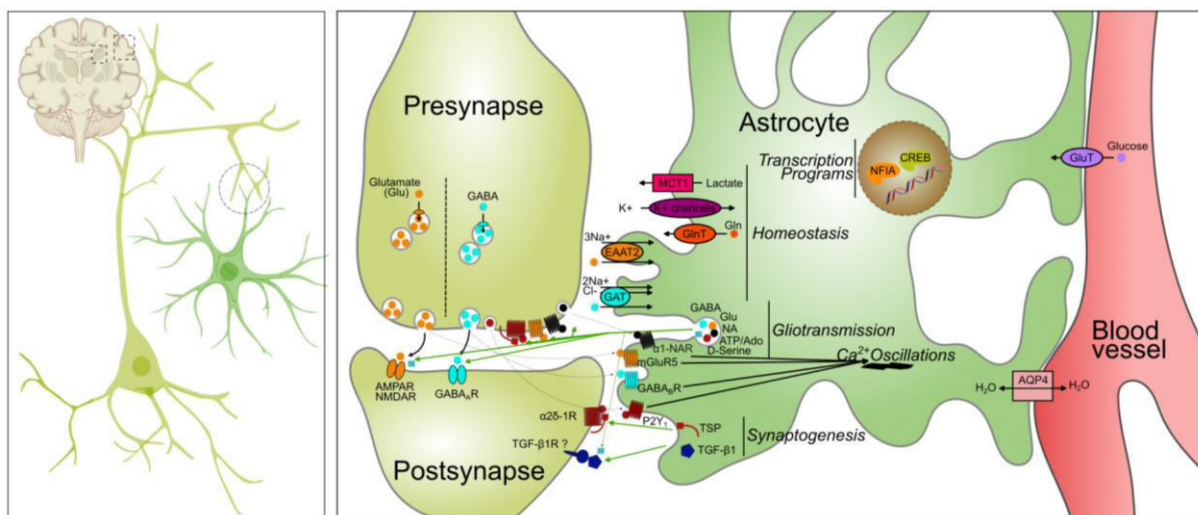


Figure 2. The tripartite synapse.

Astrocytic roles in transmitter homeostasis, gliotransmission and synaptogenesis. Green arrows show astrocytic-neuronal signals, black arrows pre-to-postsynaptic and Ca^{2+} signals, dashed arrows neuronal-astrocytic signals. Adapted from Bazargani N et al. 2016 [13]; tools: SciDraw.com and Inkscape.

Abbreviations: AMPAR, α -amino-3-hydroxy-5-methyl-4-isoxazolepropionic acid receptor; AQP4, aquaporin-4; ATP/Ado, adenosine tri-phosphate/adenosine; CREB, cAMP response element-binding protein; EAAT2, excitatory amino acid transporter 2; GABA_{(A,B)R}, γ -aminobutyric acid (receptor); GAT, GABA transporters; Gln/Glu, glutamate/glutamine; GluT, glucose transporter; MCT1, monocarboxylate-transporter 1; mGluR, metabotropic glutamate receptor; NA, noradrenaline; NAR, noradrenaline receptor; NFIA, nuclear factor IA; NMDA, N-methyl-D-aspartate-receptor; P2Y₁R, purinergic-2-Y-receptor TGF- β 1(R), transforming growth factor-beta-1 (receptor); TSP, thrombospondin.

2.2.2 Astrocytes in Tau Degradation and Propagation

Astrocytes are central for brain interstitial fluid homeostasis as explained in *section 2.2*. Linked to this outward capability, the equilibrium between protein synthesis, modification and degradation is crucial for *intracellular* homeostasis. Dysfunctional degradation is one explanation for aggregation of aberrant proteins, as typically observed in proteinopathies or lysosomal storage disorders [39, 115, 146]. The role of astrocytes in normal and pathological clearance pathways of Tau has been studied in *in vitro* and *in vivo* models of oligomeric Tau and monogenic tauopathies, respectively [95, 98, 112, 121].

Multiple pathways such as autophagy (macroautophagy; chaperone-mediated autophagy, CMA), the ubiquitin-proteasome system (UPS), and the unfolded protein response (UPR) have been identified to mediate the degradation of aggregated or misfolded proteins in neuroglial cell types [18, 70].

Autophagy is a major process for macromolecular degradation, that is chiefly orchestrated by the transcription factor of endolysosomal biogenesis (TFEB) [127]. Macroautophagy serves the lysosome-dependent degradation of membrane-engulfed material. This process is competitively regulated by mTORC1 and AMPK, which integrate the cellular energetic status (reviewed in [138]). Conversely, the

CMA is induced upon recognition of cytoplasmic proteins containing a 'KFERQ' pentapeptide sequence by chaperones (heat-shock proteins, e.g., HSC70, HSP90, HSP40), followed by their unfolding and translocation across the lysosomal membrane for final degradation. Curiously, *in vitro* HSP90 stabilizes oligomeric Tau rather than higher-order aggregates, thus its activity might even evoke harmful effects in tauopathies [149].

The second major degradation mechanism, the UPS, uses polyubiquitination tags to target proteins, with E1 (ubiquitin activating enzyme), E2 (ubiquitin conjugating enzyme), and E3 (ubiquitin ligase) enzymes, and to forward them to proteolysis in the 26S proteasome (reviewed in [125]). Physiological functioning is relevant for antigen processing and presentation, as well as for the degradation of transcription factors (TFs), cytokines, tumor suppressor and proto-oncogenes.

Unlike the latter, the UPR is a cytoprotective response to misfolded proteins in the endoplasmic reticulum. Along with a parallel induction of autophagy, the UPR initiates a series of processes: the attenuation of protein translation through the PERK pathway, as well as the upregulation of chaperones and degradation enzymes through ATF4/6 and IRE1, respectively (reviewed in [152]).

However, as evidence to date suggests, autophagy and the UPS represent the major processes for macromolecular degradation of Tau aggregates in astrocytes [138]. Importantly, where Tau aggregates originate from is essential for intervention strategies. Although at sub-neuronal levels, astrocytes have intrinsic *MAPT*/Tau expression (CELLxGENE browser: [158]) and conditional 4R Tau overexpression is sufficient for astrocytic tangle formation in mice [120]. Nevertheless, the largest share of aggregated Tau is presumably taken up from the extracellular space [95, 98, 121]. Astrocytic Tau internalization mechanisms are incompletely characterized, but evidently occur via endolysosomal activity, heparan sulfate proteoglycans, and low-density lipoprotein receptor-related protein 1 (LRP1) [95, 112, 116]. Initially protective, this mechanism could once become functionally overloaded with disease progression. Thereby, astrocytes could join in to accelerate templated Tau misfolding and spread, to exert synaptic toxicity, and promote pro-inflammatory signaling [132].

Hence, several preclinical and up to phase III clinical trials in FTD/AD have tested to harness astrocytic (and neuronal) abilities in Tau internalization and degradation to slow tauopathy progression, e.g., via lithium, methylene blue, trehalose, or nilotinib (see *section 2.2.3*). Another novel proposed, yet preclinical approach employs TFEB inducers to promote astrocytic Tau clearance [70, 75, 95].

2.2.3 Pharmacological Strategies and Perspectives in Tauopathies

Thus far, therapeutic approaches tackling 4R tauopathies are based on symptomatic multimodal management comprising several non-pharmacological as well as pharmacological interventions [19, 83, 148]. The latter mainly aim at modulating neurotransmitter systems, and include levodopa and amantadine to attenuate motor symptoms, cholinesterase inhibitors for improved cognition, or antidepressant and antipsychotic drugs for psychiatric co-morbidities.

In contrast, disease-modifying strategies recently emerge which target the causative agent of neurodegeneration in tauopathies: misfolded and aggregated Tau [25, 119, 135]. Essentially, three broader concepts are currently under investigation (Table 2; AD trials listed in Appendix B Table 2):

- i) *Reducing Tau expression* (antisense oligonucleotides [ASO], TF modulation)
- ii) *Reducing pathogenic effects of Tau species* (aggregation inhibitors, immunization, post-translational modifications, aggregate degradation, downstream neuroprotection)
- iii) *Reinstating Tau's physiological functions* (microtubule stabilization)

Past trials unsuccessfully tested repurposing drugs such as GSK3-beta kinase inhibitors (unselective: valproate [82], lithium [NCT00703677]; selective: tideglusib [142]), davunetide [20], and riluzole [15], given their effect on reduction of Tau hyperphosphorylation, microtubule stabilization, or anti-excitotoxic effects, respectively [19, 148]. From such candidates, only the antioxidant coenzyme Q10 has been translated into clinical praxis, based on the results of equivocal phase II studies [7, 136].

PRIMARY TAUOPATHY TRIALS							
TRIAL PHASE: INDICATION	Agent	CADRO mechanism class	Mechanism of action	Status (CT.gov ID)	Sponsor	Start date	End date
I: PSP, AMONG MANY OTHERS	autologous bone marrow stem cells (BMSC)	Cell death	Nasal administration of BMSC to the CNS	Recruiting: (NCT02795052)	MD Stem Cells	Jun-16	Jul-24
I: nfvPPA	AADvac-1	Tau	Active immunization (vaccine)	Active, not recruiting: (NCT03174886) (AIDA)	Axon Neuroscience SE	Jul-17	Nov-20
I: PSP	NIO752	Tau	ASO against <i>MAPT</i> /Tau transcript	Recruiting: (NCT04539041)	Novartis Pharmaceuticals	Feb-21	May-24
II: PSP	TPN-101	Inflammation	Inhibiting LINE1 reverse transcriptase, to reduce "antiviral" tau/RNA-mediated immune response	Active, not recruiting: (NCT04993768)	Transposon Therapeutics, Inc.	Oct-21	Jul-23
II: PSP-RS	ASN120290 (ASN-561)	Tau	OGA inhibitor, tau aggregation	Not yet recruiting not yet listed; sponsor website	AsceNeuron	NA	NA
II: PSP-RS	AZP2006	Tau	Tau aggregation inhibitor	Not yet recruiting: (NCT04008355)	AlzProtect SAS	Jun-22	Jul-22
II: PSP-RS	UCB 0107/Beprenemab	Tau	Anti-tau monoclonal antibody (near MTBR)	Completed, results pending: (NCT04185415)	UCB Biopharma SRL	Dec-19	Nov-25
II: PSP-RS	Tolfenamic acid	Tau	Degrades tau transcription factor SP1	Unknown, results pending: (NCT04253132)	NeuroTau	Jan-21	Dec-22
II: PSP/CBS	Fasudil	Tau/proteostasis/proteinopathies	ROCK1 /2 inhibitor, tau aggregation and degradation	Active, not recruiting: (NCT04734379)	Woolsey Pharmaceuticals	Jan-21	Nov-23

Table 2. Current clinical trials in 4R tauopathies as registered at clinicaltrials.gov. Retrieved 7th January 2023. **Abbreviations:** ASO, antisense oligonucleotide; BMSC, bone marrow stem cells, CADRO, Common Alzheimer's and Related Dementias Research Ontology; LINE1, long interspersed nuclear elements; MTBR, microtubule binding region.

Given the rationale for downsizing the pool of available aggregative elements, it was found that halving Tau expression reduced tangle burden, neuron loss and behavioral deficits in the P301S mouse model [34]. Subsequently, two phase I trials were registered for AD and PSP, that aim to reduce total Tau expression via the ASOs BIIB080/NIO752 and NIO752, respectively (reviewed in [22]). In another ongoing study, tolfenamic acid is employed to enhance degradation of SP1, a *MAPT*/Tau transcriptional activator, in PSP-RS patients (NCT04253132). Limitations of both strategies might lie in pleiotropic effects elicited by unspecific modulation of Tau expression across cell types and states, as well as in potential off-target effects as has been observed in patients with Huntington disease, cystic fibrosis or transthyretin receptor amyloidosis treated with ASOs [22].

Beyond (epi-) genetic approaches, the largest group of compounds addresses the pathological aggregation process and aggregate elimination. These encompass monoclonal antibodies raised against two different Tau epitopes. Mid-region-binding antibodies (e.g., bepranemab or E2814 in AD) are currently attested higher expectations than those directed against N-terminal Tau, due to lack of efficacy (i.e., tilavanemab and gosuranemab) [14] and suboptimal epitope engagement in the latter ones [28]. Such passive immunization is believed to halt Tau assemblage and promote microglial FcR-mediated endocytosis [122]. Comparable mechanisms must be assumed for active immunization strategies (i.e., AADva-1 tested in nfVPPA). Upcoming candidates enhancing the cellular degradation machinery,

mainly autophagy, are numerous in clinical trials, and act via mTOR (rapamycin, AD), p38 MAPK (neflamapimod, AD), tyrosine kinase (nilotinib, AD) or ROCK1/2 inhibition (fasudil, PSP/CBS). Direct aggregation inhibitors have advanced until phase III trials (i.e., TRx0237/LMTX in AD), while several candidates acting on PTMs are under examination in phase I/II trials for PSP and CBS (i.e., ASN120290, AZP2006, fasudil). TPN-101, a LINE1 reverse transcriptase inhibitor, has a particularly interesting mechanism of action in slowing PSP-RS, as it is expected to prevent the downstream activation of retrotransposons by Tau and the subsequent immune response [53, 102].

Thirdly, restoring the physiological function of Tau solely targets microtubule stabilizing as a concrete mechanism. Besides the clinically insignificant and even harmful candidates davunetide and TPI-287 [20, 144], only one compound with similar properties is tested in an AD cohort (nicotinamide, Appendix B Table 2). From such trials registered for AD, spill-over effects for other tauopathies are expected.

2.3 Motivation and Research Contributions

Motivated by the lack of effective treatments and a controversy regarding the classification of the 4R tauopathies PSP and CBD [58, 86], the main objective of this doctoral thesis is to disentangle contributions of cellular inclusion pathology to their pathogenesis in comparative studies. The leading hypothesis is that synaptic structure, degradation pathways and TF regulatory networks are differentially affected and linked to the distinct neuropathological features in PSP and CBD.

To this end, *Paper I* presents the analysis of immunofluorescence synapse labeling in *postmortem* brain tissue of a selected cohort of PSP (n=3), CBD (n=3) and control (Ctrl, n=3) cases. Synapse densities were quantified independently, in correlation with neuropathological traits, and within the astrocytic domain of pTau+ astrocytes. Synapse loss was a non-trait-correlated phenomenon in the PSP cortex, while in CBD it was correlated with the presence of APs. Interestingly, in both diseases, synapse density alterations showed a spatial dependency within astrocytic domains.

Paper II demonstrates a comprehensive investigation of the single-nucleus epigenetic profiles of neurons, microglia, oligodendrocytes, and astrocytes yielded from *postmortem* cortical brain tissue of a selected PSP (n=4), CBD (n=4) and Ctrl (n=5) cohort. These data were complemented by published GWAS and bulkRNA-seq datasets to delineate cell type-specific genetic risk variant enrichment, and to identify distinct and shared pathomechanisms across both 4R tauopathies. Finally, disease-specific TF signatures were identified that are associated with the characteristic astrocytic 4R Tau inclusion pathology.

2.3.1 Contribution of This Thesis to Synapse Maintenance in 4R Tauopathies

Evidence provided by *Paper I* supports the importance of the tripartite synapse in human primary tauopathies. Most intriguing were the reduced general synapse densities in frequently involved anatomical regions (i.e., frontal cortex and Striatum), that paralleled the neuropathological hallmarks (AP, trending with neuropil threads), and showed a spatial relationship with pTau-positive astrocytes in distinct ways in PSP and CBD (*Paper I*, Fig. 2&3). This aligns well with the deregulated epigenetic activity at synaptic genes in CBD (*DLG4* [11], *Paper II*, Fig. 2a, Suppl. Fig. 10B) and deregulated synapse gene hub TFs (CREB, NFIA; *Paper II*, Figure 6b). These findings corroborate astrocytes as promising therapeutic targets, to alleviate the synaptic phenotype and presumably cognitive deficits.

2.3.2 Contribution of This Thesis to Degradation Pathways in 4R Tauopathies

As provided in *Paper II*, astrocytes obtained from PSP and CBD cortices exhibited alterations in degradation systems on four levels:

- i) The autophagy marker CTSD was detected at decreased levels in TAs (*Paper II*, Fig. 7b).
- ii) Tauopathy-associated degradation genes were differentially accessible in tauopathy astrocytes (*HSP90AA1*, *UBB*, *EIF2AK3*; *Paper II*, Fig. 2a).
- iii) System-level enrichment of CMA showed trending upregulation in CBD astrocytes, while UPS was significantly downregulated. In PSP microglia, CMA genes were upregulated (*Paper II*, Fig. 2c).
- iv) Astrocytic TF activity of autophagy (TFEB) and UPR (ATF4) master regulators was downregulated in PSP and CBD (*Paper II*, Fig. 5h&6b).

2.3.3 Contribution of This Thesis to Pharmacological Targets in 4R Tauopathies

Evidence from *Paper II* adds to existing therapeutic considerations:

- i) GWAS risk variants were exclusively enriched in astrocytes, and not in microglia, as it is known from the secondary tauopathy AD [52] (*Paper II*, Fig. 2d). Inherited genetic risk is therefore likely reflected by astroglipathy, contemporaneously indicating a promising population for targeted therapies.
- ii) As described in *sections 2.3.2* and *2.2.2*, defective autophagy and UPR mechanisms imply disease-specific and/or disease state-specific modulation of astrocytic degradation pathways could be beneficial [95, 152].
- iii) The observed SP1 TF upregulation in astrocytes of both tauopathies endorses the use of tolfenamic acid as SP1 degradative agent (*Paper II*, Fig. 6b). However, because of cell type transcriptional pleiotropy, mis-regulating Tau expression could produce unfavorable effects.
- iv) Confinement of GSK3-beta gene accessibility upregulation to neuronal and oligodendroglial, or *MAPK8* to astrocytic and oligodendroglial populations, marks target cells of kinase modulation concepts.
- v) Upregulation of innate immunity TFs and genes as a probable result of Tau-mediated activation of retrotransposons [53, 102] encourages approaches employing LINE1 reverse transcriptase inhibitor such as TPN-101.

3. Summary

Neurodegenerative diseases are characterized by the presence of aggregated pathological proteins associated with cell degeneration in vulnerable brain areas. Research efforts have been undertaken to reveal the underlying molecular mechanisms of neurodegeneration and astrogliopathies. The latter are diseases with significant contributions by astrocytes such as Progressive Supranuclear Palsy (PSP) and Corticobasal Degeneration (CBD). However, their molecular pathogenesis remains insufficiently understood.

This work is dedicated to the investigation of astrocytes in PSP and CBD. In the first project, immunofluorescence synapse labelling was applied with automated puncta quantification in *postmortem* brain tissue of a selected PSP/CBD cohort. To gather a deeper molecular understanding, we then generated and analyzed a single-nucleus chromatin accessibility dataset from *postmortem* cortical tissue of a separate tauopathy cohort. The overarching research aims were to identify contributions of the astrocytic Tau inclusion pathology to alterations in synaptic structure and epigenetic networks.

The findings suggest that a general synapse loss in PSP is not associated with astrocytic Tau inclusions, while in CBD synapse density is negatively correlated with the typical astrocytic Tau pathology. Furthermore, synapse alterations within astrocytic spatial domains reflect the distribution of proximal versus peripheral Tau aggregates in PSP and CBD, respectively. This underpins the importance of these cells in maintaining synaptic contacts, which are considered as correlates of cognitive function. We integrated our generated chromatin accessibility data with publicly available genetic risk variant and bulkRNA-sequencing data to identify pathways and transcription factors (TFs) that are linked to Tau pathology. Genetic risk variants associated with PSP and FTD diagnoses were exclusively enriched in astrocytic accessible chromatin regions. Protein degradation systems were differentially deregulated across neuroglial populations in both tauopathies, with highly increased ubiquitin proteasome system and autophagy in PSP microglia and trending autophagy upregulation in CBD astrocytes. In pseudotime analyses of astrocytic nuclei, immediate early response (IER) and homeostasis transcription factors (TFs) (e.g., JUN, FOS, TFEB) were increased at the expense of early differentiation candidates (e.g., LHX9, EMX1/2). Modeling of TF representations emphasized the relevance of IER-related TFs. Furthermore, in combination with an external dataset, we defined astrocytic Tau TF signatures comprising JUN/FOS, NFIA, SP1, and TFEB, among others. At the protein level, the JUN/FOS target and upstream regulator MAP3K8, and TFEB's effector lysosomal protease CTSD essentially showed concordant deregulation.

These results establish a strong association of disease-relevant molecular and synaptic changes with astrocytes and demonstrate that genetic risk for disease manifestation is tightly linked to astrocytic chromatin accessibility profiles. We also identified marked differences related to protein homeostasis and TF networks between both diseases. Altogether, these findings emphasize the interactions between astrocytes and Tau as an important subject of prospective research.

4. Zusammenfassung

Neurodegenerative Erkrankungen sind durch das Vorhandensein aggregierter pathologischer Proteine gekennzeichnet, das mit der Zelldegeneration in vulnerablen Hirnregionen einhergeht. Einige Forschungsarbeiten wurden unternommen, um die zugrundeliegenden molekularen Mechanismen der Neurodegeneration und der Astrogliopathien zu erforschen. Letztere sind Krankheiten mit signifikantem Beitrag durch astrozytäre Zellen, wie z. B. die Progressive Supranukleäre Lähmung (PSP) und die Kortikobasale Degeneration (CBD). Die Pathogenese dieser Krankheiten ist jedoch nach wie vor unzureichend verstanden.

Diese Arbeit widmet sich der Untersuchung von Astrozyten bei PSP und CBD. Im ersten Projekt wurden Immunfluoreszenz-Synapsenmarkierung zur automatisierten Puncta-Quantifizierung in postmortalem Hirngewebe einer ausgewählten PSP/CBD-Kohorte verwendet. Um ein detaillierteres molekulares Verständnis zu erlangen, generierten und analysierten wir einen Datensatz der Einzelzell-Chromatin-Akzessibilität aus postmortalem kortikalem Gewebe einer separaten Tauopathie-Kohorte. Die übergreifenden Forschungsziele waren die Identifizierung des Einflusses der astrozytären Tau-Einschluss-Pathologie an Veränderungen synaptischer Strukturen und epigenetischer Netzwerke.

Die Ergebnisse deuten darauf hin, dass ein allgemeiner Synapsenverlust bei PSP nicht mit astrozytären Tau-Einschlüssen assoziiert ist, während bei CBD die Synapsendichte negativ mit der typischen astrozytären Tau-Pathologie korreliert ist. Darüber hinaus spiegeln Synapsenveränderungen innerhalb astrozytärer räumlicher Domänen die Verteilung proximaler bzw. peripherer Tau-Aggregate bei PSP und CBD wider. Dies verdeutlicht die Wichtigkeit dieser Zellen für die Aufrechterhaltung synaptischer Kontakte, die als Korrelate der kognitiven Funktion angesehen werden. Unsere Daten zur Chromatin-Akzessibilität integrierten wir mit öffentlich verfügbaren Daten zu genetischen Risikovarianten und Bulk-RNA-Sequenzierung, um „Pathways“ und Transkriptionsfaktoren (TFs) zu identifizieren, die mit der Tau-Pathologie in Verbindung stehen. Genetische Risikovarianten, die mit PSP- und FTD-Diagnosen assoziiert sind, waren ausschließlich in astrozytären Chromatin-Akzessibilitätsregionen angereichert. Protein-Degradationssysteme waren in beiden Tauopathien über Neuroglia-Populationen hinweg unterschiedlich dereguliert, mit einem stark erhöhten Ubiquitin-Proteasom-System und Autophagie in PSP-Mikroglia und einer tendenziellen Hochregulierung der Autophagie in CBD-Astrozyten. In Pseudozeitanalysen astrozytärer Kerne waren die Transkriptionsfaktoren (TF) der „immediate early reponse“ (IER) und der Proteinhomöostase (z. B. JUN, FOS, TFEB) zuungunsten von Kandidaten früher Differenzierungsstufen (z. B. LHX9, EMX1/2) erhöht. Modellierung der TF-Repräsentationen bestätigte die Bedeutung der IER TF. Darüber hinaus definierten wir in Kombination mit einem externen Datensatz astrozytäre Tau-TF-Signaturen, die u. a. JUN/FOS, NFIA, SP1 und TFEB umfassen. Auf Proteinebene wiesen sowohl das JUN/FOS-Zielgen und „Upstream“-Regulator MAP3K8 als auch die lysosomale Protease CTSD, ein Effektor von TFEB, weitgehend kongruente Deregulation auf.

Diese Ergebnisse stellen eine starke Assoziation von krankheitsrelevanten molekularen und synaptischen Veränderungen mit Astrozyten her und zeigen, dass das genetische Risiko für die Krankheitsmanifestation eng mit astrozytären Chromatin-Akzessibilitätsprofilen verbunden ist. Wir identifizierten zudem signifikante Unterschiede hinsichtlich Mechanismen der Proteinhomöostase und TF-Netzwerken zwischen beiden Krankheiten. Zusammenfassend stellen diese Ergebnisse die Wechselwirkungen zwischen Astrozyten und Tau als relevanten Fokus zukünftiger Forschung heraus.

5. *Paper I*

Contribution of the Astrocytic Tau Pathology to Synapse Loss in Progressive Supranuclear Palsy and Corticobasal Degeneration

AUTHORS

Nils Briel^{1,2,4}

Katrin Pratsch^{1,2}

Sigrun Roeber²

Thomas Arzberger^{1,2,5}

Jochen Herms^{1,2,3}

1. German Center for Neurodegenerative Diseases (DZNE) e.V., Site Munich, Feodor-Lynen-Str. 17, 81377 Munich, Germany
2. Center for Neuropathology and Prion Research, University Hospital Munich, Ludwig–Maximilians-University, Feodor-Lynen-Str. 23, 81377 Munich, Germany
3. Munich Cluster of Systems Neurology (SyNergy), Ludwig-Maximilians-University, Feodor-Lynen-Str. 17, 81377 Munich, Germany
4. Munich Medical Research School, Ludwig-Maximilians-University, Faculty of Medicine, Bavariaring 19, 80336 Munich, Germany
5. Department of Psychiatry and Psychotherapy, University Hospital Munich, Ludwig-Maximilians-University, Nussbaumstr. 7, 80336 Munich, Germany

This work is published in Brain Pathol. Epub 2020 Dec 29. 2021 Jul;31(4):e12914.

<https://doi.org/10.1111/bpa.12914>. PMID: 33089580; PMCID: PMC8412068.

Supplementary material is available online at: <https://onlinelibrary.wiley.com/action/downloadSupplement?doi=10.1111%2Fbpa.12914&file=bpa12914-sup-0001-Supinfo.pdf>

RESEARCH ARTICLE

Contribution of the astrocytic tau pathology to synapse loss in progressive supranuclear palsy and corticobasal degeneration

Nils Briel^{1,2,3}  | Katrin Pratsch^{1,2} | Sigrun Roeber² | Thomas Arzberger^{1,2,4} | Jochen Herms^{1,2,5}

¹German Center for Neurodegenerative Diseases (DZNE) e.V., Site Munich, Munich, Germany

²Center for Neuropathology and Prion Research, University Hospital Munich, Ludwig-Maximilians-University, Munich, Germany

³Munich Medical Research School, Faculty of Medicine, Ludwig-Maximilians-University, Munich, Germany

⁴Department of Psychiatry and Psychotherapy, University Hospital Munich, Ludwig-Maximilians-University, Munich, Germany

⁵Munich Cluster of Systems Neurology (SyNergy), Ludwig-Maximilians-University, Munich, Germany

Correspondence

Jochen Herms, Center for Neuropathology and Prion Research, University Hospital Munich, Ludwig-Maximilians-University, Feodor-Lynen-Str. 23, 81377 Munich, Germany.

Email: jochen.herms@med.uni-muenchen.de

Funding information

Munich Cluster of Systems Neurology (SyNergy; project ID EXC 2145 / ID 390857198); Marie Skłodowska-Curie actions grant, Grant/Award Number: ITN SynDegen (721802); German Academic Scholarship Foundation

Abstract

Primary 4-repeat tauopathies with frontotemporal lobar degeneration (FTLD) like Progressive Supranuclear Palsy (PSP) or Corticobasal Degeneration (CBD) show diverse cellular pathology in various brain regions. Besides shared characteristics of neuronal and oligodendroglial cytoplasmic inclusions of accumulated hyperphosphorylated tau protein (pTau), astrocytes in PSP and CBD contain pathognomonic pTau aggregates — hence, lending the designation tufted astrocytes (TA) or astrocytic plaques (AP), respectively. pTau toxicity is most commonly assigned to neurons, whereas the implications of astrocytic pTau for maintaining neurotransmission within the tripartite synapse of human brains is not well understood. We performed immunofluorescent synapse labeling and automated puncta quantification in the medial frontal gyrus (MFG) and striatal regions from PSP and CBD postmortem samples to capture morphometric synaptic alterations. This approach indicated general synaptic losses of both, excitatory and inhibitory bipartite synapses in the frontal cortex of PSP cases, whereas in CBD lower synapse densities were only related to astrocytic plaques. In contrast to tufted astrocytes in PSP, affected astrocytes in CBD could not preserve synaptic integrity within their spatial domains, when compared to non-affected internal astrocytes or astrocytes in healthy controls. These findings suggest a pTau pathology-associated role of astrocytes in maintaining connections within neuronal circuits, considered as the microscopic substrate of cognitive dysfunction in CBD. By contrasting astrocytic-synaptic associations in both diseases, we hereby highlight astrocytic pTau as an important subject of prospective research and as a potential cellular target for therapeutic approaches in the primary tauopathies PSP and CBD.

Abbreviations: AD, Alzheimer's disease; ANOVA, analysis of variance; AP, astrocytic plaque; APP, amyloid precursor protein; CA, control astrocyte(s); CB, coiled bodies; CBD, corticobasal degeneration; Ctrl, control; DF, degrees of freedom; dpi, dots per inch; EAAT2, excitatory amino acid transporter 2; fCtx, frontal cortex of the middle frontal gyrus; FTD, frontotemporal dementia; FTLT, frontotemporal lobar degeneration; GFAP, glial fibrillary acidic protein; GLT1, glutamate transporter 1; KO, knock-out; LSM, light sheet microscope; MFG, middle frontal gyrus; NA, numerical aperture; NFT, neurofibrillary tangles; NT, neuropil threads; PBS, phosphate-buffered saline; PET, positron emission tomography; PSP, Progressive Supranuclear Palsy; pTau, hyperphosphorylated tau; ROI, region of interest; SB, Sudan Black; Str, striatum; SV2A, synaptic vesicle protein 2A; TA, tufted astrocyte; vGAT, vesicular GABA transporter; vGLUT1, vesicular glutamate transporter 1.

This is an open access article under the terms of the Creative Commons Attribution License, which permits use, distribution and reproduction in any medium, provided the original work is properly cited.

© 2020 The Authors. *Brain Pathology* published by John Wiley & Sons Ltd on behalf of International Society of Neuropathology

KEY WORDS

astrocytic plaques, corticobasal degeneration, progressive supranuclear palsy, synapse loss, tauopathy, tufted astrocytes

1 | INTRODUCTION

The neuropathological classification of frontotemporal lobar degeneration of the tau-type (FTLD-tau), a group of neurodegenerative diseases with predominant cognitive (frontotemporal dementia, FTD) and motor impairments, primarily bases on heterogeneous patterns of cytoplasmic inclusions of aggregated hyperphosphorylated *microtubule-associated protein tau* (pTau) in neurons and glia (9, 16, 18, 27, 48). Differential splicing of exon 10 transcripts of the tau gene leads to 3-repeat and 4-repeat tau isoforms. Typical cases of PSP and CBD are associated with a predominant aggregation of 4-repeat (4R) pTau isoforms (28). In histopathology, the AT8 monoclonal antibody recognizing pTau phosphorylated at both serine 202 and threonine 205 is widely used for visualizing pathological tau deposits (27, 48). Typical CBD cases are characterized by neuronal (pre-) tangles and ballooned neurons, dense neuropil threads (NT), a prominent white matter pathology with oligodendrocytic coiled bodies (CB) and corona-like astrocytic plaques (AP), which mainly involve the fronto-parietal cortices, the striatum as well as the substantia nigra (9, 48).

In contrast, the typical neuropathological traits of PSP are widespread pTau aggregates forming neurofibrillary tangles (NFT), which are sometimes globose, numerous CB, and tufted astrocytes (TA) mainly in the basal ganglia, brainstem, cerebellum and to varying degrees in neocortical areas. The described pathognomonic astrocytic pTau pathology is emphasized in the soma-distant processes of APs in CBD, whereas in PSP TAs' inclusions are rather localized in soma-proximal cell compartments (9, 16, 27, 48).

While higher order pTau assemblies in the form of so-called "tangles" are thought to have an arguably toxic effect in neurons, lower order pTau oligomers appear to be more potent cellular or synaptic noxae (2, 7, 12, 21, 41). Indeed, recent PET-imaging studies in human FTD and Alzheimer's Disease (AD) patients reported (i) a remarkably high synapse loss, (ii) elevated mitochondrial stress marker binding levels, and (iii) a positive correlation between both (preprint: Holland et. al. 2020, medRxiv: 2020.01.24.20018697 and conference report: <https://www.alzforum.org/news/conference-coverage/multimodal-imaging-neurodegenerative-diseases-links-pathology-and-cellular>). Additionally, densitometric approaches with brain lysates obtained from the frontal cortex of AD and PSP subjects showed ca. 50% reductions of synaptophysin protein levels to those of controls, concordant with putatively depleted presynaptic vesicle

pools (5, 26). However, a histological validation of a supposed morphological synaptic decrease in FTDs, as suggested by those radio-ligand or densitometry studies, is lacking to date. Furthermore, whether the synaptic phenotype relates to a cell type-specific pathology remains unexplored.

Synapse loss is not only a common and characteristic finding in animal models for tau pathology (21, 47, 49), but also a presumptive cause of cognitive deficits in PSP and AD (4, 46). Though, the latter view is challenged by the finding of lower synaptophysin levels in non-demented vs. demented PSP subjects (5) as well as by more recent findings, which could not confirm decreased binding of the synaptic vesicle protein 2A (SV2A) targeting radio-ligand [³H]UCB-J to presynaptic vesicle pools in postmortem sections of AD patients in comparison to non-AD control cases (30).

At the level of cell complexes, the functioning of neuronal circuits in the mammalian brain does not exclusively depend on the cell type-autonomous physiology of interconnected neurons. There are external factors provided by glial cells that regulate the integrity of neurons and their cellular compartments *in vitro* (25) and *in vivo* (43, 44). The spatial unit an astrocyte is responsible for often is referred to as the "astrocytic domain" or "synaptic island," when specifying the synaptic responsibility (15, 35). As assessed by comparative studies in humans, non-human primates, and other species, such domains measure in average about 142 μm in diameter and encompass about 2 million synapses (34, 35). The fine perisynaptic astrocytic processes, being long time presumed as passive bystanders of neuronal communication, emerged as essential components of the tripartite synapse to provide support structurally, trophically, and functionally (36, 38, 43) (preprint: Holt et al. 2019, bioRxiv: 10.1101/518787v1). Furthermore, an impaired astroglial support has previously been implicated in a pTau- and amyloid precursor protein (APP)-related disease context, including mouse models recapitulating tauopathies with mutant pTau (P301S, P301L (42), rTg4510 (39)), brain culture internalization approaches (38) and the APP-KO mouse line (31). In murine hippocampal neuronal-astrocytic co-cultures pTau accumulation in astrocytes was followed by diminished gliotransmission and consequent synapse dysfunctions, indicating a direct involvement of astrocytes in the upstream mechanisms of synaptotoxicity (38). Interpreting the neuropathology and astrocytic roles as described before, pTau-mediated synaptic dysfunction in primary tauopathies is likely to be a joint result of neuronal and astroglial effects.

To address this, we assessed the synaptic density in cortical and striatal areas of PSP and CBD subjects from a morphometry-centric perspective. We then disentangled cell type-distinct contributions to the synaptic phenotype and differentiated these effects by the disease context.

2 | MATERIALS AND METHODS

2.1 | Human tissue of PSP, CBD and control subjects

2.1.1 | Neuropathological evaluation

The neuropathological diagnosis of all cases included was conducted at the Center for Neuropathology, German national reference center for neurodegenerative disorders (23).

At autopsy, the whole brain was dissected out. One hemisphere was frozen immediately. The other one was fixed in formalin for at least two weeks and later cut into 1 cm thick coronal slices. From these, regions of interest including neo- and archicortical, basal ganglia, brainstem, cerebellar, spinal areas as well as the hypophysis were cut out, embedded in paraffin and stained for diagnostic evaluation. A board-examined neuropathologist examined the tissue blocks of all underlying cases. The PSP- and CBD cases were classified according to the *NINDS Neuropathologic Diagnostic Criteria* for PSP (16, 27) and the *Office of Rare Diseases Neuropathologic Criteria* for CBD (9).

2.1.2 | Selection of cases

4R tauopathy (PSP, CBD) or control cases with significant co-pathology in areas of interest were excluded from the study. Neurologically and psychiatrically non-diseased subjects were chosen as control cases. The investigated cohorts were matched for age, postmortem interval (PMI), disease duration, and fixation-time, and none of these covariates differed significantly between the cohorts (Table 1, Figures S1a–c and S2e). Exclusion criteria for 4R tauopathy (PSP, CBD) cases were immunopositivity for A β ₄₂, TDP-43, or RD3 (3R tau) in examined regions and lack of pathognomonic cellular pTau inclusion pattern; exclusion criteria for control cases were immunopositivity for A β ₄₂, TDP-43, AT8, RD3, or RD4 (4R tau) in examined regions. The age at death ranged from 52 to 82 years. To address the potential bias of differing fixation durations on the analysis of detected synaptic puncta, studies of correlation showed neither significant relations across all cohorts nor in a cohort-differentiated view (Figure S2). Thus, the synapse quantification is unlikely biased by this and the other covariates (Figure S1d–k). To be noted,

TABLE 1 Covariates of included PSP, CBD and control subjects

Code	Diagnosis	Age (years)	PMI (hr)	Gender	Fixation time (years)	CERAD	BRAAK & BRAAK (NFT)	THAL-phase (A β)	TDP-43	Disease duration (years)	Locus
103	Ctrl	61	15	Female	9.0	0	1	0	neg	–	MFG/NCau
110	Ctrl	72	23	Male	8.8	0	2	0	neg	–	MFG/Put
111	Ctrl	82	63	Male	7.5	0	1	1 ^a	neg	–	MFG/NCau
102	PSP	68	38	Male	3.3	0	1	0	neg	6.0	MFG/NCau
105	PSP	77	78	Female	6.8	0	0	0	neg	2.5	MFG/NCau
107	PSP	64	106	Male	5.2	0	0	0	neg	4.5	MFG/NCau
104	CBD	52	14	Female	7.7	0	0	0	neg	4.5	MFG/NCau
108	CBD	56	44	Male	3.5	0	1	0	neg	2.5	MFG/Put
109	CBD	75	33	Female	5.9	0	0	0	neg	3.0	MFG/NCau

^aA β plaques were not observed in the frontal cortex.

Abbreviations: A β , amyloid beta; Ctrl, control; MFG, medial frontal gyrus; NCau, caudate nucleus; NFT, neurofibrillary tangles; Put, putamen; neg, negative.

we were limited by the availability of (i) rare formalin-fixed brain tissue of PSP and CBD cases, in which the astrocytic domain had to be captured within thick vibratome-sections in its largest diameter and (ii) of those cases with pure tau-pathology to exclude additional confounding effects by other proteinaceous aggregates.

2.1.3 | Regions of interest

PSP, CBD, and control samples used for this study stem from formalin-fixed archival brain tissue and corresponding paraffin-embedded specimen. In coronal brain slices, we sampled circa 1 cm³-measuring tissue blocks from the medial frontal gyrus at the height of the anterior striatum (MFG, Brodmann area: 46) and from the anterior striatum (caudate nucleus at the coronal height of the Ncl. accumbens until the height of the pallidum or from the putamen) of grey and parts of white matter (see Table 1 for information on subjects).

2.2 | Immunofluorescence staining for synapse analysis

Starting with formalin-fixed archival coronal brain slices of 1 cm thickness fixed for 3.5 to ca. 9 years, samples containing the regions of interest were cut out and divided into smaller blocks of ca. (1 × 1 × 0.5) cm³ volume. Then, these blocks were placed in 2 mL reagent tubes and first subjected to antigen retrieval. For this purpose, tissue blocks were incubated in citrate buffer (10 mM,

pH 6) overnight before incubating in fresh medium for 20 minutes at 95°C and subsequent cooling to room temperature. Next, using a Leica VT1000E vibratome, 50 µm-thick sections were prepared. To avoid batch bias, all samples were processed within one common run for each staining combination. The free-floating immunofluorescent staining procedure was introduced by permeabilization with 2% Triton X-100 in 1× PBS (PBST) for 16 hr at 4°C. Unspecific potential binding sites were blocked with 10% (v/v) appropriate serum (donkey, #D9663; goat #G9023; Sigma-Aldrich, Germany) in 0.3% PBST for 5–6 hr at room temperature. Next, primary antibodies diluted in 5% serum in 0.3% PBST were applied in appropriate, previously experimentally determined concentrations (Table 2) at 4°C on a shaking platform for three consecutive days. After washing, secondary antibodies were applied in a 1:1000 dilution in 5% serum in 0.3% PBST at room temperature for 4 hours before washing. Quenching of mainly lipid-caused autofluorescence was achieved by an immersion in 0.02% (w/v) Sudan Black (SB) in 70% (v/v) ethanol for 2 minutes. Finally, sections were mounted onto Superfrost[®]-plus slides (Thermo Fisher Scientific, Germany) and covered with Fluorescence Mounting Medium (#S302380-2, Agilent Dako, Germany) and #1.5H high-precision imaging coverslips.

Antibodies used for *excitatory* synapse analysis were rabbit anti-vGLUT1 and guinea pig anti-HOMER1 and the fluorescent-labeled goat anti-rabbit AlexaFluor[®]647 and goat anti-guinea pig AlexaFluor[®]488. Mouse anti-AT8 labeled with goat anti-mouse AlexaFluor[®]568 was co-stained to aid orientation, but not used in analysis.

TABLE 2 Antibodies and respective usage specifications

Antibodies list	Dilution	Identifier and source
<i>Primary</i>		
Anti-AT8, mouse	1:200	MN1020, Thermo Fisher Scientific, Germany
Anti-GEPHYRIN, mouse	1:150	147 011, Synaptic Systems Ltd, Germany
Anti-GFAP, goat	1:150	ab53554, Abcam, Germany
Anti-GLT1/ EAAT2, guinea pig	1:250	AB1783, Merck Chemicals Ltd, Germany
Anti-HOMER1, guinea pig	1:110	160 004, Synaptic Systems Ltd, Germany
Anti-HOMER1, rabbit	1:100	160 002, Synaptic Systems Ltd, Germany
Anti-vGAT, rabbit	1:200	131 008, Synaptic Systems Ltd, Germany
Anti-vGLUT1, rabbit	1:100	ZRB2374, Sigma-Aldrich Chemie Ltd, Germany
<i>Secondary</i>		
Anti-goat, Alexa Fluor [®] 647, donkey	1:1000	A21447, Thermo Fisher Scientific, Germany
Anti-guinea pig, Alexa Fluor [®] 488, goat	1:1000	A11073, Thermo Fisher Scientific, Germany
Anti-guinea pig, AlexaFluor [®] 647, goat	1:1000	A21450, Thermo Fisher Scientific, Germany
Anti-mouse, Alexa Fluor [®] 568, donkey	1:1000	A10037, Thermo Fisher Scientific, Germany
Anti-mouse, Alexa Fluor [®] 568, goat	1:1000	A11031, Thermo Fisher Scientific, Germany
Anti-rabbit, Alexa Fluor [®] 647, goat	1:1000	A21244, Thermo Fisher Scientific, Germany
Anti-rabbit, AlexaFluor [®] 488, donkey	1:1000	A21206, Thermo Fisher Scientific, Germany
Anti-rabbit, AlexaFluor [®] 488, goat	1:1000	A11008, Thermo Fisher Scientific, Germany

Antibodies used for *inhibitory* synapse analysis were rabbit anti-vGAT and mouse anti-GEPHYRIN and the fluorescent-labeled donkey anti-rabbit AlexaFluor[®]488 and donkey anti-goat AlexaFluor[®]647. Goat anti-GFAP labeled with donkey anti-goat AlexaFluor[®]647 was co-stained to aid orientation, but not used for further analysis.

For *astrocytic domain* analyses, we used mouse anti-AT8, rabbit anti-HOMER1, guinea pig anti-GLT1/EAAT2, and the fluorescent-labeled goat anti-mouse AlexaFluor[®]568, goat anti-rabbit AlexaFluor[®]488, and goat anti-guinea pig AlexaFluor[®]647. See Table 2 for information about antibodies and applied dilutions.

2.3 | Image acquisition, processing, and synapse analysis

Cover-slipped tri-labeled sections were inspected using a Zeiss LSM780 confocal microscopy system (Zeiss, Germany) assisted by the “ZEN black” software and equipped with a Plan Aplanachromat 40×/NA 1.4 oil DIC M27 objective. Isocortical layers II-IV or striatal grey matter were identified by their nuclei density or reduced amount of myelinated axon tracts appearing black in SB lipid stain, respectively. Five (50 × 50) μm² large 2-channel images (pre- and postsynaptic) were randomly sampled within the predefined histological area for general synapse quantifications using standardized microscope settings (1024 dpi; 16-bit, 0.049 μm lateral resolution, pinhole set to 29 (488 nm channel) and 39 μm (647 nm channel)). When investigating synapse densities related to astrocytic pathology, 11–14 individual characteristic AT8⁺ astrocytes and 4–6 AT8⁻/EAAT2⁺ control astrocytes were identified in two representative cases (PSP = 1, CBD = 1, Ctrl = 1) with less pronounced pathology in the cortex of the MFG. The acquisition of a sectioning plane was standardized to the respective astrocyte’s centroid core, recognized as round, “empty” structure in the AT8 or EAAT2 channel (Figure 3b). Then, a (212 × 212) μm²-large 3-channel image was acquired with standardized settings (HOMER1/AT8/EAAT2, 4096 dpi; 16-bit, 0.052 μm lateral resolution, pinhole set to 32 (488 nm channel) or 30 μm (568 nm, 647 nm channels)).

A custom ImageJ-written macro script was used for pre-processing raw bipartite synapses images, including background subtraction, bandpass filtering, despeckling, sharpening, and thresholding (Figure S3) to account for fixation and staining artifacts. Next, intermediate files were subjected to colocalization and single channel analyses in the “*Synapse Counter*” tool with size parameters adjusted corresponding to developer’s recommendations (<https://github.com/SynPuCo/SynapseCounter>; accessed 6 Mar 2020).

In contrast, astrocytic domains (plus surrounding area) were binned into 17 (27 × 27) μm²-large ROIs. Aiming at differentiating the synapse density distribution

within these domains, we defined 5 Sholl-like concentric circles represented by center ($n = 1$), close ($n = 4$), mid ($n = 4$), distant ($n = 4$), and out ($n = 4$) bins around each astrocyte’s core. Such circles were referred to as “Sholl-like area representations.” The “synapse density distribution” was then defined as the consecutive set of “Sholl-like area representations” from “center” to “out” present in the raw image of one single astrocytic domain (center, close, mid) plus surrounding area (distant, out; Figure 3a,b). Then, a similar pipeline was run on each of these images as described above, with the final outcome measured by “*Analyze Particles...*” in *ImageJ/FIJI*. The custom scripts and a guided analysis workflow are accessible via the public repository GitHub (<https://github.com/nes-b/AstSyns>). Single ROI-values were reorganized into distance circles along area representations, means calculated for each circle in R 3.6.3 and subsequently processed for statistical analysis and graph generation.

2.4 | Quantification of neuropathological traits

In order to quantify the extent of neuropathological pTau traits such as NFT, TA/AP, and CB, 5 μm-thick paraffin sections of the MFG were stained by the AT8 antibody (1:200) on a Roche BenchMark Ultra system (CCI standard program with preboiling). Stained slides were inspected using an Olympus BX50 equipped with a UPlanFI 20× objective (NA 0.50). By randomly sampling 10 visual fields per MFG sample and by manually counting the number of positive cells, total cell counts were reported for respective traits in all fields. For NTs, though, we estimated the extent on a semi-quantitative scale ranging from 0 = “no thread” to 5 = “dense meshwork.”

2.5 | Statistics and plots

All statistical tests were calculated in RStudio (version 1.2.5001, R 3.6.3). Shapiro–Wilk testing of normality distribution on single outcome measurements was used to determine downstream group-wise comparisons of either means (two-sided parametric *t*-test) or medians (two-sided nonparametric Mann–Whitney *U*-test). For comparisons of more than two groups, pair-wise testing with Holm–Sidak correction was applied. Bound analyses, e.g. of astrocyte domain synapse density distributions, were done using two-way ANOVA and Levene-test of normality confirmation (<https://rpubs.com/tmcurlay/twowayanova>; accessed 6 Mar 2020) followed by the Games–Howell test for data sets with unequal variance (<https://rpubs.com/aaronsc32/games-howell-test>; accessed 6 Mar 2020). Statistical assessment and graphic illustration in the R environment was mainly supported by the “ggpubr” (<https://github.com/kassambara/ggpubr>; accessed 10 Mar 2020)

and “ggstatsplot” (<https://github.com/IndrajeetPatil/ggstatsplot>; accessed 10 Mar 2020) packages.

3 | RESULTS

3.1 | Excitatory and inhibitory bipartite synapses are reduced in PSP

In order to morphometrically assess alterations in synapse densities, postmortem brain samples from non-diseased control subjects were compared with those of neuropathologically confirmed PSP and CBD cases with abundant cortical pTau aggregates, but without immunohistochemical signs of cortical or striatal copathology ($n = 3$ per cohort; Table 1). In specimen from cortical tissue from the MFG (fCtx), layer II to IV as well as in grey matter from rostral striatal caudate nucleus or anterior putamen (Str) bipartite synapses were quantified. A bipartite synapse was defined as the unity of colocalized pre- and postsynaptic signal to a certain spatial extent (overlap presynaptic channel, postsynaptic channel ≥ 0.33). Here, we used previously established markers for presynapses (excitatory vesicular Glutamate Transporter 1: vGLUT1, inhibitory vesicular GABA Transporter: vGAT; Figure 1b,d) and postsynapses (excitatory HOMER1, inhibitory GEPHYRIN; Figure 1b,d).

Differentiated by synaptic qualities and disease entity, a significant loss of bipartite *excitatory synapses* (vGLUT1+/HOMER1+) could be mapped to the fCtx of PSP patients (Figure 1a 1st row; t -test, $p = 0.038$). No significant alterations were observed in the excitatory bipartite synapse density of the Str in PSP. Noteworthy, while excitatory presynapses remained unchanged, nonsignificant trends became apparent for reduced excitatory postsynapses (HOMER1+) in the PSP-fCtx (Figure 1a, 3rd row; t -test, $p = 0.099$) and PSP-Str analysis branches (Figure 1a, 3rd row; t -test, $p = 0.099$), hinting toward possible latent, isolated excitatory postsynaptic reductions. In the CBD cohort, we did not find any significant synaptic alterations, neither among the anatomical regions of investigation, nor among the separate pre-, post-, or bipartite synapse sub-analyses. However, the excitatory postsynapses’ (HOMER1+) density was trending toward reductions in the CBD-fCtx analysis branch compared with controls (Figure 1a, 3rd row; t -test, $p = 0.072$).

The analysis of bipartite *inhibitory synapses* (vGAT+/GEPHYRIN+) revealed a similar loss pattern regarding colocalization as apparent for excitatory synapses (Figure 1c, 1st row; 3 groups one-way-ANOVA, $p = 0.023$). In PSP, there were significantly less inhibitory bipartite synapses in the fCtx (Figure 1c, 1st row; t -test, $p = 0.047$), but not in the Str. Regarding the separated analyses of single synaptic densities there were almost no significant differences between the PSP and the control

group. Interestingly, these counts indicated a significant increase of vGAT+ presynapses in the Str of PSP patients (Figure 1c, 2nd row; t -test, $p = 0.022$) — a severely affected brain region in this tauopathy. In the CBD cohort though, neither significant nor trending differences of bipartite or single inhibitory synapse densities were detectable when compared to the levels of the control cohort. Together, in PSP excitatory and inhibitory synapses were reduced in the fCtx, while in the Str only inhibitory presynapses were significantly increased. The assessment of synapses in CBD yielded no significant differences; neither in the fCtx nor in the Str. Nevertheless, there was a trend toward reduced excitatory postsynapses in the fCtx in both PSP and CBD (see Table S1). However, the consistent high synapse density scores of CBD case #109 impelled to ask for a more differentiated questioning toward variable neuropathological features in this disease. Due to clearer results regarding synapse alterations in the cortical than in the striatal regions in these subjects, we focused on the fCtx in the following analyses.

3.2 | Astrocytic plaques are indicators of a reduced excitatory synapse density in CBD

Since proteinaceous aggregates like pTau assemblies are known for their cell-harming properties (12, 13), general synaptic alterations, as often observed in neurodegenerative disease (21, 46), would expectedly be linked to the number of cells with pTau aggregates within a certain anatomical region. Thus, we hypothesized, the synaptic density might negatively correlate with the extent of cellular pTau pathology.

In order to proof this hypothesis, AT8-labeled paraffin sections adjacent to those samples investigated for synapse counting (MFG, fCtx) were used for obtaining total numbers of cells with different types of pTau aggregates (NFT, TA/AP, CB) and for a semi-quantitative assessment of pTau positive NT. These values correspond to the observations from 10 randomly sampled fields of 250x magnification (Table 3). Strikingly, when inspecting AT8+ cell-specific pTau traits of individual CBD cases, #109 had only very few cortical APs, several NFTs and CBs and only few NT in comparison to #108 (Figure 2a). When correlating a given pTau trait with the synaptic density, the extent of astrocytic pTau pathology was the only significant one (Figure 2b, grey; $R_{\text{PEARSON}} = -1$, $p = 0.043$) to estimate excitatory synapse density in CBD, while NT grading was close to significance (Figure 2b, grey; $R_{\text{PEARSON}} = -0.99$, $p = 0.075$). Contrarily, in the PSP cohort none of the pTau aggregate types correlated with synapse reductions (Figure 2b, yellow). In summary, structural synaptotrophic degradation was linked with pTau+ astrocytes in CBD and possibly with neuropil thread pathology. In the investigated PSP cohort though, the factual synaptic reduction was not linked to a singular neuropathological pTau trait.

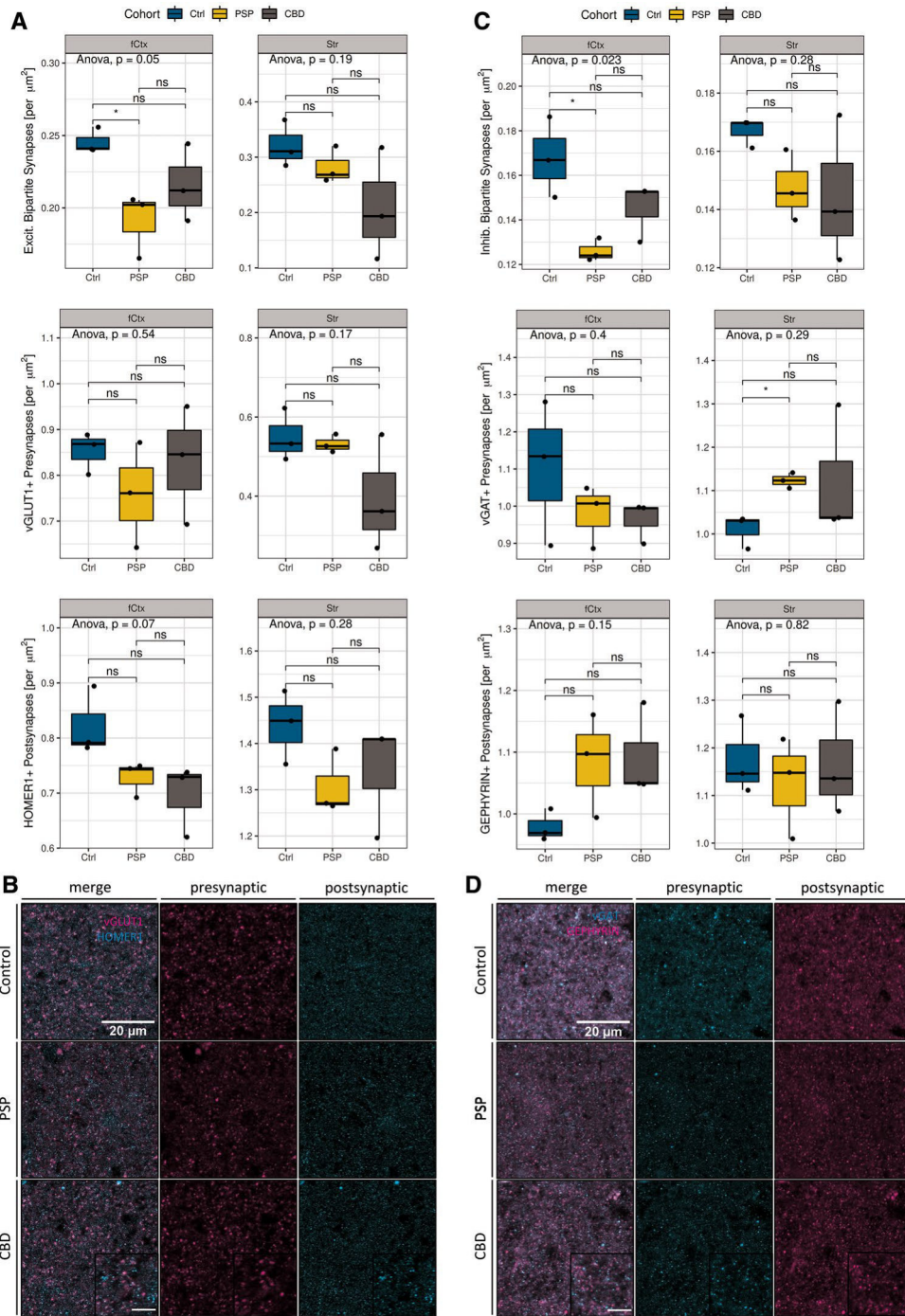


FIGURE 1 Bipartite synapse quantifications. (a) Statistical analysis of excitatory synapses (# synapses per μm^2) faceted by region (left column: fCtx, right column: Str) and markers (vGLUT1, HOMER1). Significant reductions of bipartite excitatory synapses in PSP-fCtx and trending isolated postsynaptic loss in PSP- and CBD-fCtx. Boxplots show synapse densities for colocalized pre- and postsynaptic positive (+) signal (1st row), presynapses only (2nd row), and postsynapses (3rd row) in the fCtx and Str. The color code indicates disease entity. Black dots depict values of single cases. The upper and lower hinges of each box correspond to the 75th and 25th percentiles, while median values are represented by a black bar. Whiskers display the range of data within 1.5 of the inter-quartile range. Significance statements are depicted according to the analysis of variance (ANOVA) with Tukey post hoc correction (entire groups) or *t*-test (pair-wise group comparisons). Results are expressed as decimal (ANOVA) or indicated as $*p < 0.05$ and ns = “not significant” (*t*-test). (b) Confocal *ex vivo* images of the merged pre- and postsynaptic markers for excitatory synapses (vGLUT1 and HOMER1, left), presynaptic (middle column), and postsynaptic (right) in the fCtx of controls (1st row), PSP (2nd row), and CBD (3rd row) subjects. Scale bars: 20 μm (main), 10 μm (inset). (c) Statistical analysis of inhibitory synapses (# synapses per μm^2) faceted by region (left column: fCtx, right: Str) and markers (vGAT, GEPHYRIN). Significant reductions of inhibitory synapse density in the fCtx and significant increases of inhibitory presynapses in the Str of PSP patients. Depiction and statistical assessment according to (a). (d) Confocal *ex vivo* images of the merged pre- and postsynaptic markers for inhibitory synapses (vGAT and GEPHYRIN, left), presynaptic (middle column), and postsynaptic (right) in the fCtx of controls, PSP and CBD subjects. Scale bars according to (c). fCtx, cortex of the MFG; Str, striatum

TABLE 3 Quantification of neuropathological traits

Case	Diagnosis	TA/ AP	NFT/ Pretangles	CB	Threads
102	PSP	137	48	146	1
105	PSP	38	30	61	2
107	PSP	49	42	128	3
104	CBD	68	62	36	3
108	CBD	94	134	34	5
109	CBD	17	31	5	1

Note: Total counts of neuropathological traits per 10 visual 250 \times -magnification fields or threads grading in the PSP and CBD fCtx.

Abbreviations: Abbreviations: AP, astrocytic plaque; CB, coiled bodies; NFT, neurofibrillary tangle; TA, tufted astrocytes.

3.3 | Synapse loss is evident within spatial domains of pTau-affected astrocytes

In review with the previously assigned reductions in general bipartite synapse counts of both synapse types, we wondered, whether this effect can be ascribed to the single-cell level. Therefore, we quantified postsynaptic puncta within and surrounding the astrocytic domain, the spatial unit an astrocyte is responsible for 11–14 AT8+ astrocytes as well as 4–6 control astrocytes expressing a marker of neurotransmitter clearance (excitatory amino acid transporter 2, EAAT2) residing in fCtx layers II to VI were identified in 50 μm -thick sections and imaged. Within this approach synapse densities were determined as HOMER1+ puncta in 17 (27 \times 27) μm^2 -large squared bins placed at concentric circles around each astrocyte's core (Figure 3a,b). Thereby a total area of ca. 12,400 μm^2 was covered, the actual astrocytic domain accounting for 6600 μm^2 (corresponding to 9 squared bins) thereof.

When comparing only *domain*-assigned bin-means of synapse densities of pTau+ and pTau- astrocytes, APs showed significantly lower values than their internal control astrocytes (CBD_AP vs. CBD_CA, Figure 3c; *t*-test, $p = 0.014$). In comparison to EAAT2+ astrocytes from non-diseased subjects, AP domains exhibited at least a trend to sparser synapses (Figure 3c; *t*-test, $p = 0.054$), whereas examined TA domains did not show such reductions. Instead, TA domains seemed to be less vulnerable to their pTau inclusions, when compared to APs (Figure 3c; *t*-test, $p = 0.044$).

To elaborate a potential pTau+ astrocyte-related synapse depletion as a function of distance, mean densities of all five distances (“center” = 0 μm , “close” = 30 μm , “mid” = 60 μm , “distant” = 90 μm , and “out” = 120 μm) were determined in an ordered fashion, resulting in bound center-to-out Sholl-like area representations of the astrocytic domain (Figure 3a,b). We found first, a consistent initial increment of synaptic densities in the soma-proximal distance “close” with a subsequent decrease, which was unique to pTau- astrocytes (Figures 3d and 4a,c; distance: “close”). Second, the highest mean loss could be assigned to this first distance in TAs in

PSP (Figure 4b; “close” vs. “out”; *t*-test, $p = 0.033$), while the lowest density was measured in the fourth distance of APs in CBD (Figure 4d; “distant” vs. “out”; *t*-test, $p = 0.007$), which might correspond to an enlarged astrocytic territory size as determined by Oberheim et al. (34) (Figure 3b.2) or to functional consequences extending beyond this arbitrary boundary. Third, these significant differences in spatial synapse distributions levelled out when reaching the last distance (“out”) for TAs in PSP (Figure 4b, two-way-ANOVA, $p = 0.024$). Fourth, spatial synapse distributions of APs in CBD were inherently different from those of internal control astrocytes (Figure 3d, Table 4; two-way-ANOVA, $p = 0.003$) as well as external control astrocytes (Figure 3d, Table 4; two-way-ANOVA, $p = 0.017$). In summary, in this domain-centered analysis single APs displayed an abnormal synapse distribution at principally reduced density levels, while TAs exhibited only minor declines within the most proximal part of their synaptic islands.

4 | DISCUSSION

Neurodegeneration in tauopathies has been widely researched in both mouse models and human disease (1, 19, 49). Astrocytes, with specialized responsibilities for structural and functional support within spatially divided territories, modulate neuronal signaling via gliotransmission at the tripartite synapse (3, 22, 32) — an association of pre- and postsynaptic neuronal terminals and astrocytic perisynaptic processes (14, 15, 17). Evidently, this led to assumptions of whether and how neuronal circuits depend on the intact function of astrocytes and their peripheral cellular compartments in neurodegenerative disease. Especially, those entities comprising prominent astrocytic inclusion pathology, such as PSP or CBD, attract interest to address these questions.

As synaptic reductions in tauopathies are incompletely characterized (30) (preprint: Holland et al. 2020, medRxiv: 2020.01.24.20018697), we examined synapse alterations in PSP and CBD brains in this study. In addition to morphometric assessments of synapse densities in the frontal cortex and striatal regions of deceased individuals, we integrated the extent of neuropathological traits to elaborate cell type-differentiated contributions. Further, we found a spatial dependency of synapse densities from pTau+ astrocytes. Thereby, for the first time, our work stresses the pivotal role of astrocytes in maintaining tripartite synapse stability in CBD and confirms a substantial synapse loss in PSP with only minor associations with astrocytic, neuronal, or oligodendroglial pathology.

In general, cognitive decline or motor symptoms might be attributed to (i) synaptic dysfunction occurring primarily on a sub-synaptic level with only minor morphological synaptic degradation or (ii) to co-occurring synaptic dysfunction and structural depletion (5, 26, 46).

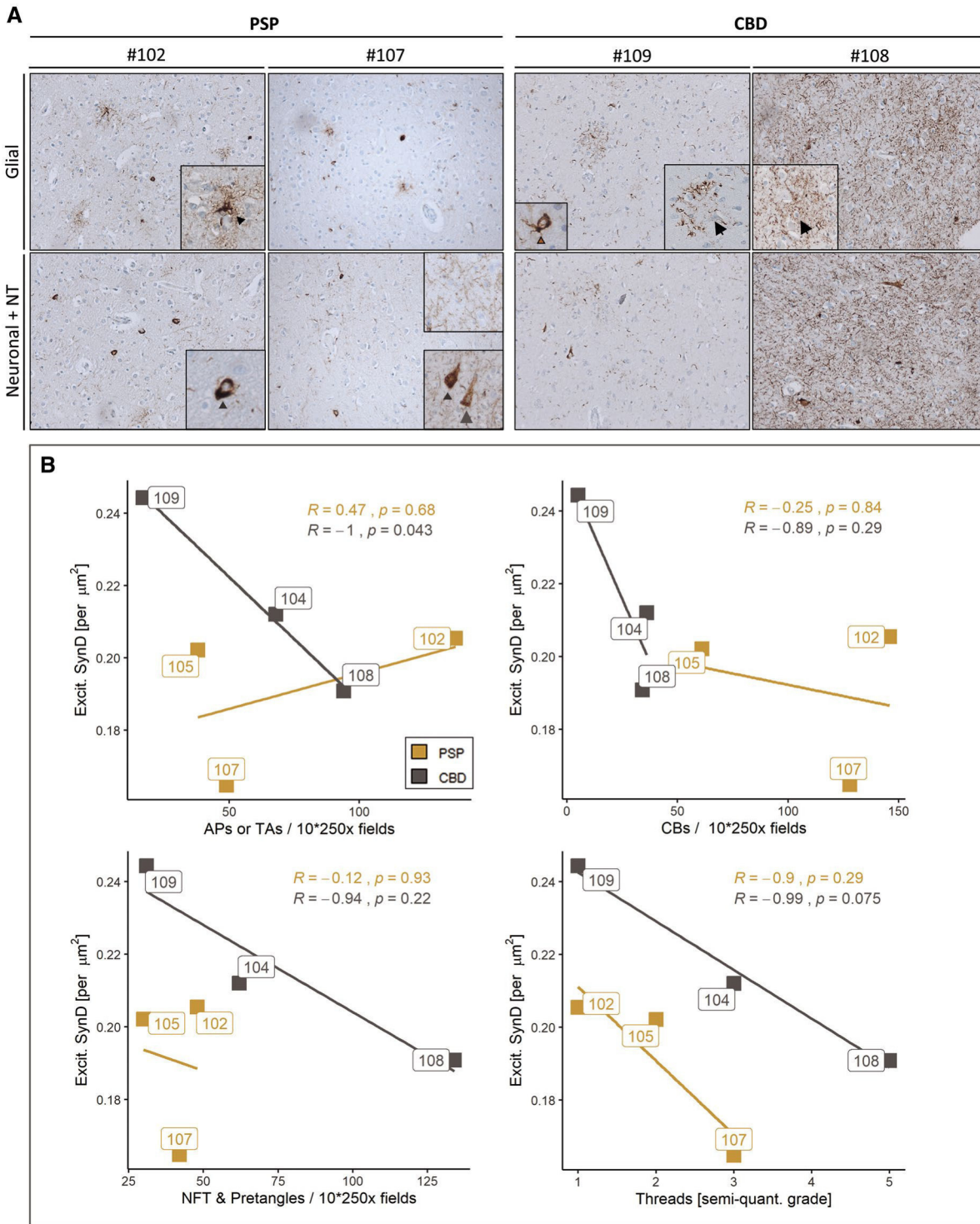


FIGURE 2 Synapse densities correlate with the occurrence of APs but not TAs in the frontal cortex. (a) Diverse AT8 inclusion pathology in fCtx of investigated PSP and CBD cases visualized by immunohistochemistry using the AT8 antibody. Representative light microscopy images depicting the extent of AT8+ cell type-assigned neuropathology in those two PSP cases (left panel) and those two CBD cases (right panel) with the highest synapse counts (left column of each panel) and lowest synapse counts (right column of each panel). Insets depict particular AT8 traits of affected brain cell types. The upper row shows glial pathology with TA (arrowhead), APs (arrow), and a CB (brown arrow); the lower row depicts neuronal pathology including pretangles (grey arrowhead), NFTs (grey arrow), together with NT of varying degrees. (b) In the fCtx the density of synapses correlates with neuropathological traits present in CBD (APs, trending with NT/threads), but not with the assessed traits seen in PSP (TAs, NFT, CB, NT/threads). Correlation scatter plots for excitatory synapse density (“Excit. SynD,” synapses per μm^2 area) in the fCtx faceted by each of the assessed neuropathological traits: TAs and APs (upper left), CBs (upper right), NFTs and pretangles (lower left) as well as NTs (lower right). Color code indicates disease entity. Boxed labels show single case identifiers. Statistical results are expressed as Pearson’s *R* and respective decimal *p* values (see also Table 2). AP, astrocytic plaque; TA, tufted astrocyte

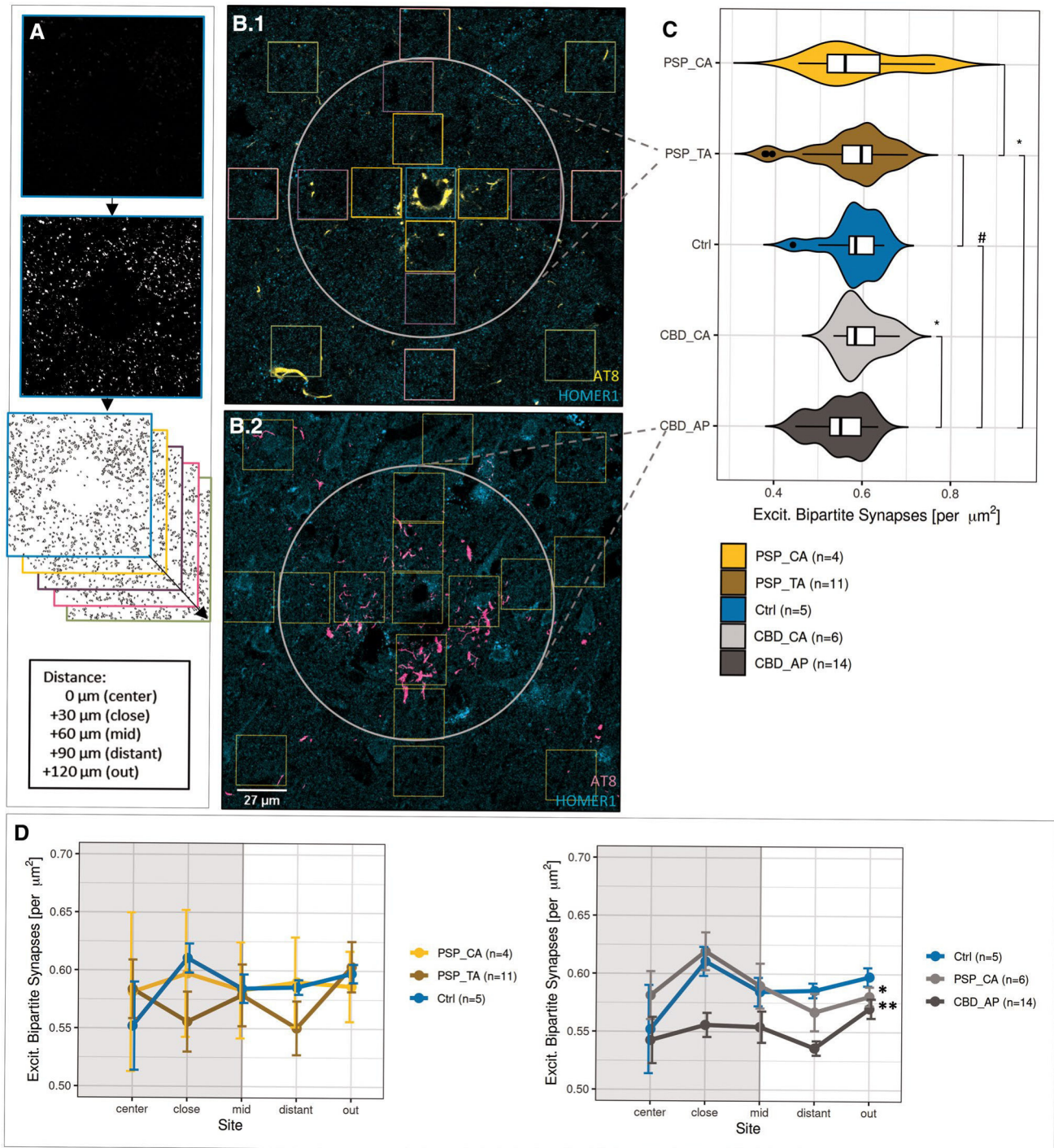


FIGURE 3 Synapse loss is associated with the territory of APs. (a) Workflow for evaluating astrocytic domain-associated synapse densities. Bins/ROIs (colored boxes in b) are placed at Sholl-like, concentric circles surrounding the astrocyte's core, while somatic targets of the HOMER1 antibody are excluded. Once extracted from the raw image, all bins belonging to one of the five distance representations from "center" to "out" were individually processed and subjected to puncta detection. Merged values of bins belonging to the same distance representation were positioned accordingly and the resulting sequence defined as "synapse distribution." (b) Exemplifying the image source for the analysis of domain-associated synapse density AT8 and HOMER1 in TAs in PSP (b.1) and APs in CBD cortices (b.2), where squares delineate bins to extract synapses from. The white circle delimits the astrocytic domain by a priori knowledge. Assignments were given as follows: "center" = light blue, "close" = orange, "mid" = purple, "distant" = pink, "out" = light green. (c) Reduced synapse density in the territory of APs. Combined box-violin plots depicting the synapse densities of only those bins, which were located within the ascribed astrocytic domain (white circle in b). Comparisons between TAs (golden yellow) / APs (dark grey) and internal AT8- control astrocytes (yellow, light grey) of the same condition or external AT8-controls (blue) of non-diseased control subjects. Boxplot description follows Figure 1a. *T*-test assuming normal distribution, where #: $p < 0.075$, * $p < 0.05$ and ns: "not significant". (d) Inherent differences among synapse density distributions within the domains of APs. Means of synapse densities are plotted against area representation assignment for TA and CA in PSP, AP, and CA in CBD and astrocytes in corresponding control cases (left: PSP, right: CBD). The extent of the presumed astrocytic domain is delimited as grey, boxed background. Results are expressed as \pm SEM, * $p < 0.05$, ** $p < 0.01$, two-way-ANOVA with Leven's testing for normality and Games-Howell post hoc test. CA, control astrocytes

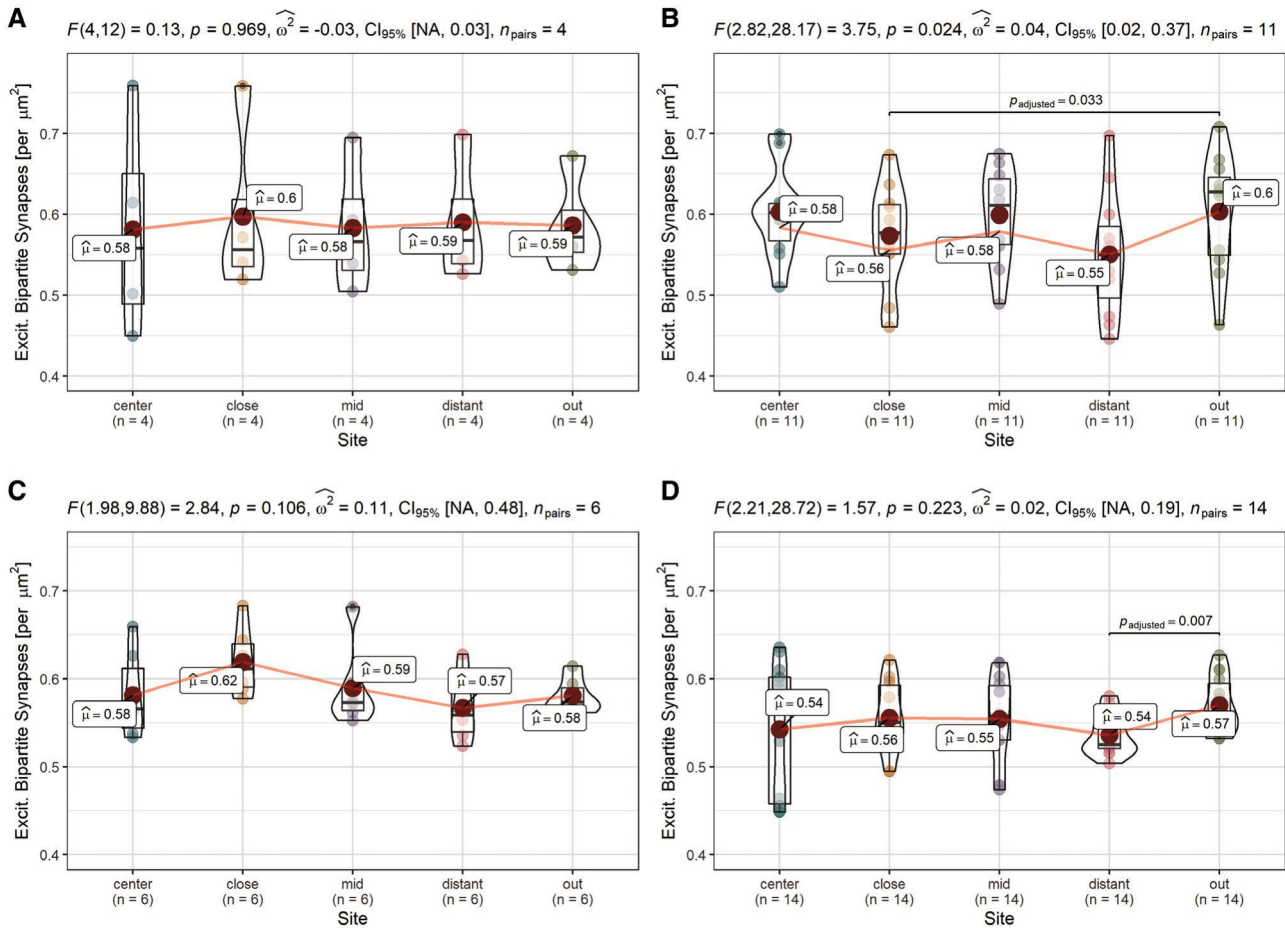


FIGURE 4 Altered synapse density distributions in domains of APs and TAs. Distribution analysis of single astrocyte cohorts shows unchanged distributions in domains of internal control astrocytes (PSP_CA/CBD_CA donors, AT8-) and significant differences in the overall distribution in CBD_APs, respective significant between-bin-differences to the outermost part around PSP_TAs and CBD_APs approximating a normal synapse density. (a–d) Pair-wise comparisons of synaptic density among predefined sites within cohorts of astrocyte classes in the fCtx of PSP and CBD subjects. PSP_CA (a), PSP_TA (b), CBD_CA (c), and CBD_AP (d). Graphs show combined box-violin plots. Small colored dots represent values of single domains at this site, while larger colored dots depict the calculated mean (mean values indicated as boxed labels). Boxed labels provide information on the mean (μ). Assuming a normal distribution, Fisher’s repeated measures one-way ANOVA was used to estimate F -values, p values, to determine the effect size (ω^2) and range of the confidence interval ($CI_{95\%}$) given a certain samples size (n), as indicated in the caption of each frame. T -testing with Holm–Sidak adjustment was applied for pairwise comparison. Adjusted p values of between-bin-comparisons are specified as decimals within each of the graphs

TABLE 4 Results of astrocytic domain analysis

Groups	Mean difference	Standard error	T -value	d.f.	p value	Upper limit	Lower limit
PSP_CA: PSP_TA	-0.013	0.016	0.593	31.836	0.975	0.051	-0.077
PSP_CA: Ctrl	-0.002	0.015	0.072	26.789	1.000	0.061	-0.064
PSP_TA: CBD_AP	-0.023	0.009	1.845	82.311	0.356	0.012	-0.057
PSP_TA: Ctrl	0.012	0.001	0.829	75.278	0.921	0.051	-0.028
CBD_CA : CBD_AP	-0.036	0.007	3.763	61.596	0.003**	-0.009	-0.063
CBD_CA: Ctrl	-0.002	0.008	0.131	50.205	1.000	0.032	-0.035
CBD_AP: Ctrl	0.034	0.007	3.273	45.153	0.017*	0.064	0.005

Note: Two-way-ANOVA with Games-Howell post hoc correction.

* $p < 0.05$; ** $p < 0.01$.

Abbreviations: AP, astrocytic plaque; CA, control astrocyte; Ctrl, control; d.f., degrees of freedom; TA, tufted astrocyte.

Our findings support the last-mentioned scenario for both PSP and CBD, as we observed reduced general, non-trait-associated synapse reductions in the PSP

cohort, while CBD cases exhibited such losses only in correlation with AP pathology or trending with NT. To our knowledge, any differentiation of synaptic losses

along with the human pathological astrocytic phenotype, as observed here, has not been shown yet. On the one hand, underestimating the actual effect in territories of PSP-typical TAs might be due to asymmetrical configuration and distribution of pTau accumulations within the astrocytic domain. On the other hand, this follows a biological notion, in which peripheral pTau deposits in CBD hinder AP astrocytes to sustain intracellular transport to their perivascular endfeet or perisynaptic processes, consequently impairing their neurosupportive functions. On the contrary, TAs being loaded with pTau aggregates more proximally, show only declines in synapse density in this soma-near part and rather normal levels in the remaining parts of their domains. This could be explained by differences in the distribution of transmembrane transporters or ion channels important for establishing microdomains (e.g. Ca^{2+} channels) along the astrocytic branches (31) and which might allow for compensating compartmentalized dysfunction to different extents between TAs and AP-astrocytes. In a pathogenetic model shared by TAs and APs, astrocytic tau uptake mechanisms comparable with those involving other potentially neurotoxic compounds to ensure extracellular milieu regulation could take place. Such have been postulated for different tau-species in a heparin-sulfate-dependent manner (29, 40) or in independent, rather unspecified mechanisms in the case of monomeric tau (37). Consequently, in an early phase the AP- or TA-in-progress might accumulate extracellular tau via suggested import molecules, deposit it as a less toxic aggregated form similar to NFTs and only at a later stage develop dysfunctional synapse support (2, 7, 11, 41).

Hence, another critical component of understanding pTau aggregates and their pathophysiological implications is the discrimination of several tau-species of hierarchical order (regarding their quaternary structures), phosphorylation patterns and other posttranslational modifications, which are thought to govern disease characteristics (6, 8, 10–12, 24, 45). To date, determined toxicity is less assigned to higher molecular aggregates such as sarkosyl-insoluble tau tangles (~1000 monomers) or filaments than rather to truncated, sarkosyl-soluble forms like oligomeric (~10–100) tau assemblies, which might precede in early tauopathy disease stages (2, 6, 24).

Since a toxic potential of pTau seems to be more evident in relation to APs than to TAs in our study, affected astrocytic subpopulations might be differentially vulnerable to intracellular pTau deposits. Alternatively, disease-determining cell-harming properties of astrocytic PSP- or CBD-pTau might underlie this observation. Indeed, PHF-seeding experiments with PSP and CBD brain extracts in wild-type mice showed strain-inherent characteristics in pTau propagation and cellular distribution, further suggesting a diagnostic and etiological separation of these tauopathies is appropriate and necessary (33).

Interestingly, as assessed in the first experiment general synaptic alterations in the CBD cohort were not statistically significant. Given the range of pTau+ cell load in the samples of this cohort in the subsequent correlation analysis, the pathology spread in #109 may not have progressed far enough to reveal a complete region-assigned synapse loss as detectable by the general synapse density analysis. Nevertheless, a decline was already evident in the synaptic islands of APs in this case, potentially indicating a stage of beginning synaptotoxicity associated with astrocytic pTau inclusions in CBD.

In respect of a vulnerability of synapses differentiated by their excitatory or inhibitory quality, described alterations in PSP argue against gliotransmission-determined favoring of either one of them. Thus, we assume similar mechanisms to take action in tau-mediated synaptic deprivation in excitatory as in inhibitory synapses in this disease. Besides this, we did not observe major synaptic derangements in the striatal regions, although inhibitory presynapses were more frequent in this region in PSP brains compared with controls, suggestive of a potential compensation of synaptic dysfunction.

However, it should be noted, that we primarily focused on cases with abundant pTau pathology in the frontal cortex — a rather rare condition in PSP — and without co-pathology (20). We relied on the availability of archival, non-embedded brain tissue for free-floating immunofluorescent staining to allow capturing a sufficient amount of synapses and astrocytic domains in thicker (50 μm) sections. Given the marked synapse loss evident in PET- as well as biochemical studies of brains from FTD patients (5) (preprint: Holland et al. 2020, medRxiv: 2020.01.24.20018697), we expected a considerable effect size for synaptic alterations. Therefore, our analysis included only a selected subset of PSP and CBD cases.

In review, this study sets out cellular contributors to synaptic loss in the primary 4R-tauopathies PSP and CBD, suggesting astrocyte-mediated synapse loss and the overall pTau pathology as an attribute for general synapse reductions in PSP. Therefore, this study identifies a potential cellular therapeutic target in CBD and emphasizes the usefulness of differentiated pathogenetic and diagnostic considerations regarding these tauopathies. For complementing, our current understanding of the pathogenesis of these diseases, follow-up studies are needed to validate the neuropathological traits as predictors of synaptic, i.e. factual cognitive impairments in suitable disease models and in larger cohorts of human individuals.

5 | CONCLUSIONS

Astrocytes as mediators of synaptic transmission and as indicators of pTau inclusion pathology were investigated



in the context of the 4R-tauopathies PSP and CBD. Here, we present evidence for synapse loss associated with APs, the neuropathological hallmark of CBD. In PSP the effects of TA pTau to indicate synapse loss remain behind the impact of the overall pathology. These results implicate pTau-affected astroglia as contributors to the pathophysiology of synapse loss rather in CBD than in PSP, which is suggestive of cognitive dysfunction in affected patients.

ACKNOWLEDGEMENTS

We thank all patients and their families for enabling research with primary human brain tissue. We thank all members of the *Neurobiobank Munich* for their structural and conceptual support, Dr. C. Sgobio for valuable input and reading the manuscript, J. M. Luque, T. Blume, K. Ochs, and Dr. O. Windl for fruitful discussions, Dr. N. Buresch and M. Schmidt for their excellent technical support as well as Prof. Dr. A. Danek and PD Dr. J. Levin for professional input from neurological specialists' view. This project was funded by the Munich Cluster of Systems Neurology (SyNergy; project ID EXC 2145 / ID 390857198), LMU Munich, Munich, Germany. All authors are affiliated with the University Hospital Munich, Germany. NB, KP, TA, and JH are affiliated with the German Center for Neurodegenerative Diseases. NB holds a scholarship from the German Academic Scholarship Foundation, KP is funded by the Marie Skłodowska-Curie actions grant, ITN SynDegen (721802).

ETHICS APPROVAL

Collection and distribution of human brain tissue obtained from the Neurobiobank Munich (NBM) respected the principles of informed consent, along with the Code of Conduct established by the BrainNet Europe (23) and were in accordance with the guidelines of the Ethics Committee of the LMU Munich (registration code: 345-13) and with the 1964 Helsinki Declaration and its later amendments or comparable ethical standards. Prior to death, all individuals donating to the NBM had agreed for autopsy and usage of brain samples in the interest of biomedical research. All cases were double-pseudonymized in order to account for personal privacy. All experiments of this study were approved by this committee (registration code: 19-442 KB).

CONFLICT OF INTEREST

The authors declare that they have no competing interests.

AUTHOR CONTRIBUTIONS

All authors contributed to the study conception and design. Material preparation, data collection and analysis were performed by NB and KP. The first draft of the manuscript was written by NB and all authors commented on previous versions of the manuscript. All authors read and approved the final manuscript.

DATA AVAILABILITY STATEMENT

Scripts for pre-processing and quantifying synaptic puncta images are available on GitHub (<https://github.com/nes-b/AstSyns>). Raw data that support the findings of this study are available from the corresponding author upon request.

ORCID

Nils Briel  <https://orcid.org/0000-0002-4349-3277>

REFERENCES

- Ahmed Z, Cooper J, Murray TK, Garn K, McNaughton E, Clarke H, et al. A novel in vivo model of tau propagation with rapid and progressive neurofibrillary tangle pathology: the pattern of spread is determined by connectivity, not proximity. *Acta Neuropathol.* 2014;127:667–83.
- Berger Z, Roder H, Hanna A, Carlson A, Rangachari V, Yue M, et al. Accumulation of pathological tau species and memory loss in a conditional model of tauopathy. *J Neurosci.* 2007;27:3650–62.
- Bernardinelli Y, Randall J, Janett E, Nikonenko I, König S, Jones EV, et al. Activity-dependent structural plasticity of perisynaptic astrocytic domains promotes excitatory synapse stability. *Curr Biol.* 2014;24:1679–88.
- Bigio EH, Brown DF, White CL. Progressive supranuclear palsy with dementia: cortical pathology. *J Neuropathol Exp Neurol.* 1999;58:359–64.
- Bigio EH, Vono MB, Satumtira S, Adamson J, Sontag E, Hynan LS, et al. Cortical synapse loss in progressive supranuclear palsy. *J Neuropathol Exp Neurol.* 2001;60:403–10.
- Castillo-Carranza DL, Gerson JE, Sengupta U, Guerrero-Muñoz MJ, Lasagna-Reeves CA, Kaye R. Specific targeting of tau oligomers in Htau mice prevents cognitive impairment and tau toxicity following injection with brain-derived tau oligomeric seeds. *J Alzheimer's Dis.* 2014;40:S97–111.
- Corbett GT, Wang Z, Hong W, Colom-Cadena M, Rose J, Liao M, et al. PrP is a central player in toxicity mediated by soluble aggregates of neurodegeneration-causing proteins. *Acta Neuropathol.* 2019;139:503–26.
- Cripps D, Thomas SN, Jeng Y, Yang F, Davies P, Yang AJ. Alzheimer disease-specific conformation of hyperphosphorylated paired helical filament-Tau is polyubiquitinated through Lys-48, Lys-11, and Lys-6 ubiquitin conjugation. *J Biol Chem.* 2006;281:10825–38.
- Dickson DW, Bergeron C, Chin SS, Duyckaerts C, Horoupian D, Ikeda K, et al. Office of rare diseases neuropathologic criteria for corticobasal degeneration. *J Neuropathol Exp Neurol.* 2002;61:935–46.
- Ferrer I, López-González I, Carmona M, Arregui L, Dalfó E, Torrejón-Escribano B, et al. Glial and neuronal tau pathology in tauopathies. *J Neuropathol Exp Neurol.* 2014;73:81–97.
- Fox LM, William CM, Adamowicz DH, Pitstick R, Carlson GA, Spires-Jones TL, et al. Soluble tau species, not neurofibrillary aggregates, disrupt neural system integration in a tau transgenic model. *J Neuropathol Exp Neurol.* 2011;70:588–95.
- Goedert M. The ordered assembly of tau is the gain-of-toxic function that causes human tauopathies. *Alzheimer's Dement.* 2016;12:1040–50.
- Goedert M, Eisenberg DS, Crowther RA. Propagation of tau aggregates and neurodegeneration. *Annu Rev Neurosci.* 2017;40:189–210.
- Halassa MM, Fellin T, Haydon PG. The tripartite synapse: roles for gliotransmission in health and disease. *Trends Mol Med.* 2007;13:54–63.
- Halassa MM, Fellin T, Takano H, Dong J-H, Haydon PG. Synaptic islands defined by the territory of a single astrocyte. *J Neurosci.* 2007;27:6473–7.

16. Hauw JJ, Daniel SE, Dickson D, Horoupian DS, Jellinger K, Lantos PL, et al. Preliminary NINDS neuropathologic criteria for steele-richardson-olszewski syndrome (progressive supranuclear palsy). *Neurology*. 1994;44:2015–9.
17. Heller JP, Rusakov DA. Morphological plasticity of astroglia: understanding synaptic microenvironment. *Glia*. 2015;63:2133–51.
18. Höglinger GU, Respondek G, Stamelou M, Kurz C, Josephs KA, Lang AE, et al. Clinical diagnosis of progressive supranuclear palsy: the movement disorder society criteria. *Mov Disord*. 2017;32:853–64.
19. Jackson JS, Witton J, Johnson JD, Ahmed Z, Ward M, Randall AD, et al. Altered synapse stability in the early stages of tauopathy. *Cell Rep*. 2017;18:3063–8.
20. Jecmenica Lukic M, Kurz C, Respondek G, Grau-Rivera O, Compta Y, Gelpi E, et al. Copathology in progressive supranuclear palsy: does it matter? *Mov Disord*. 2020;35:984–93.
21. Kaniyappan S, Chandupatla RR, Mandelkow EM, Mandelkow E. Extracellular low-n oligomers of tau cause selective synaptotoxicity without affecting cell viability. *Alzheimer's Dement*. 2017;13:1270–91.
22. Kim SK, Nabekura J, Koizumi S. Astrocyte-mediated synapse remodeling in the pathological brain. *Glia*. 2017;65:1719–27.
23. Klioueva NM, Rademaker MC, Dexter DT, Al-Sarraj S, Seilhean D, Streichenberger N, et al. BrainNet Europe's code of conduct for brain banking. *J Neural Transm*. 2015;122:937–40.
24. Lasagna-Reeves CA, Castillo-Carranza DL, Sengupta U, Sarmiento J, Troncoso J, Jackson GR, et al. Identification of oligomers at early stages of tau aggregation in Alzheimer's disease. *FASEB J*. 2012;26:1946–59.
25. Liddel SA, Guttenplan KA, Clarke LE, Bennett FC, Bohlen CJ, Schirmer L, et al. Neurotoxic reactive astrocytes are induced by activated microglia. *Nature*. 2017;541:481–7.
26. Lipton AM, Munro Cullum C, Satumtira S, Sontag E, Hynan LS, White CL, et al. Contribution of asymmetric synapse loss to lateralizing clinical deficits in frontotemporal dementias. *Arch Neurol*. 2001;58:1233–9.
27. Litvan I, Hauw JJ, Bartko JJ, Lantos PL, Daniel SE, Horoupian DS, et al. Validity and reliability of the preliminary NINDS neuropathologic criteria for progressive supranuclear palsy and related disorders. *J Neuropathol Exp Neurol*. 1996;55:97–105.
28. Mackenzie IRA, Neumann M, Bigio EH, Cairns NJ, Alafuzoff I, Kril J, et al. Nomenclature and nosology for neuropathologic subtypes of frontotemporal lobar degeneration: an update. *Acta Neuropathol*. 2010;119:1–4.
29. Martini-Stoica H, Cole AL, Swartzlander DB, Chen F, Wan Y-W, Bajaj L, et al. TFEB enhances astroglial uptake of extracellular tau species and reduces tau spreading. *J Exp Med*. 2018;215:2355–77.
30. Metaxas A, Thygesen C, Briting SRR, Landau AM, Darvesh S, Finsen B. Increased inflammation and unchanged density of synaptic vesicle glycoprotein 2A (SV2A) in the postmortem frontal cortex of Alzheimer's disease patients. *Front Cell Neurosci*. 2019;13:538.
31. Montagna E, Crux S, Luckner M, Herber J, Colombo AV, Marinković P, et al. In vivo Ca²⁺ imaging of astrocytic microdomains reveals a critical role of the amyloid precursor protein for mitochondria. *Glia*. 2019;67:985–98.
32. Murai KK, Pasquale EB. Eph receptors and ephrins in neuron-astrocyte communication at synapses. *Glia*. 2011;59:1567–78.
33. Narasimhan S, Guo JL, Changolkar L, Stieber A, McBride JD, Silva LV, et al. Pathological tau strains from human brains recapitulate the diversity of tauopathies in nontransgenic mouse brain. *J Neurosci*. 2017;37:11406–23.
34. Oberheim NA, Takano T, Han X, He W, Lin JHC, Wang F, et al. Uniquely hominid features of adult human astrocytes. *J Neurosci*. 2009;29:3276–87.
35. Oberheim NA, Wang X, Goldman S, Nedergaard M. Astrocytic complexity distinguishes the human brain. *Trends Neurosci*. 2006;29:547–53.
36. Papouin T, Dunphy J, Tolman M, Foley JC, Haydon PG. Astrocytic control of synaptic function. *Philos Trans R Soc B Biol Sci*. 2017;372:20160154. <https://doi.org/10.1098/rstb.2016.0154>.
37. Perea JR, López E, Diez-Ballesteros JC, Ávila J, Hernández F, Bolós M. Extracellular monomeric tau is internalized by astrocytes. *Front Neurosci*. 2019;13:442.
38. Piacentini R, Li Puma DD, Mainardi M, Lazzarino G, Tavazzi B, Arancio O, et al. Reduced gliotransmitter release from astrocytes mediates tau-induced synaptic dysfunction in cultured hippocampal neurons. *Glia*. 2017;65:1302–16.
39. Pickett EK, Henstridge CM, Allison E, Pitstick R, Pooler A, Wegmann S, et al. Spread of tau down neural circuits precedes synapse and neuronal loss in the rTgTauEC mouse model of early Alzheimer's disease. *Synapse*. 2017;71:1–8.
40. Rauch JN, Chen JJ, Sorum AW, Miller GM, Sharf T, See SK, et al. Tau internalization is regulated by 6-O sulfation on heparan sulfate proteoglycans (HSPGs). *Sci Rep*. 2018;8:1–10.
41. Santacruz K, Lewis J, Spire T, Paulson J, Kotilinek L, Ingelsson M, et al. Tau suppression in a neurodegenerative mouse model improves memory function. *Science*. 2005;309:476–81.
42. Sidoryk-Wegrzynowicz M, Gerber YN, Ries M, Sastre M, Tolkovsky AM, Spillantini MG. Astrocytes in mouse models of tauopathies acquire early deficits and lose neurosupportive functions. *Acta Neuropathol Commun*. 2017;5:89.
43. Stogsdill JA, Ramirez J, Liu D, Kim YH, Baldwin KT, Enustun E, et al. Astrocytic neurotrophins control astrocyte morphogenesis and synaptogenesis. *Nature*. 2017;551:192–7.
44. Sun X-D, Li L, Liu F, Huang Z-H, Bean JC, Jiao H-F, et al. Lrp4 in astrocytes modulates glutamatergic transmission. *Nat Neurosci*. 2016;19:1010–8.
45. Taniguchi-Watanabe S, Arai T, Kametani F, Nonaka T, Masuda-Suzukake M, Tarutani A, et al. Biochemical classification of tauopathies by immunoblot, protein sequence and mass spectrometric analyses of sarkosyl-insoluble and trypsin-resistant tau. *Acta Neuropathol*. 2016;131:267–80.
46. Terry RD, Masliah E, Salmon DP, Butters N, Deteresa R, Hill R, et al. Physical basis of cognitive alterations in Alzheimer's disease: synapse loss is the major correlate of cognitive impairment. *Annals Neur*. 1991;2004:572–80.
47. Wagner J, Krauss S, Shi S, Ryazanov S, Steffen J, Miklitz C, et al. Reducing tau aggregates with anle138b delays disease progression in a mouse model of tauopathies. *Acta Neuropathol*. 2015;130:619–31.
48. Yoshida M. Astrocytic inclusions in progressive supranuclear palsy and corticobasal degeneration. *Neuropathology*. 2014;34:555–70.
49. Yoshiyama Y, Higuchi M, Zhang B, Huang SM, Iwata N, Saido TCC, et al. Synapse loss and microglial activation precede tangles in a P301S tauopathy mouse model. *Neuron*. 2007;53:337–51.

SUPPORTING INFORMATION

Additional supporting information may be found online in the Supporting Information section.

How to cite this article: Briel N, Pratsch K, Roeber S, Arzberger T, Herms J. Contribution of the astrocytic tau pathology to synapse loss in progressive supranuclear palsy and corticobasal degeneration. *Brain Pathology*. 2021;31:e12914. <https://doi.org/10.1111/bpa.12914>

6. *Paper II*

Single-Nucleus Chromatin Accessibility Profiling Highlights Distinct Astrocyte Signatures in Progressive Supranuclear Palsy and Corticobasal Degeneration

AUTHORS

Nils Briel^{1,2,3}

Viktoria C Ruf¹

Katrin Pratsch^{1,2}

Sigrun Roeber¹

Jeannine Widmann¹

Janina Mielke¹

Mario M Dorostkar¹

Otto Windl¹

Thomas Arzberger^{1,2,5}

Jochen Herms^{1,2,4 *}

Felix L Struebing^{1,2 *}

* These authors contributed equally

1. Center for Neuropathology and Prion Research, Ludwig-Maximilians-University, Feodor-Lynen-Str. 23, 81377 Munich, Germany
2. German Center for Neurodegenerative Diseases, Feodor-Lynen-Str. 17, 81377 Munich, Germany
3. Munich Medical Research School, Ludwig-Maximilians-University, Faculty of Medicine, Bavariaring 19, 80336 Munich, Germany
4. Munich Cluster of Systems Neurology (SyNergy), Feodor-Lynen-Str. 17, 81377 Munich, Germany
5. Department of Psychiatry and Psychotherapy, University Hospital Munich, Ludwig-Maximilians-University, Nussbaumstr. 7, 80336 Munich, Germany

This work is published in: *Acta Neuropathol* 144, 615–635 (2022). <https://doi.org/10.1007/s00401-022-02483-8>. PMID: 35976433. PMCID: PMC9468099.

Supplementary material is available online at: <https://link.springer.com/article/10.1007/s00401-022-02483-8#Sec23>



Single-nucleus chromatin accessibility profiling highlights distinct astrocyte signatures in progressive supranuclear palsy and corticobasal degeneration

Nils Briel^{1,2,3} · Viktoria C. Ruf¹ · Katrin Pratsch^{1,2} · Sigrun Roeber¹ · Jeannine Widmann¹ · Janina Mielke¹ · Mario M. Dorostkar¹ · Otto Windl¹ · Thomas Arzberger^{1,2,5} · Jochen Herms^{1,2,4} · Felix L. Struebing^{1,2}

Received: 15 June 2022 / Revised: 3 August 2022 / Accepted: 8 August 2022 / Published online: 17 August 2022

© The Author(s) 2022

Abstract

Tauopathies such as progressive supranuclear palsy (PSP) and corticobasal degeneration (CBD) exhibit characteristic neuronal and glial inclusions of hyperphosphorylated Tau (pTau). Although the astrocytic pTau phenotype upon neuropathological examination is the most guiding feature in distinguishing both diseases, regulatory mechanisms controlling their transitions into disease-specific states are poorly understood to date. Here, we provide accessible chromatin data of more than 45,000 single nuclei isolated from the frontal cortex of PSP, CBD, and control individuals. We found a strong association of disease-relevant molecular changes with astrocytes and demonstrate that tauopathy-relevant genetic risk variants are tightly linked to astrocytic chromatin accessibility profiles in the brains of PSP and CBD patients. Unlike the established pathogenesis in the secondary tauopathy Alzheimer disease, microglial alterations were relatively sparse. Transcription factor (TF) motif enrichments in pseudotime as well as modeling of the astrocytic TF interplay suggested a common pTau signature for CBD and PSP that is reminiscent of an inflammatory immediate-early response. Nonetheless, machine learning models also predicted discriminatory features, and we observed marked differences in molecular entities related to protein homeostasis between both diseases. Predicted TF involvement was supported by immunofluorescence analyses in postmortem brain tissue for their highly correlated target genes. Collectively, our data expand the current knowledge on risk gene involvement (e.g., *MAPT*, *MAPK8*, and *NFE2L2*) and molecular pathways leading to the phenotypic changes associated with CBD and PSP.

Keywords Progressive supranuclear palsy · Corticobasal degeneration · Tauopathy · snATAC-seq · Astrocytes · Neurodegeneration

Abbreviations

(bv)FTD	(Behavioral variant) frontotemporal dementia
(q)PCR	(Quantitative) polymerase chain reaction
AD	Alzheimer's disease
ALS	Amyotrophic lateral sclerosis

ARTAG	Aging-related Tau-astrogliopathy
Ast	Astrocytes
ATAC-seq	Assay for transposase-accessible chromatin using sequencing
BH	Benjamini–Hochberg
bp	Base pairs
BP	Biological process

Jochen Herms and Felix L. Struebing contributed equally.

✉ Jochen Herms
Jochen.Herms@med.uni-muenchen.de

✉ Felix L. Struebing
Felix.Struebing@med.uni-muenchen.de

¹ Center for Neuropathology and Prion Research, University Hospital Munich, Ludwig–Maximilians–University, Feodor-Lynen-Str. 23, 81377 Munich, Germany

² German Center for Neurodegenerative Diseases, Feodor-Lynen-Str. 17, 81377 Munich, Germany

³ Munich Medical Research School, Faculty of Medicine, Ludwig–Maximilians–University, Bavariaring 19, 80336 Munich, Germany

⁴ Munich Cluster of Systems Neurology (SyNergy), Feodor-Lynen-Str. 17, 81377 Munich, Germany

⁵ Department of Psychiatry and Psychotherapy, University Hospital Munich, Ludwig–Maximilians–University, Nussbaumstr. 7, 80336 Munich, Germany

CBD	Corticobasal degeneration
CBS	Corticobasal syndrome
CC	Cellular compartment
CMA	Chaperon-mediated autophagy
CRE	<i>cis</i> -Regulatory element
CTSD	Cathepsin D
DAR	Differentially accessible region
DEG	Differentially expressed gene
DLN	Deep-layer neurons
DNA	Desoxyribonucleic acid
Exc.	Excitatory
FDR	False discovery rate
GA	Gene accessibility
Gb	Giga bases
GEM	Gel-bead in emulsion
GO	Gene ontology
GSEA	Gene-set enrichment analysis
GWAS	Genome-wide association study
Inh.	Inhibitory
LB(D)	Lewy body (dementia)
Lime	Local interpretable model-agnostic explanations
Log2-FC	Binary logarithm fold-change
MAP(3)K8	Mitogen-activated protein (3) kinase 8
MAPT	Microtubule-associated protein Tau
MF	Molecular function
Mic	Microglia
ML	Machine learning
MND	Motor neuron disease
MSA	Multiple system atrophy
NFT	Neurofibrillary tangles
Oli	Oligodendrocytes
OPC	Oligodendrocytic precursor cells
PART	Primary aging-related tauopathy
PD	Parkinson disease
PMI	<i>Postmortem</i> Interval
PSP(-RS)	Progressive supranuclear palsy-(Richardson syndrome)
pTau	Hyperphosphorylated tau
RAP	Regulon activity profile
RNA-seq	Ribonucleotide acid sequencing
RTN	Reconstruction of transcriptional regulatory networks
sn*	Single nuclei
SNP	Single nucleotide polymorphism
TA	Tufted astrocyte
TF(M)(E)	Transcription factor (motif) (enrichment)
ULN	Upper-layer neurons
UMAP	Uniform manifold approximation and projection
UPR	Unfolded protein response
UPS	Ubiquitin proteasome system
XGB	Extreme gradient boosting

Introduction

Most neurodegenerative disorders are characterized by misfolded, intracellular protein aggregates that can disrupt neuronal and glial homeostasis. Among these, tauopathies represent a group of diseases in which deposits of hyperphosphorylated tau (pTau) protein can be seen upon neuropathological examination [25]. Examples of tauopathies are Alzheimer's disease (AD) and Progressive Supranuclear Palsy (PSP) as well as the less common Corticobasal Degeneration (CBD). Because clinical symptoms of those three diseases can overlap, definite diagnosis requires postmortem neuropathological examination [2, 38, 64]. Besides the distribution pattern of pTau inclusions throughout the central nervous system, two histological features are used to distinguish tauopathies: affected cell types and the immunohistochemical ratio of isoform-specific Tau antibodies [18, 64].

In regard to the latter, the Tau harboring gene *MAPT*, located on chromosome 17q21.23, gives rise to six isoforms by differential splicing involving exons 2, 3, and 10 [18, 21]. The microtubule-binding domain, consisting of 3 or 4 repeats (3R/4R) depending on inclusion of exon 10, not only defines the affinity of Tau to microtubules, but also its aggregation properties [25]. While AD can be regarded a mixed 3R/4R tauopathy, 4R isoforms predominate in PSP and CBD. As for affected cell types, AD, PSP, and CBD all share neuronal pTau inclusions such as neurofibrillary tangles or neuropilic threads. Glial inclusions are rare in AD, but common in CBD or PSP [16]. The most prominent immunoreactive feature to discriminate PSP from CBD is the astrocytic pTau phenotype: with tufted astrocytes (TA) being a hallmark for PSP and astrocytic plaques (AP) for CBD as shown in Fig. 1 [11, 38, 64].

Postmortem transcriptome studies can help in identifying disease-associated signatures and, when performed in single-cell resolution, even quantify the degree of cell type-specific involvement. This has been achieved primarily in the context of AD, and through integration of multiple “omics” studies such as single-cell and genome-wide association studies (GWAS), it is now believed that microglia are key players in AD pathogenesis [22, 40, 46, 54]. This insight is already being translated in a therapeutic context, with studies underway that seek to restore microglial fitness [26]. In contrast, postmortem “omics”-studies are sparse in PSP and CBD [1, 7, 22, 24, 34], and to date non-existent in single-cell resolution.

The lack of cell type-resolved molecular data for PSP and CBD compelled us to perform this study. We hypothesized that their neuropathological phenotype would be mirrored by molecular changes in specific cell types, and we wondered whether we could find molecular features

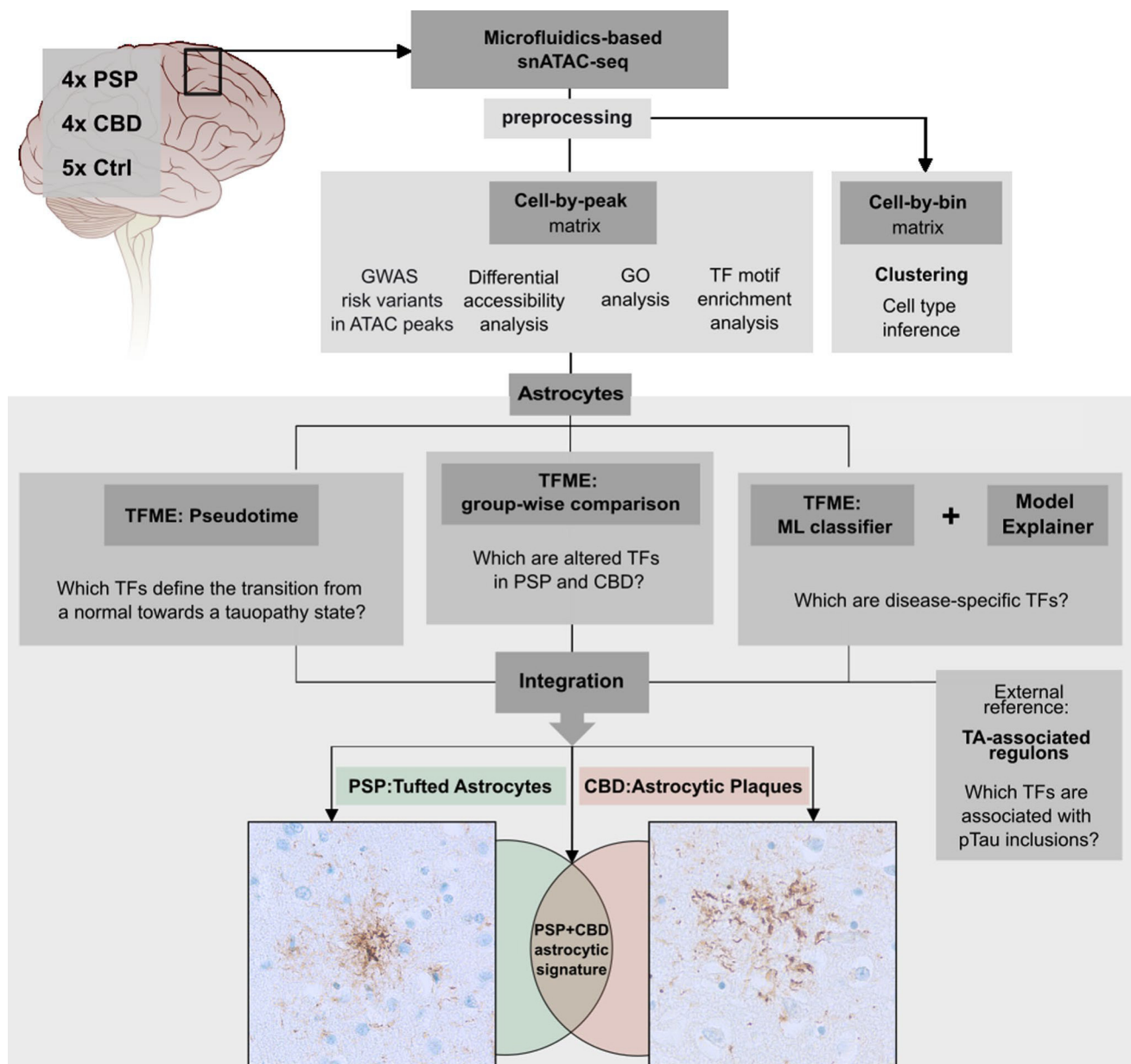


Fig. 1 Concept of the bioinformatical analysis. SnATAC-sequencing was applied to snap-frozen frontal cortex samples from deceased PSP, CBD, and Ctrl individuals. Raw sequencing reads were pre-processed and resulting matrices were then used (i) for graph-based clustering and cell type inference (using a binned genome), and (ii) for GWAS risk variant-association with cell types, differential accessibility analysis and GO, as well as TF-motif analysis (using the peak matrix). Downstream, only the astrocytic cluster was investigated (boxed lower part). To find significantly altered TFs in tauopathy-derived astrocytes, disease-wise comparisons of TFME were conducted (mid panel). TFME changes along pseudotime trajectories were assessed to identify TFs linked with pathogenesis (left). An ML-based disease classifier was utilized to delineate disease-specific

TFs in a more unbiased approach (right). Significant results from these three branches were refined by a TF profile linked to the presence of astrocytic pTau inclusions in PSP (Tufted Astrocytes, TA). Finally, this multilayered regulon pattern was integrated to define a general astrocytic tauopathy TF signature, or entity-specific astrocytic TF signatures. These are presumed to mirror the neuropathological context of characteristic pTau inclusions in astrocytes, namely TA in PSP and AP in CBD. *AP* astrocytic plaque, *GO* gene ontology, *GWAS* genome wide association studies, *ML* machine learning, *pTau* hyperphosphorylated Tau, *TA* tufted astrocyte, *TFME* transcription factor motif enrichment. The brain illustration was modified from https://de.m.wikipedia.org/wiki/Datei:Brain_stem_normal_human.svg (CC-Attribution-2.5 License 2006)

that distinguished both diseases. We chose an epigenetic assay—the single-nucleus assay for transposase accessible chromatin sequencing (snATAC-seq) as compared to

a transcriptomic assay (snRNA-seq). The read-out of snATAC-seq corresponds to regions of open chromatin in the genome, and these are commonly associated with loci of

active transcription or epigenetic regulation [8, 33]. This assay relies on DNA instead of RNA as input material; hence, degradation of RNA, which is commonly associated with long postmortem intervals and agony phases, is not a cause of concern. Furthermore, since the coordinated expression of genes has been shown to be regulated by effects of transcription factors (TFs) on the compaction of chromatin [33, 60], altered TF dynamics might have an impact on pathogenesis in these diseases. This can be explored optimally with an open chromatin assay such as snATAC-seq. Direct TF effects are usually guided by DNA sequence motifs, so-called TF binding sites, which are located in non-coding *cis*-regulatory elements (CREs) like enhancers, silencers, or promoters [57]. Their interaction is perturbed in diseases with a complex genetic background [31], probably explaining the large contribution of non-coding mutations to pathogenesis. More precisely, mutations in CREs can affect TF binding dynamics to varying degrees [12]. Thus, viewed from a higher perspective, the TF interplay within a given cell type can be regarded as an integration point of genetic background, epigenetic information, and as effector of intra- and extracellular signaling pathways. Because TF binding sites within CREs outnumber genes and their transcripts by several orders of magnitude, the feature space is larger in snATAC-seq compared to snRNA-seq data, which can be leveraged for increased discriminatory power.

Figure 1 outlines our discovery-driven approach: first, we demonstrate the importance of astrocytes to CBD and PSP disease pathology by combining tauopathy-associated genes and GWAS risk variants with our data. Then we explore their transition into a tauopathy state via TF profiling. Incorporating separate analyses such as pseudotemporal imputations, group-wise comparisons of TF information, external data, and machine learning models, we ultimately attempt to delineate disease-specific astrocytic TF signatures in a comprehensive data integration part. To validate these findings, we finally detect protein expression alterations of highly correlated target genes in archival brain tissue of PSP and CBD cases using an immunofluorescent staining approach.

Materials and methods

Neuropathological assessment and case selection

The complete brain was prepared at autopsy. Hemispheres were treated differently: the left hemisphere was fixed in formalin for a duration of two weeks or longer before coronal slicing of 1 cm step size, while the right hemisphere was snap-frozen immediately. From the former, paraffin-embedded specimen sampled across the whole cerebrum, brain

stem, cerebellum, and spinal cord were used for diagnostic examination.

Cases (4 PSP, 4 CBD) and controls (5 Ctrl) were selected based on the amount of additional co-pathology and matched by age (PSP 72.8 ± 4.8 , CBD 56.5 ± 2.9 , Ctrl 69.4 ± 14), postmortem interval (PSP 41.2 ± 34.2 , CBD 33.8 ± 20.2 , Ctrl 26.2 ± 6.8), and sex (males, PSP = 50%, CBD = 50%, Ctrl = 60%) at its best (see Table 1). Ctrl cases were chosen based on the absence of neurologic or psychiatric disease history. Those Ctrl or tauopathy cases exhibiting substantial co-pathology (i.e., $A\beta_{42}$, α -synuclein, TDP-43, pTau (AT8), Aging-related Tau-Astroglialopathy (ARTAG), Primary Aging-related Tauopathy (PART), 3R Tau (RD3), or 4R Tau (RD4; in case of Ctrl)) in study-relevant regions were excluded.

Region of interest

Approximately 1 cm³-thick tissue blocks of grey and appending white matter were excised from snap-frozen coronal cerebral slices using a diamond band saw. The regions of interest were parts of the medial and superior frontal gyrus at the level of the anterior striatum (MFG, SFG) in the coronal view corresponding to Brodmann areas 6/8/9. The corresponding regions were sampled from the contralateral formalin-fixed hemisphere for validation studies.

Single-nucleus ATAC-sequencing

Nuclei preparation and quantification

To isolate nuclei, 200 mg of brain tissue was homogenized in 3.75 mL of chilled lysis buffer (10 mM Tris-HCl pH 8.0, 0.32 M sucrose, 0.34 mM DTT, 0.1 mM PMSF, 3 mM MgAc₂, 5 mM CaCl₂, 0.1 mM EDTA, 0.1% Igepal, and 1 protease inhibitor cocktail tablet (complete mini protease inhibitor cocktail, Roche Diagnostics, Mannheim, Germany) per 50 mL) using a Dounce homogenizer and transferred to 15 mL-ultracentrifugation tubes (Seton Open-top polyallomer centrifuge Tubes) with additional 2.25 mL lysis buffer. Homogenates were underlaid with 6.75 mL sucrose buffer (10 mM Tris-HCl, pH 8.0, 1.8 M sucrose, 0.34 mM DTT, 0.1 mM PMSF, 3 mM MgAc₂, and 1 protease inhibitor cocktail tablet per 50 mL) and centrifuged for 1 h at 24,000 rpm at 4 °C. The nuclei pellet was resuspended in 1 × nuclei buffer (10 × Genomics) and nuclei were quantified using a Neubauer haemocytometer.

Single nuclei partitioning and snATAC-Seq library construction

Single nuclei partitioning and subsequent snATAC-Seq library construction were performed using the

Table 1 Covariates of PSP, CBD, and Ctrl subjects

Case ID	Neuro-pathological diagnosis	Neuro-logical diagnosis (last ante mortem)	Age at death [years]	PMI [hours]	Sex	Disease duration [years]	Brain weight [g]	Tau isoform [#] [IHC: 4R/3R]	AGD (NFT)	Braak&Braak (NFT)	CERAD-plaque density	Thal-Phase	Aβ42 (4G8)	α-synuclein (Braak; LBs)	TDP-43	FUS
PSP1	PSP	PSP-RS	68	38	Male	6.0	1460	±	-	1	0	0	No	0	neg	neg
PSP2	PSP	PSP-ns	77	78	Female	2.5	1112	±	-	0	0	0	No	0	neg	neg
PSP3	PSP	PSP-ns	78	42	Male	9.0	NA	±	+	1	0	1*	Yes*	0	neg	neg
PSP4	PSP	bvFTD-tauopathy	68	7	Female	7.0	1005	±	-	0	0	0	No	0	neg	neg
CBD1	CBD	PSP-RS	52	14	Female	4.5	1260	±	-	0	0	0	No	0	neg	neg
CBD2	CBD	bvFTD	56	44	Male	2.5	NA	±	+	1	0	0	No	0	neg	neg
CBD3	CBD	bvFTD-CBS	59	23	Female	7.0	1220	±	-	1	-	1*	Yes*	0	pos	neg
CBD4	CBD	bvFTD-MIND	59	54	Male	1.5	1330	±	+	1	0	3*	Yes*	0	neg	neg
C1	Ctrl	-	58	22	Male	-	NA	-/-	-	1	-	0	-	0	pos	-
C2	Ctrl	-	82	27	Male	-	1230	-/-	-	2	-	1*	-	0	neg	neg
C3	Ctrl	-	86	20	Female	-	1035	-/-	-	1	-	0	-	0	-	-
C4	Ctrl	-	64	33	Female	-	NA	-/-	-	1	-	0	-	0	neg	neg
C5	Ctrl	-	53	29	Male	-	1792	-/-	-	0	-	2*	-	0	neg	neg

Aβ42 amyloid beta 42, AGD Argyrophilic Grain Disease, bvFTD behavioral variant Frontotemporal Dementia, CBS Corticobasal Syndrome, CERAD Consortium to Establish a Registry for Alzheimer's Disease, Ctrl control, IHC immunohistochemistry, LBs Lewy bodies, MND motor neuron disease, NA not assessable, neg negative, NFT neurofibrillary tangles, ns not specified, PMI postmortem interval, RS Richardson Syndrome. See also comprehensive data (Supplementary Data, T0, online resource)

[#]In study-relevant region. *No 4G8/Aβ42-positivity or Aβ-plaques in the study-relevant region

Chromium Next GEM Single Cell ATAC Reagent Kit v1.1 (10×Genomics, Pleasanton, CA, USA) according to the manufacturer's protocol. Briefly, following incubation with ATAC Enzyme for 1 h at 37 °C, nuclei were loaded onto a Chromium Next GEM Chip H for a targeted recovery of 5000 or 10,000 nuclei per PSP/CBD and Ctrl sample, respectively. After partitioning of the nuclei and DNA cleanup, sample indices were added, and double-sided size selection was performed. Finally, libraries were eluted in 20 µl Buffer EB (Qiagen, Hilden, Germany) and stored at –20 °C. Correct fragment size distribution of the libraries was checked via the Agilent Bioanalyzer System using an Agilent bioanalyzer High-sensitivity DNA chip (Agilent, Santa Clara, CA, USA). Library concentrations were determined using the KAPA library Quantification Kit for Illumina Platforms (Roche Diagnostics, Mannheim, Germany).

Sequencing of snATAC-seq libraries

Quantified and quality-controlled snATAC libraries were pooled at equimolar concentrations, denatured, and sequenced on an Illumina NovaSeq6000 platform according to the 10×Genomics sequencing requirements for single-indexed snATAC-Seq libraries, aiming at a minimum sequencing depth of 25,000 read pairs per nucleus.

Analysis of snATAC-seq data

The main bioinformatical workflow is illustrated in Fig. 1 and consists of 8 parts (a detailed description of bioinformatical analyses is included separately as a Supplementary Methods section, online resource). Initially, sequencing data were subjected to the 10×Genomics™ *cellranger-atac-1.2.0* pipeline and *Snaptools/SnapATAC* packages [14] for pre-processing and quality control (QC), respectively. Barcodes were filtered for mapping quality, fragment sizes, and correct alignment flags. *SnapATAC*'s representations of chromatin accessibility as either bins (equally sized genomic windows of 1,000 bp overlapping with sequenced DNA-fragments) or peaks (exact genomic ranges of cluster-aggregated DNA-fragments) were the basis for all downstream single-nucleus analyses. Gene accessibility (GA) as a surrogate of a gene's transcriptional activity was calculated as a *z* score-based metric in *SnapATAC* [14].

The cell-by-bin matrix was used for clustering (Supplementary Fig. 1, online resource) and barcode embedding using uniform manifold approximation and projection (UMAP) metrics. Technical covariates were identified, and batch effect correction applied to the primary UMAP embedding (Supplementary Figs. 1 and 2, online resource). Furthermore, graph-based cell type inference was conducted in the UMAP embedding, while RNA- and ATAC-seq data-derived marker gene lists from McKenzie et al. [41] and

Lake et al. [35] served as references (Supplementary Figs. 3 and 4, Supplementary Data, T01, online resource).

The cell-by-peak matrix was leveraged for identifying GWAS risk variants in ATAC peaks [28], differential gene accessibility analysis, gene ontology (GO) analysis, and TF motif enrichment (TFME) analysis. To assess cell type enrichment of GWAS risk variants, publicly available disease-specific GWAS [24, 34] summary statistics were downloaded from <https://www.ebi.ac.uk/gwas/> for PSP (Orphanet_683), CBD (Orphanet_278), AD (EFO_0000249), Frontotemporal Dementia (FTD, Orphanet_282), Parkinson Disease (PD, EFO_0002508), Multiple System Atrophy (MSA, EFO_1001050), Lewy Body Dementia (LBD, EFO_0006792), and Amyotrophic Lateral Sclerosis (ALS, EFO_0000253).

Quantification of alterations assigned to biological pathway terms was enabled by the *amiGO2* database (<http://amigo.geneontology.org/amigo/search/bioentity>) filtered for the terms 'chaperon-mediated autophagy' (CMA), ubiquitin–proteasome-system (UPS), and unfolded-protein-response (UPR) or 'microglial cell activation' in *Homo sapiens*.

The subsequent steps were exclusively conducted with the astrocytic cluster: first, we assessed group-wise differences of TFME using *Wilcoxon* rank-sum tests and the *Bonferroni* method to adjust for multiple hypothesis testing.

Employing the package *Cicero* [49], we constructed pseudotime trajectories on the re-embedded astrocyte cluster, which was filtered for Ctrl- and CBD-derived astrocytic nuclei. High TFME levels of an epigenetic indicator of astrocytic immaturity (i.e., the TF *EMX2*) served to define the origin of the trajectory. To evaluate GA and TFME changes along these trajectories, *tradeSeq* [3], its modeling framework, and *Wald*-test-based functions were used.

To identify features that are most distinctive in predicting the group entity (Ctrl, PSP, or CBD), a supervised machine learning (ML) algorithm called extreme gradient boosting tree (XGB) was trained on the astrocytic TFME. Train-test set splits consisted of 80% or 20% of the complete astrocytic population, respectively. The model's predictive performance was primarily measured by *overall accuracy* and *Cohen's kappa* in the test set; further classification performance indicators (e.g., sensitivity, specificity, negative and positive predictive values) were reported for a more detailed characterization. To interpret the model's predictive process and to weigh its input features (i.e., TFs) by their importance for a particular prediction, the ML explanation framework *Lime* was used [52].

We identified TFs associated with the classical neuropathological phenotype in PSP (tufted astrocyte, TA) by applying the *Reconstruction of Transcriptional Regulatory Networks*. To this end, we utilized a public transcriptomic data set derived from temporal cortices of 176 PSP cases [1].

Using gene-set enrichment analysis (GSEA), the inferred transcriptional regulatory network was integrated with differentially expressed genes as well as covariate-adjusted neuropathology-gene expression correlation coefficients, which both were reported in the original study. The unit of a given TF with all the genes regulated by it was termed *regulon*.

To ultimately distill a set of shared and disease-specific pTau-associated TF candidates, we integrated the results of all previous analyses. These multidimensional overlaps were visualized as upset plots.

The Supplementary Methods, online resource, offer a more detailed description of the bioinformatical workflow.

TF target gene validation—bioinformatics, immunofluorescence staining and data analysis

To retrieve the most important target genes of JUNB and TFEB TFs in this astrocyte dataset, correlations between TFME and the GA of all genes in the dataset were computed group-wise. Significant correlations in the Ctrl data were excluded in the following step to reduce false positive, thus unspecific findings. Next, potential target genes were ranked per disease by *BH*-adjusted *p* values and *Pearson R* before searching for genomic overlaps of *Cicero CRE* links and each specific gene locus (± 10 kb). Visual inspection of co-accessibility plots at highly correlated and overlapping gene loci guided identification of the top candidate genes.

Ten micrometer-thick sections were prepared from formalin-fixed paraffin-embedded brain samples of the MFG, which were deparaffinized with HistoClear (VWR Life science, #H103-4L) and rehydrated in descending ethanol series. Antigen retrieval was performed with 1× Sodium citrate solution, pH 6 in a pressure cooker for 20 min. Auto-fluorescence quenching/photobleaching was applied using 25,000 Lux LED lights for 2×45 min with slides submerged in quenching solution (4.5% H₂O₂ and 20 mM NaOH in 1X PBS). Blocking was performed with 5% Goat Serum (GS) and 0.3% Triton X-100 in 1X PBS. Primary antibodies raised in rabbit against the candidate gene products MAP3K8 (1:500, abcam, #ab137589), or CTSD (1:200, abcam, #ab75852) were incubated together with mouse anti-AT8 (1:500, ThermoFisher Scientific, #MN1020) and guinea pig anti-GFAP (in combination with MAP3K8, 1:500, SynapticSystems, #173,004) or chicken anti-GFAP (in combination with CTSD, 1:500, EMD Millipore AB5541), respectively, over night at 4 °C. After washing, secondary antibody incubation followed (1:1000, goat anti-guinea pig / anti-chicken AlexaFluor®488, anti-mouse AlexaFluor®568, anti-rabbit AlexaFluor®647) with an incubation period of 60 min. Finally, slides were covered with mounting medium containing DAPI (#S302380-2, Agilent Dako, Germany) and #1.5H high-precision imaging coverslips.

Images were acquired from the MFG cortex with a Leica Stellaris 5 confocal microscope. pTau + astrocytes were identified based on the prototypical morphology and cellular distribution of aggregates. TAs were defined by bush-like, soma-proximally arranged pTau conglomerate with processes of different thickness. APs were defined by corona-like, soma-distantly arranged fine pTau processes. Then, z-stacks were acquired, using an HC Plan Apochromat CS2 63x/NA 1.40 Oil objective (2048×2048 pixels, 181.93² μm height/width, 8–9 μm depth). Images were preprocessed including min and max pixel value cut-offs using custom macro scripts (see also GitHub repository).

Marker-positive (CTSD +, MAP3K8 +) and -negative astrocytes with detectable signal after standardized thresholding were counted using the *CellCounter* tool provided with ImageJ/Fiji. Ratios of GFAP + [Marker] + and GFAP^{only} + cells were compared with ratios of AT8 + (TA/AP) [Marker] + and AT8^{only} + cells.

General statement: computing environment and statistics

Preprocessing was run in RStudio Server with R3.6 and Python2.7 for Debian Server. The subsequent bioinformatical analysis including statistical testing was conducted within RStudio Desktop running on R3.6.3 (*SnapATAC*) and R4.0.4 (remaining analyses) for Linux (Ubuntu 20.04 LTS). To determine the applicability of hypothesis testing methods, the *Shapiro–Wilk* method was used to test for normal distributions. Consequently, *Welch's t*-test was used in normally distributed and *Wilcoxon's* rank-sum test in non-normally distributed populations. *Welch* and *Wilcoxon* tests were conducted as two-tailed versions, unless otherwise stated. For multiple comparison correction, the *BH* method to obtain the false discovery rate (FDR), or the *Bonferroni* method to report family-wise errors were applied to unadjusted *p* values. Significant distribution differences as estimated by the *tradeSeq*-gene models along pseudotime were determined based on their *Wald*-statistic and corrected according to the *Bonferroni* method, unless otherwise stated.

Results

Characterization of PSP and CBD frontal lobe brain nuclei via snATAC-seq

Isolated nuclei from fresh-frozen frontal cortex tissue from 13 samples underwent single-nucleus library preparation and short-read sequencing, yielding open chromatin profiles for 45,205 nuclei. After quality control and dimensionality reduction, clusters were defined from the snATAC-seq data to assess cell type identity (Fig. 2a). The

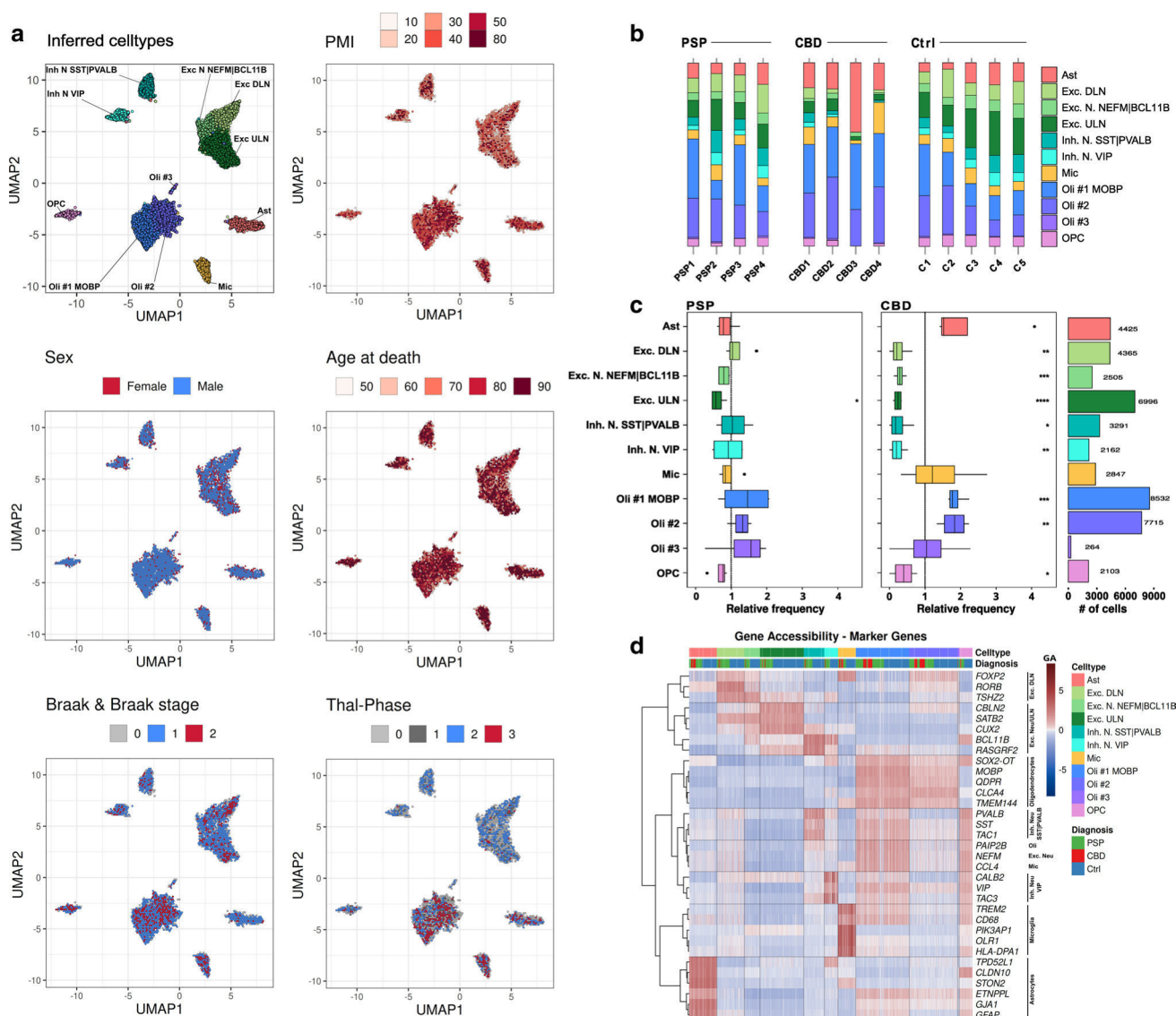


Fig. 2 Cell type inference and shifted cell type proportions in primary tauopathies. **a** Projections of cluster-cell type assignments and metadata onto the UMAP embedding of barcodes indicating their dissimilarity in distance between single barcodes (nuclei) as well as the respective variable as color code. Color coding and labels indicate the cell type or sub-cell type identity where applicable. The case-related covariates *postmortem* interval (PMI), sex, age at death, *Braak&Braak* stages did not overtly influence the embedding. Neuronal clusters were rather composited of nuclei originating from cases with *Thal* phase 0–2. Hex-binning was used to visualize overlapping puncta as pixel-wise means in case of PMI, sex, age at death, *Braak&Braak* stages, and *Thal* phases. **b** Bar plots representing relative sample-wise cell type frequencies of PSP, CBD, and Ctrl samples. Color coding indicates the cell type identity. CBD cases exhibit higher relative numbers of astrocytes (esp. CBD3). **c** Boxplots of relative cell type frequencies show excitatory neuron loss in PSP (left) and reductions in all neuronal populations with higher oligodendrocyte frequencies in CBD (mid) samples, when compared to theCtrls’

mean (vertical dashed line). Outliers are depicted as black dots. The hinges of each box correspond to the 25th and 75th percentiles with medians drawn as black bar. The 1.5-times inter-quartile ranges are shown as black whiskers. Total numbers of cells (# of cells) are indicated as bar plots on the right. Color coding indicates the cell type identity where applicable, while asterisks display the degree of significance with $*p < .05$, $**p < .01$, $***p < .001$, and $****p < .0001$. **d** Heatmap of gene body accessibility (GA) scores at marker gene loci to guide cell type identification. Every column corresponds to a single barcode, every row to a gene. Color shading indicates the extent of GA from low (blue) to high (red). Rows were clustered hierarchically (Euclidean distance, Ward-D2 method) and results depicted as dendrogram on the left. Cell/barcode order was fixed, but the overlay informs about the definitive cell type and the neuropathological diagnosis. Gene names comply with the *Ensembl* gene IDs. *Exc. DLN* excitatory deep-layer neurons, *Exc. ULN* excitatory upper-layer neurons, *Inh. N.* inhibitory neurons, *Mic* microglia, *Oli* oligodendrocytes, *OPC* oligodendrocytic precursor cells, *PMI postmortem* interval

total number of clusters and their respective sizes were found to be robust to downsampling, indicating appropriate clustering metrics (Supplementary Figs. 1 and 2, online resource). We detected a total of 11 major clusters, with negligible confounding effects by PMI, sex, age at death, *Thal* phase or *Braak & Braak* stage. Nevertheless, divergent regional atrophy patterns between PSP and CBD cases cannot completely be excluded. For cell type annotations, we gathered canonical marker genes from the literature and aggregated their gene accessibility (GA) score per cluster (Fig. 2d; Supplementary Fig. 3; Supplementary Data, T01, online resource). The GA score is derived from the sum of open chromatin loci overlapping a gene and its respective regulatory elements and can thus be understood as a proxy for gene transcription.

While neurons were represented by 5 and oligodendrocytes by 3 distinct clusters, microglia (Mic), astrocytes (Ast), and oligodendrocyte precursor cells (OPC) were each assigned to a single cluster. Neuronal subtypes were classified as (i) excitatory upper-layer neurons (Exc. ULN) with increased GA of *CBLN2*, *CUX2*, and *RASGRF2*, (ii) excitatory deep-layer neurons (Exc. DLN) with *RORB*, *FOXP2*, and *TSHZ2*, (iii) *NEFM*- and *BCL11B*-positive excitatory neurons (Exc. N. NEFM/BCL11B) as well as (iv) inhibitory neurons with either *PVALB* and *TAC1* or *SST* GA (Inh. N. SST/PVALB), and (v) inhibitory neurons with high *VIP*, *TAC3*, and *CALB2* GA. Oligodendrocytes were identified based on high GA for *MOBP* (Oli #1 MOBP) and numbered consecutively (Oli #2, Oli #3). Across all cells, Oli #1 MOBP was the most and Oli #3 the least abundant cell type (Fig. 2b, c). Because visual inspection of the *Thal* phase projection in UMAP suggested an uneven distribution across cell types, we performed a post hoc correlation analysis. This revealed only a positive association ($R=0.65$, $p=0.017$) between microglia and the cerebral distribution of A β + plaques (i.e., *Thal* phases) in our dataset (Supplementary Fig. 4, online resource), an association that has been described in the context of AD [20].

Gene ontology (GO) enrichment analyses supported cluster identities by recapitulation of known, commonly ascribed biological functions (Supplementary Fig. 5, online resource). Interestingly, microglial and astrocytic annotations were largely overlapping, hinting at an immune-regulatory role also for astrocytes in PSP/CBD. Transcription factor motif enrichment (TFME) comparisons demonstrated cluster-specific TF patterns, e.g., for Mic (SPI, RUNX2, IRF family), neurons in general (ZBTB18, RORA), and Ast (UNCX, LMX1A/B, HOXB2/3) (Supplementary Fig. 6A, online resource). Finally, cross-correlation of TFME matrices showed strong overlap within the major glial and neuronal cell types (Supplementary Fig. 6B, online resource), altogether indicating a technically and biologically consistent definition of clusters.

The frontal cortex is frequently affected by neurodegeneration and glial pathology in CBD and PSP [64]. Thus, we hypothesized that cell type proportions might appear shifted towards more glial cells in such areas and sought to calculate cell type frequencies per case (Fig. 2b). Comparing disease groups after normalization to Ctrl indicated a statistically significant decrease of neurons, OPCs, and oligodendrocytes in CBD, whereas there was only a reduction of Exc. ULN in PSP (*Welch t* test, Fig. 2c). However, we noted a greater cell type proportion variance in the CBD group. Because it is generally believed that qualitative immunohistochemical changes in tauopathies can be observed in both hemispheres, cases in this study were evaluated for inclusion with immunohistochemistry on the contralateral side. Thus, we cannot exclude the possibility that neurodegeneration or gliosis differed between hemispheres for certain cases. While only few reports regarding the asymmetry of immunohistochemical changes in PSP exist, this was previously described in the context of CBD [18, 64].

Broad chromatin changes at tauopathy-associated and protein degradation-related gene loci

To gain insight into disease-specific epigenetic alterations, we retrieved tauopathy-associated genes from *DisGeNET*, a database that integrates GWAS results, animal model experiments, and literature references [47]. We assessed their z -scored accessibilities in the disease and Ctrl groups (*Wilcoxon* rank-sum test, *Bonferroni* correction). We found altered GA scores of the top 50-ranked tauopathy-associated genes in all primary cell types except for the Mic cluster, which showed no significant changes at the selected genes in both disease entities (Fig. 3a). Due to the prominent involvement of microglia in AD [42, 45, 46]—another tauopathy—this finding was unexpected. Nevertheless, we could additionally show that there was no GA difference between groups when aggregating scores for all genes associated with the GO term “microglial activation”, supporting the notion that this phenomenon is not driven by epigenetic mechanisms in CBD or PSP (Fig. 3b).

Of note, *MAPT* showed reduced GA scores in one oligodendroglial and one neuronal cluster (Oli #1 MOBP and Exc. DLN) for both diseases, with a more pronounced reduction in CBD and unchanged conditions in Ast. The most significant positive GA change was observed in *NFE2L2* (Nuclear factor erythroid 2-related factor 2) in excitatory neurons, with a stronger gain in CBD compared to PSP. While in PSP, most significant hits were attributed to Exc. DLN, Exc. ULN were affected by the most extensive changes in CBD (Fig. 3a, Supplementary Fig. 7A&B, online resource).

Many tauopathy-related genes, including MAP-kinases and lysosomal enzymes, are associated with protein homeostasis [29, 66]. Thus, we aggregated GA scores for three

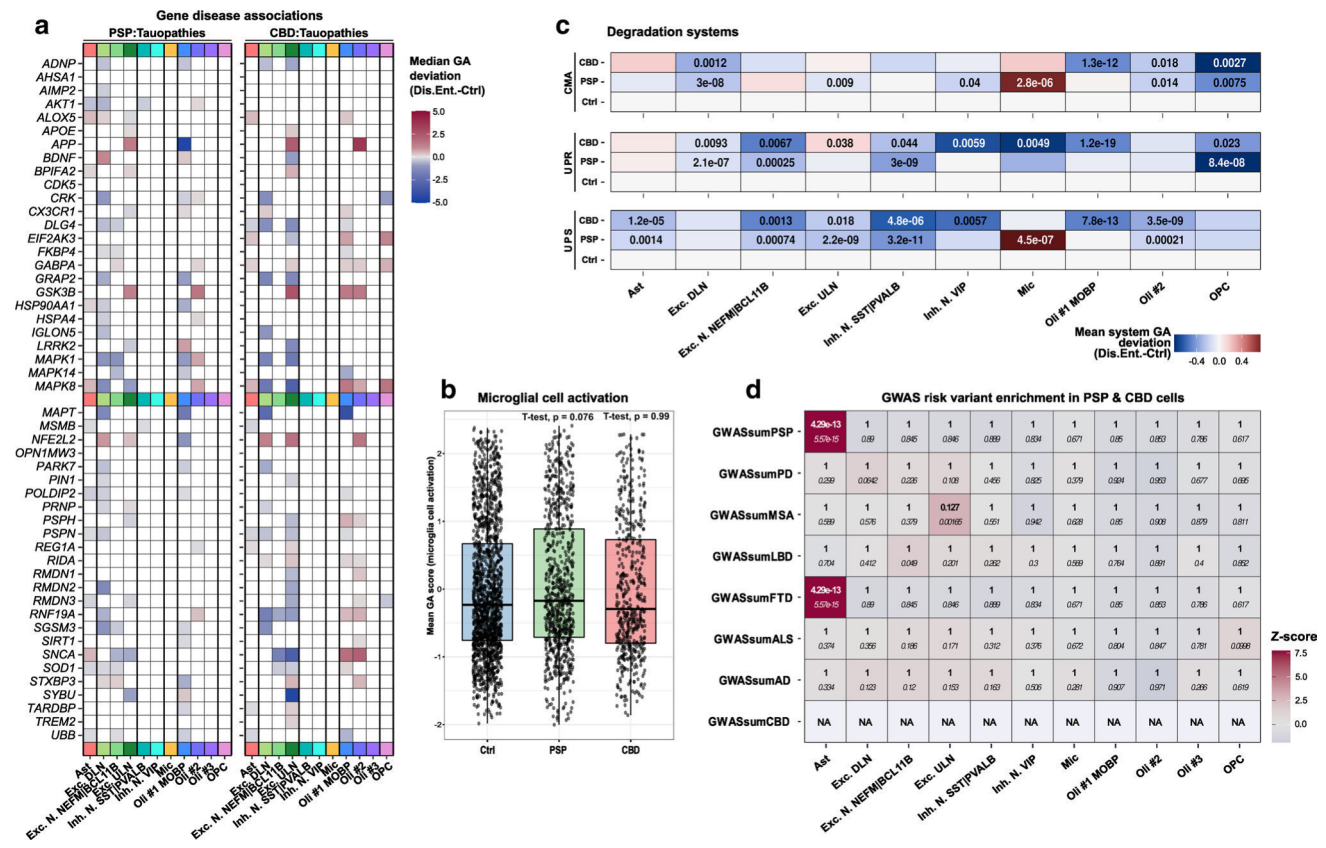


Fig. 3 Differential accessibility analysis reveals prominent changes in tauopathy-associated genes in neurons and glia. **a** Heatmap indicating significance and magnitude of GA changes at the top50 tauopathy-associated gene loci in PSP-(left) and CBD-(right) assigned cells and their gene-cell type pairs. Color shading represents the difference from reference gene-cell type pairs inCtrls. Only gene-cell type pairs with $p < .05$ are depicted (*Wilcoxon* rank-sum test, *BH*-correction). All major cell types except for microglia (and OPCs in PSP) exhibit significant GA changes in respect of these tauopathy-associated candidates. **b** Boxplots of *microglial cell activation*-associated GA patterns (AmiGO database) in microglia of the snATAC-seq dataset indicate no significant differences between compared groups. Nuclei-specific GA means of genes related to this GO term are given on the y-axis and compared between group entities on the x-axis. Single nuclei are depicted as black dots. The hinges of each box correspond to the 25th and 75th percentiles with medians drawn as black bar. The 1.5-times inter-quartile ranges are shown as black whiskers. Two-tailed *Welch's t*-test, referencing the Ctrl set, p values as indicated. **c** Protein homeostasis-related genes across all cell types differentiated

by group entity and degradation pathway show reduced system-level GA in Ast, most neuronal, and Oli populations, while Mic exhibit marked CMA and UPS inductions in PSP. Color coding shows aggregated mean scores of accessibility values at genes that were altered significantly and associated with either the CMA (top), UPR (middle), or UPS degradation systems (bottom). P values are given for each group vs. Ctrl comparison (two-tailed *Welch t* test, if $p < .05$). **d** Heatmap of genetic risk variant enrichment results in tauopathy cortices resolved by cell type assignments (x -axis) and GWAS data set (y -axis) highlight Ast, which exhibit strong enrichment. Color code indicates z scores and text inserts depict the uncorrected p value (*italic*) as well as the *BH*-corrected p values (bold, *Wilcoxon* rank-sum test). *Abs.diff.* absolute difference, *CMA* chaperon-mediated autophagy, *Dis.Ent.* disease entity, *Exc. DLN* excitatory deep-layer neurons, *Exc. ULN* excitatory upper-layer neurons, *FDR* false discovery rate, *GA* gene accessibility, *Inh. N.* inhibitory neurons, *Mic* microglia, *NA* not assessable, *Oli* oligodendrocytes, *OPC* oligodendrocytic precursor cells, *UPS* ubiquitin–proteasome-system, *UPR* unfolded-protein-response

molecular entities known to be involved in protein degradation (Fig. 3c): the ubiquitin proteasome system (UPS), the unfolded protein response (UPR), and chaperone-mediated autophagy (CMA). All three pathways were downregulated in oligodendrocytic populations in CBD with primarily downregulated CMA and UPS in PSP-derived Oli #2. We observed concordant UPS reductions in CBD and PSP Ast ($p < 0.005$) with simultaneously reduced microglial UPR ($p < 0.001$). Contrarily, PSP Mic exhibited a marked activation of both CMA and UPS ($p < 0.001$). With respect to the

neuronal populations, downregulation of all three systems was apparent. However, in CBD-derived Exc. ULN, the UPR system was induced, reflecting neuronal heterogeneity also in terms of degradative pathways.

On the DNA sequence level, GWAS risk variants associated with neurodegenerative diseases might be linked to ATAC-seq peaks, which are several hundred bp long regions of open chromatin, aggregated by cluster. Assuming that this relation would likewise affect certain cell types more than others, we compiled GWAS summary statistics

for tauopathies and related neurodegenerative syndromes, namely PSP, CBD, AD, Frontotemporal Dementia (FTD), Parkinson Disease (PD), Multiple System Atrophy (MSA), Lewy Body Dementia (LBD), and Amyotrophic Lateral Sclerosis (ALS). We then inferred cell type-associated risk variants in our dataset (as pooled tauopathy nuclei) segregated by disease-specific peaks (Fig. 3d, see Methods). This analysis showed pairs of high z scores and highly significant enrichment for FTD- and PSP-associated risk variants in astrocyte-specific peaks. We were unable to calculate cell type enrichments for CBD risk variants due to the sparsity of CBD GWAS (the significance-filtered CBD GWAS list consisted of only 6 SNPs). Strikingly, we did not observe GWAS enrichments for any of the above neurodegenerative diseases in microglia-specific peaks—not even AD, for which other studies have clearly attributed a large genetic risk proportion to microglia [42, 45, 46], suggesting that PSP- and CBD-specific microglial peaks are distinct from AD-specific ones.

Collectively, this investigation demonstrates that genetic risk variants previously associated with the clinical spectrum of primary tauopathies (i.e., PSP and FTD) are tightly linked to *astrocytic* chromatin accessibility profiles in the brains of PSP and CBD patients. Nonetheless, systematic cell type and pathway annotations also point to inherent differences between these diseases.

Tracking epigenetic transition states of tauopathy astrocytes supports a context of neuroinflammation

Integrating the previous findings with the knowledge that the astrocytic phenotype constitutes a major neuropathological feature to distinguish CBD from PSP impelled us to focus our downstream investigations on the Ast cluster. Thus, we subjected all 4425 astrocyte-derived nuclei from both tauopathies and Ctrl to subclustering and annotation procedures. One astrocytic subcluster exclusively consisted of tauopathy-derived nuclei (mainly CBD) and exhibited higher accessibility at genes involved in ‘stimulus detection’ or ‘signal transduction’ (Fig. 4a, Supplementary Fig. 8A, online resource). A triangular disease-wise comparison of TF motif enrichment (TFME) values (Supplementary Data, T02-T03, online resource, *Wilcoxon* rank-sum test, *BH*-corrected) revealed that the most significant candidates were those TFs associated with immunological terms (Supplementary Fig. 9A–E, online resource), while TF deviations were stronger in CBD than in PSP astrocytes (Supplementary Fig. 9F, online resource).

To gather insight into *how* astrocytes derived from tauopathy brains might evolve from a physiological towards a diseased state, we hypothesized this transition to be a continuous process paralleled by changes in open chromatin and mirrored by differential accessibilities for specific TFs along a shared

time constant. Hence, we sought to understand TFME dynamics with pseudotemporal models, though in separate UMAP embeddings for each disease entity.

We reasoned that high accessibility for the TF EMX2, which is specific for and active in early differentiating astrocytes, would be a suitable starting point for an assumed astrocytic transition path [58] (Fig. 4b–d). For CBD, we obtained a trajectory that terminated in a population of CBD-derived astrocytes, while only few of them were embedded in proximity to Ctrl cells in the EMX2_{HIGH} population. This is consistent with the presence of unaffected astrocytes in the tauopathy brain. In PSP brains, however, no disease-defined astrocytic subcluster was evident (Supplementary Fig. 8B, online resource).

The pseudotime inference itself does not allow for statistical evaluation of single-cell feature values over pseudotemporal trajectories. Thus, a framework called *tradeSeq* [3] was employed to test for TFME changes along the astrocytic transition axis. In a first step, generative additive models were fit to the feature distributions as a function of pseudotime. Subsequently, *Wald*-statistic-based hypothesis testing allowed to discern TFMs whose respective TFME values were either associated with the trajectory course or differed significantly from starting to terminating points.

This analysis showed a diverging pattern: The immediate early response (IER)-related FOS and JUN family members as well as their co-transcriptional factors NFE2, JDP2, and MAF, known to co-act as the AP-1 complex in the regulation of cell growth, differentiation, inflammation, and apoptosis [50, 61] (Fig. 4e–g, Supplementary Fig. 10A, Supplementary Fig. 11A&B, online resource), showed significantly higher and highly correlated TFME values (*Wald*-statistic start-vs.-end comparison, *BH*-corrected p value < 0.05). In contrast, TFs related to the early stages of astrocyte differentiation (LHX9, SHOX, RFX4, HESX1, and EMX2), showed a gradual loss of their enrichment (Fig. 4g, Supplementary Fig. 10A, Supplementary Fig. 11C–E, online resource). Focusing on pseudotime-aligned GA changes, protein homeostasis-related genes (e.g., *APOE*, *HSPB8*, *LRPI*) were upregulated, while many synaptic candidates (e.g., *SNCA*, *BDNF*, *NRXN3*) gradually decreased in their GA in CBD astrocytes (Supplementary Fig. 10B, online resource).

This analysis demonstrated that in CBD astrocytes, chromatin accessibility of TFs implicated in early astroglial development appears to be reduced in favor of a neuroinflammatory response.

Reconstructing disease-specific representations of astrocytic TF networks and a phenotype-associated regulon activity profile

We wondered whether we could leverage TFME information in a more unbiased way to decipher signatures delineating

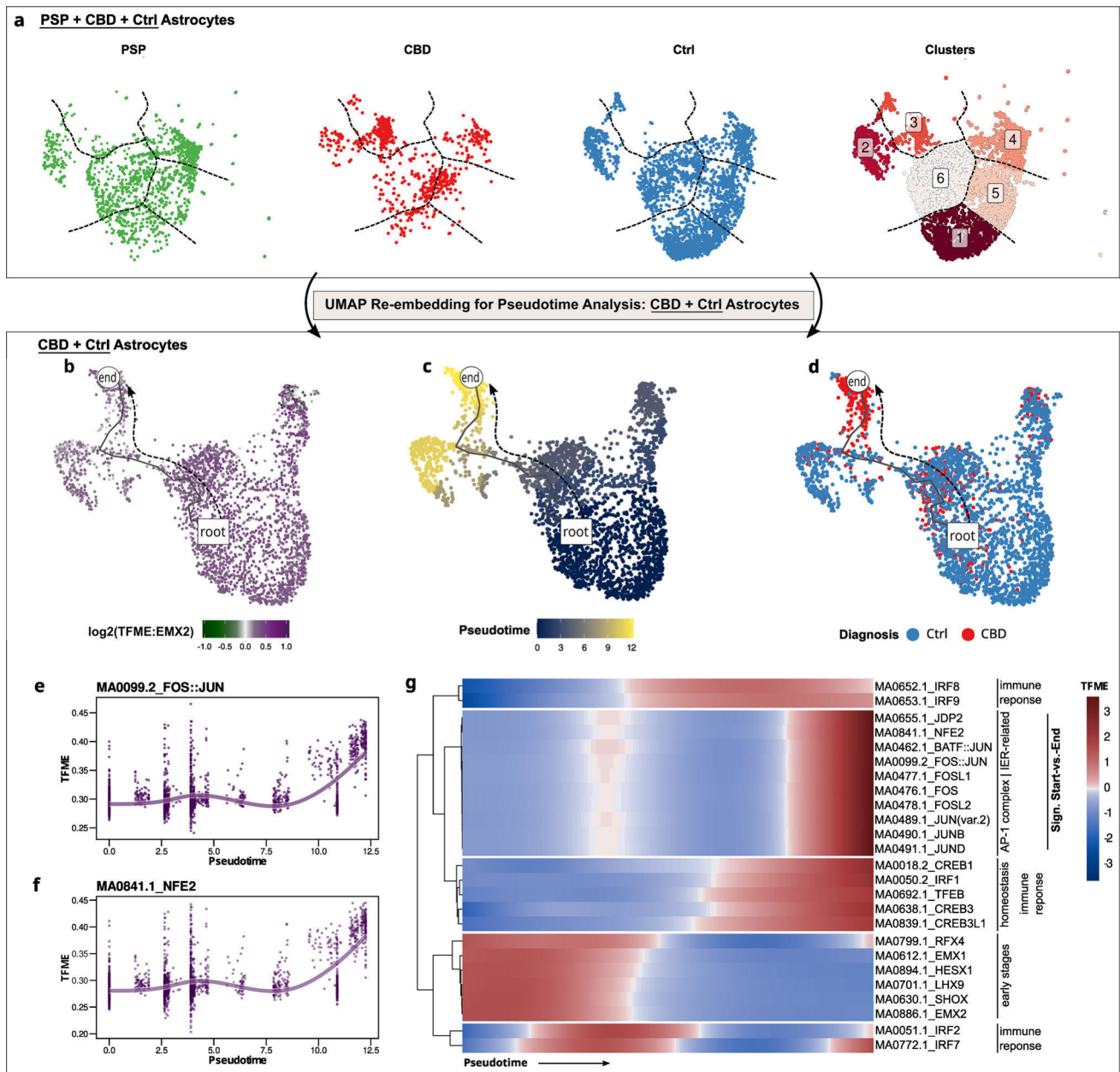


Fig. 4 CBD astrocytes acquire an epigenetic state of stress response and neuroinflammation. **a** All *PSP*-, *CBD*-, and *Ctrl*-derived astrocytes re-embedded in UMAP, stratified by group entity (first, second, third panel), and depicted after k-means clustering in a merged UMAP (fourth panel). One cluster (#3) is specific for CBD astrocytes. Color code indicates group entity or cluster assignments in the first three or the fourth panel, respectively. Dashed lines delineate cluster borders and are transferred to the group-wise depictions. **b–d** Exclusively *CBD*- and *Ctrl*-derived astrocytes re-embedded in UMAP. A pseudotime trajectory leads from a non-specific Ast pool towards a CBD-enriched population. Color code indicates EMX2 TFME (**b**), pseudotime (**c**, dimensionless), or group entity (**d**). The black line indicates the pseudotemporal trajectory from the *root*

towards the *end* cell. **e, f** Generative additive model non-linear fits of TFME values over pseudotime of the FOS-JUN (**e**) or NFE2 (**f**) motifs indicate parallel increments during the astrocytic transition towards a CBD-state. **g** Pseudotime heatmap displaying the TFME values of significantly altered TFMs in the start-vs.-end comparison (*Wald*-testing, *BH*-adjusted $p < .05$), as well as markers of early astrocytic development or immune regulation. Biological pathway associations are given on the right. TFME of astrocytic early-stage TFs is gradually decreasing, while immunologically relevant and AP-1 complex-related TFs gain in motif enrichment. *IER* immediate-early response, *TFME* transcription factor motif enrichment, *Sign* significant

PSP and CBD brains specifically from a non-diseased condition. Thus, we modeled disease-specific TF patterns by exploiting the discriminatory power of a machine-learning algorithm in a supervised classification task. Concretely, an extreme gradient boosting tree algorithm was trained on the cell-specific TFME of an 80%-split of the astrocyte subset, including data from PSP, CBD, and Ctrl astrocytes ($n=3540$). Assessing the model's performance with unseen nuclei of the remaining 20% of the astrocyte subset ($n=885$, Fig. 5a, b) yielded reliable classification regarding accuracy (overall 82.6%, balanced 84.0%), positive predictive value (82.3%), and negative predictive value (90.6%). Furthermore, when dividing by the a priori expected likelihood of predicting the correct group entity, the model's predictive ability can be considered 'substantial' with a *Cohen kappa* of 70.2% [10]. The differentiated prediction performance was most accurate for CBD vs. Ctrl tasks, followed by PSP vs. CBD, and PSP vs. Ctrl distinctions (Fig. 5a, Supplementary Fig. 12A, online resource).

In a subsequent step, overall feature importance assessment highlighted IER- and cellular immunity-related TFs (FOS, JUN, NFATC2/3, STAT1) as most useful in predicting the tauopathy or Ctrl state (Fig. 5c). Since this did not sufficiently inform about *disease-specific* importance, we used local interpretable model-agnostic explanations (*Lime*) [52] to understand the model's decision-making process in more detail. For a given astrocytic nucleus, *Lime* evaluated the contributions of TFME ranges to support or contradict the respective disease label (depicted as bar length in Fig. 5d–f). Consequently, we selected the top 10 candidates ranked by their feature weight in all test set astrocytes, which were assumed to be most helpful in predicting astrocytic identity of either PSP, CBD, or Ctrl origin specifically. Interestingly, the 'importance' metric was not only determined by the TFME deviations with the highest changes, but also by the discriminatory power of subtle TFME changes across the compared groups (Supplementary Fig. 12B, online resource).

The previous analyses highlighted changes in astrocyte TF dynamics without any respect to the underlying neuropathological phenotype. To link this information (i.e., pTau inclusions in astrocytes) with TF activities, we used the *Reconstruction of Transcriptional Regulatory Networks* approach [9] (Fig. 5g). Enabled by the availability of bulk gene expression data and correlations thereof with tufted astrocyte quantitation data (i.e., adjusted semiquantitative TA density) from the temporal cortex (TCX) of 176 PSP patients [1], we assessed genetic regulators and their target genes as so-called *regulon units* (Fig. 5g).

Utilizing these neuropathological-transcriptomic correlations, we assigned TA-related values to the given regulons (two-tailed GSEA, differential enrichment score, Fig. 5h), which we termed tufted astrocyte-associated regulon activity

profile (TA-RAP). Unsupervised clustering of regulons indicated sets with lower (top branch), mixed (mid branch), and increased (bottom branch) activity in PSP cases when compared to Ctrl. Again, IER-related and immunologically relevant TF transcripts such as *JUNB*, *NFATC2*, *NFE2L3*, or *IKZF5* were present among the set of activity enhanced regulons, while those related to developmental processes exhibited lower scores (e.g., *FOXF2*, *NRL*). Genes assigned to the TA-associated regulons shown in Fig. 5h were also enriched in biological pathways related to autophagy, peroxisomes, and (de-)ubiquitination (Supplementary Fig. 13, online resource).

These analyses highlight the importance of TF networks related to the IER or neuroinflammation in PSP and CBD astrocytes alike. Furthermore, external bulk transcriptomic data supports this notion independently from our snATAC-seq data for PSP. Nevertheless, an unbiased machine learning model also predicted discriminatory features between the two disease groups.

Definition of tauopathy signatures in astrocytes of PSP and CBD brains

The primary objective of this study was to define epigenetic signatures for PSP and CBD based on TF networks. Hence, we finally integrated the results of the four disjoint analysis branches into consensus lists (Fig. 6, for concept see also Fig. 1). The first set contained the names of all TFs that showed significant TFME changes in disease-wise statistical comparisons within the entire astrocyte population. The second set consisted of TFs whose accessibility profiles aligned tightly with the pseudotime trajectory. ML model explanations indicated the TF candidates contributing to the third set. Lastly, those TFs resulting from TA-RAP extraction in the external PSP dataset represented the members of the fourth set. To determine the consensus of candidates nominated by these different approaches, we used upset plots. We first describe a common PSP and CBD "pTau" signature that likely represents the regulatory state of pTau-positive astrocytes (Fig. 6a, b). Through hierarchical ordering by (i) the number of branches that overlap and (ii) the extent of overlap in terms of TF candidate counts, 4 ranks of confidence were assigned to TF sets with ≥ 3 set intersections. Guiding in discerning a tauopathy (PSP and/or CBD) from a Ctrl frontal cortex was the proposed astrocytic tauopathy signature depicted in Fig. 6b, with increased accessibilities for TF binding sites related to the IER such as JUN, FOS, and its ligands FOSL1 and FOSL2.

When directly comparing CBD and PSP TF binding site accessibilities, it became apparent that their changes followed almost exclusively the same direction, with the exception of TFEB and NFIC::TLX1, which showed lower accessibilities in PSP but greater ones in CBD. Meanwhile, we

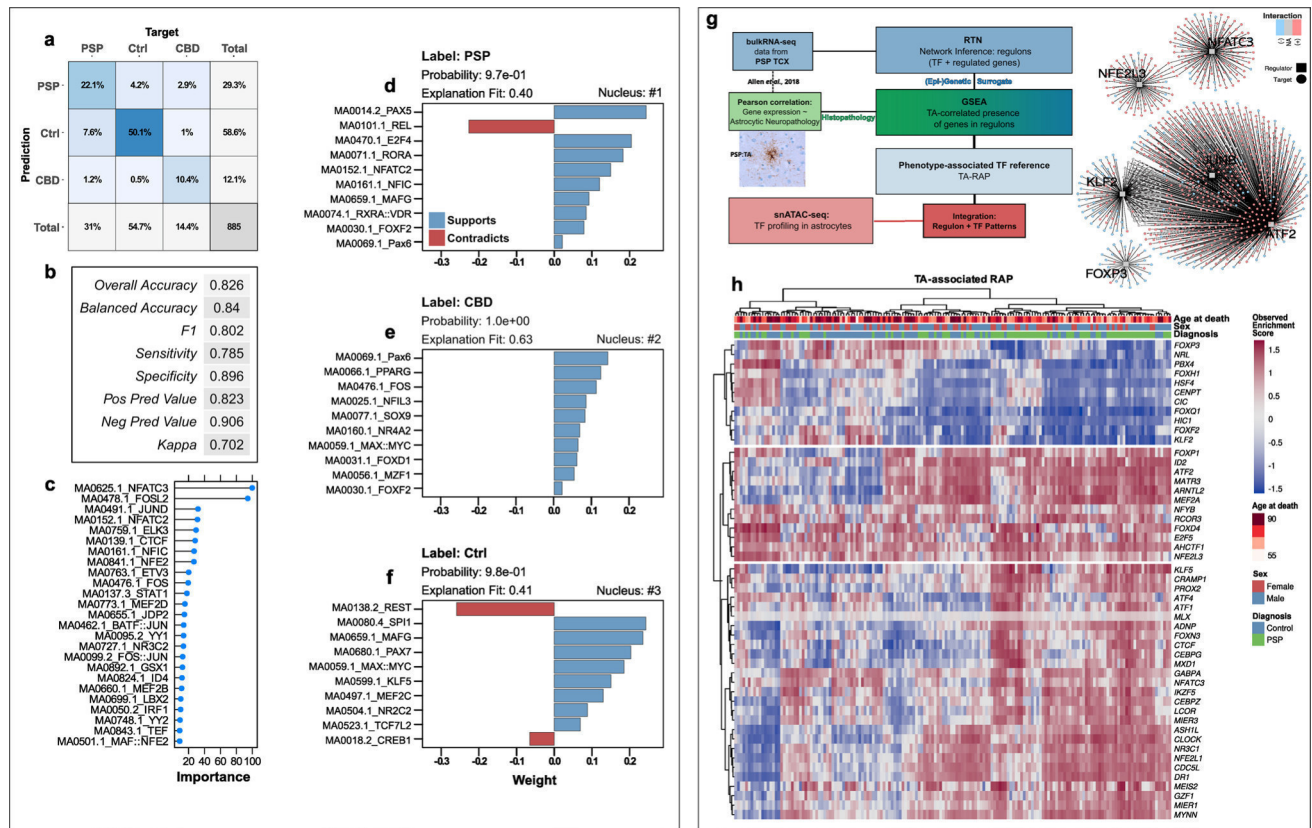


Fig. 5 TF networks associated with the astrocytic tauopathy state and regulatory correlates of tufted astrocytes. **a** Confusion matrix displaying the intersections of the XGB model's predictions (rows) and the actual labels (columns). Each square contains the percentual proportion of test set samples ($=20\%$ nuclei) with the assigned prediction–label relation. The sums of each row or column are depicted in the rightmost column or bottom row, respectively. The total sample number (i.e., nuclei of the 20% test set-split) is shown in the bottom right corner. **b** Evaluation parameters of classification performance of the trained XGB model on the 20% test set-split. Overall, more than 82% of predictions were correct (overall accuracy) and the model performs "substantially" with a *Cohen* kappa of 70.2%. **c** Overall feature importance values of the top 25 TFMs included in training the XGB model to correctly classify an astrocyte TF representation in general. The x-axis differentiates the feature importance (%) as reported by *caret*'s *varImp* function. Immediate-early response candidates (NFAT2/3) and major AP-1 constituents (FOSL2, JUN) were among the most important TFs. **d–f** Lime feature importance bar diagrams of the most certainly correctly classified barcodes of each group entity. The bar direction and bar color indicate the feature weights (\sim importance) assigned to the TFM, which are given as y-axis breaks. Feature weight was assigned to specific TFME value ranges. Each panel is complemented by the group entity label, the model's calculated probability, and the explanatory model's fit value. **g** Bioinformatical concept of the RTN analytical approach to link a neuropathological phenotype to TF information. A regulon network was inferred from published bulkRNA-seq data in PSP TCX and fil-

tered subsequently for those regulons that showed phenotype association (i.e., gene set enrichment of DEGs with histopathological TA grading in PSP cortices). Thereby, a TA-associated regulon activity profile was deduced, which was employed as TF reference in an integration part with snATAC-seq data-derived astrocytic TF activity patterns. Ultimately, this approach served to refine pTau-inclusion pathology-associated astrocytic PSP/CBD signatures. On the right, a set of TA-linked regulons illustrates the modularity of TF-gene-interactions (color code), the inter-modular connectivity suggesting co-regulation exerted by regulators on common genes, and the presumed presence of distinct groups of TFs. **h** Activity heatmap of those regulons that are enriched with TA grading in PSP TCX and whose regulon activity is significantly different between PSP and Ctrl TCX samples ($p < .05$, *BH*-corrected). Regulons in the upper part correlate negatively, those in the lower part correlate positively with TAs in PSP cortices. Every column corresponds to a single TCX sample and every row to a gene while color shade indicates the extent of regulon activity change. Rows and columns were clustered hierarchically (*Euclidean* distance, *Ward-D2* method) and results indicated as dendrograms. The colored overlay informs about the age at death, sex, and definitive neuropathological diagnosis. Gene names comply with the *Ensembl* IDs. *DEG* differentially expressed gene, *GSEA* gene set enrichment analysis, *Neg Pred Value* negative predictive value, *Pos Pred Value* positive predictive value, *RTN* Reconstruction of Transcriptional Networks, *TA* tufted astrocyte, *TCX* temporal cortex, *RAP* regulon activity profile, *XGB* extreme gradient boosting tree

observed relatively strong differences in the extent of accessibility alterations. Thus, to discriminate the two tauopathies, we hereby propose $JUN(B,D)_{HIGH}$, $FOS(L1,L2)_{HIGH}$

as well as the involvement of DUX4, KLF5, MAX::MYC, PAX6, and PPARG to support the identity of CBD-originated astrocytes (Fig. 6c–e). PSP astrocytes exhibited a

signature with additionally decreased TFEB and CREB1 accessibilities. Interestingly, subsequent pathway enrichment analyses of the PSP and CBD signatures incorporating the logic of TFME changes suggested MAPK-dependent signaling and infectious agent defense terms to play important biological roles in primary tauopathy astrocytes (Fig. 6f, g). In addition, the RELA and JUN TFs link back to protein homeostasis pathways (i.e., ‘ubiquitin protein ligase binding’), which is reflected in the gradual accessibility increments of tauopathy- and degradation system-associated genes (Supplementary Fig. 14, online resource).

Collectively, the integration of a variety of analytic approaches resulted in the identification of an astrocytic pTau signature that is strongly reminiscent of an immediate-early response. Notwithstanding, distinct molecular states of astrocytes in PSP and CBD were identified as well.

Since a conceivable confounder—case CBD3—might have introduced a sampling bias through its relatively high proportion of astrocytes, we performed a separate re-analysis without that case. Even with this approach, the major results of our study remain unaffected; however, we detected a significant increase in relative astrocyte frequencies (likely due to the lack of the outlier sample CBD3) and a more comprehensive list of TFs supporting a pTau phenotype (Supplementary Fig. 15–18, online resource).

Altered JUNB and TFEB activity influences target protein expression

Finally, we wondered whether the altered TF regulatory networks in tauopathies would manifest themselves in altered protein levels that could be observed by immunohistochemistry in post-mortem brains. We therefore identified target genes of the prominent TF candidates JUN(B) and TFEB, both of which are master regulators of essential homeostatic pathways.

To this end, we selected the top gene candidates resulting from correlating JUN(B)/TFEB TFME and GA, and which overlapped with *Cicero* co-accessibility links on the genomic level (see Methods). This approach highlighted *MAP3K8* as JUN(B)- and *CTSD* as TFEB-targeted genes (Supplementary Fig. 19, online resource). We performed immunofluorescence labeling of those candidates’ gene products in postmortem PSP and CBD samples (i.e., MFG) to validate JUNB and TFEB network dysregulation through their predicted target genes (Fig. 7a, b).

The mitogen-activated protein kinase *MAP3K8* (also known as TPL2) can transduce pro-inflammatory stimuli (i.e., IL17-receptor signaling in astrocytes) through the JUN(B)/FOS TF complex, which itself can enhance *MAP3K8* and interleukin expression [43, 63, 65]. We observed a significantly higher rate of pTau-positive astrocytes (TAs and APs) with *MAP3K8* expression compared

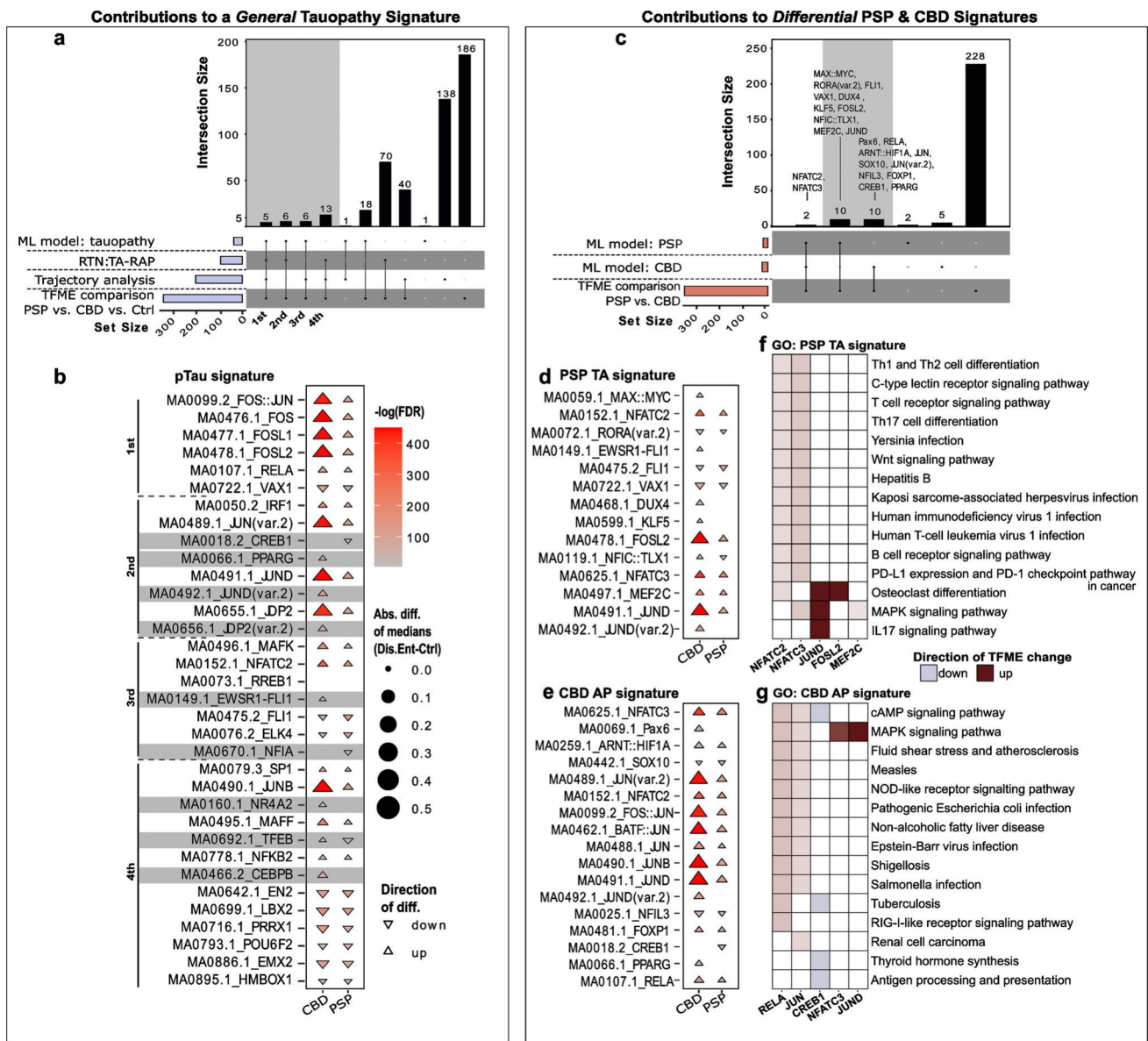
to GFAP positives in both tauopathies (PSP: 0.83 vs. 0.42, $n_{\text{cells}} = (118; 23)$, $n_{\text{cases}} = 4$; CBD: 0.79 vs. 0.37, $n = (83; 34)$, $n_{\text{cases}} = 4$) (Fig. 7a). In contrast, when investigating the expression of Cathepsin D, a lysosomal hydrolase and marker of lysosomal degradation [48], we found an inverse association with CTSD + TAs (in PSP), while the fraction of CTSD + APs (in CBD) was not significantly higher than their GFAP + counterparts (PSP 0.44 vs. 0.84, $n_{\text{cells}} = (65; 18)$, $n_{\text{cases}} = 3$; CBD 0.91 vs. 0.85, $n_{\text{cells}} = (87; 36)$, $n_{\text{cases}} = 4$) (Fig. 7b). Notably, protein expression was also visible in neuronal somata and other non-astrocytic cells. Together, we conclude that tauopathy astrocytes show signs of a JUN(B)-mediated pro-inflammatory state, while TAs in PSP additionally display a TFEB-mediated downregulation of lysosomal degradation.

Collectively, our findings are summarized in a flow chart (Fig. 7c) that can be used as an informative reference for epigenetic signatures that play a role in PSP and CBD.

Discussion

In this study, we applied an integrative systems biology approach to capture single-nucleus chromatin accessibilities in PSP and CBD frontal cortices. By combining latent characteristics of TF information and external transcriptome data, we shed light on the regulatory identity of pTau-affected astrocytes in these neurodegenerative diseases. Previous studies in bulks of brain cells repeatedly highlighted tauopathy-associated genes, or genes harboring genetic risk variants in their proximity [1, 27, 34]. However, cell type-resolved data sets have only been published for AD, where a role for microglia in its pathogenesis is now relatively well established. To our surprise, we did neither find microglia-associated accessibility changes, nor did we see an association of neurodegeneration-specific genetic risk loci with microglial specific peaks in the PSP or CBD datasets. In contrast, our data highlight astrocyte-relevant epigenetic alterations (Fig. 7c) [6, 55, 62]. Responses to pathological stimuli associated with the occurrence of pTau are likely related to astrocytic subpopulations, as delineated by differential use of TF binding sites in our study [15, 17, 30]. Nevertheless, we cannot exclude the possibility that accessibility changes in astrocytes are secondary in nature, without any direct effect of pTau on the compaction of chromatin, even though this has been described before in Tau transgenic *Drosophila* [19].

We propose that such TF signatures are meaningful (i) descriptively as indicators of disease entity, and (ii) biologically as the representation of a pathogenetically relevant gene expression program. The diagnostic value of this analysis might aid future TF-based studies with latent or missing phenotype data in a priori trait mapping. Together



with the proposed TF signature-based disease description, the underlying biology might even elicit candidates worth targeting pharmacologically. For example, one concept in AD aims at promoting lysosomal biogenesis and degradative enzyme expression. Astrocyte-specific conditional knock-out experiments in mouse models and neuronal cultures previously suggested to target TFEB, a transcriptional inductor of autophagic lysosomal degradation [5, 39]. This lysosomal master regulator significantly reduced the load of neuronal pTau and shifted extracellular Tau fibrils into astrocytes for lysosomal degradation. In our data, increased TFME values of TFEB in CBD astrocytes were paired with autophagy activation without significant rise in CTSD protein levels (in APs), while reduced TFEB activity and CTSD expression (in TAs) was evident in PSP astrocytes. This adds the notion of deficient activity in the latter and potentially

defective or inefficient lysosomal pathways in the former disease context. TFEB could thereby activate antioxidative and autophagy processes in synergy with NFE2 [32], a TF which featured increased motif enrichment in CBD astrocytes and whose deficiency is associated with exacerbation of Tau and amyloid pathology [53]. In turn, NFE2 family members are dependent on co-regulators and the AP-1 complex, a regulatory machinery implicated in neuroinflammation, apoptosis, gliotic remodeling, and axonal repair [50, 61]. This heterodimeric regulator complex exhibits cell type-specific composition and response profiles but has merely been in the focus of tauopathy research.

Immunohistochemical analysis in *postmortem* brain tissue of individuals with the very rare 3R tauopathy Pick's disease revealed colocalization of AP-1 components such as FOS, JUN, and MYC with the disease-defining intraneuronal pTau

Fig. 6 A concept of astrocytic tauopathy signatures. **a** Upset plot illustrating TFs useful in distinguishing PSP/CBD from Ctrl astrocytes that resulted from (i) interpreting the XGB classification model ('ML model: tauopathy'), (ii) the TA-related regulon activity profile in the bulkRNA-seq data set ('RTN: TA-RAP'), (iii) the pseudotime trajectory analysis in the snATAC-seq data set ('Trajectory analysis'), and (iv) group-wise TFME comparisons in the snATAC-seq data set ('TFME' comparison'). Set sizes are indicated as blue bars, while the intersection logic is shown as vertical lines and dots. Column heights depict the extent of intersection for the given sets. The first four intersections were assigned a hierarchy of importance in defining the primary tauopathy context. **b** Triangle plot indicating significance, absolute extent, and direction of TFME changes in pTau signature TFs in tauopathy-assigned astrocytes. The triangle tips point towards the direction of change while the size represents the absolute difference from the TFME reference in Ctrl. Fill shading displays the negative decadic logarithm of the *BH*-corrected p values from pair-wise *Wilcoxon* rank-sum tests. Empty coordinates inform about non-significant comparisons. Gray underlay informs about candidates with diverging TFME when collating PSP and CBD. **c** Upset plot to identify TFs useful in differentiating CBD from PSP astrocytes. The single sets resulted (i) from the most important TFs for PSP or CBD prediction according to the XGB model explainer ('ML model: PSP', 'ML model: CBD') and (ii) from pairwise statistical TFME comparisons between PSP and CBD astrocytes ('TFME comparisons'). The general plot structure equates to A. **d, e** Triangle plot indicating significance, absolute extent, and direction of TFME changes in PSP (**d**), and CBD (**e**) signature TFs in tauopathy-assigned astrocytes. The general plot structure equates to B. **f, g** Heatmaps of the GO enrichment of the PSP (**f**) and CBD TF signatures (**g**). The top 15 terms according to MF, BP, and CC enrichment scores as well as only those TFs that share at least one of these terms are depicted. Color code indicates the direction and strength of enrichment or depletion compared to Ctrl astrocytes. MAPK signaling, immunological and infectious disease terms are enriched. *Abs.diff.* absolute difference, *AP* astrocytic plaque, *CMA* chaperon-mediated autophagy, *DAR* differentially accessible region, *Dis.Ent.* disease entity, *EC* extracellular, *Exc.* *DLN* excitatory deep-layer neurons, *Exc. ULN* excitatory upper-layer neurons, *FDR* false discovery rate, *GO* gene ontology, *Mic* microglia, *ML* machine learning, *Oli* oligodendrocytes, *OPC* oligodendrocytic precursor cells, *TA-RAP* tufted astrocyte-associated regulon activity profile, *TF(ME)* transcription factor (motif enrichment), *UPS* ubiquitin-proteasome-system, *UPR* unfolded-protein-response

deposits (*Pick* bodies) and neuronal cytoplasm [44]. PSP and CBD astrocytes seem to acquire a pathological state of reactivity, cellular stress, and potentially apoptosis upon AP-1 activation (Fig. 6h). To our knowledge, an IER signature, comprising the AP-1 subunits, NFKB2, and NR4A2, has not been described in 4R tauopathies.

AP-1 itself might be induced by MAP kinases, as suggested by the simultaneous increase in the GA of *MAPK8/JNK1* and protein levels of *MAP3K8/TPL-2* in

(pTau+) astrocytes of both tauopathies. In parallel, activated *MAPK8/JNK1* in astrocytes might perpetuate Tau hyperphosphorylation, thereby contributing to a persistent cellular stress response [19, 51]. In neurons, the reduced GA of *MAPKs* (isoforms 1,8,14) and increased GA of their downstream target *GSK3B* suggest a potential target point by means of therapeutic kinase inhibition. Unfortunately, previous clinical trials with unspecific kinase inhibitors (valproic acid, lithium) and the selective *GSK3B*-inhibitor tideglusib failed to achieve considerable clinical improvements in AD or PSP patients [23, 36, 59]. Complicating the kinase modulation concept, increased GA of *MAPK8/JNK1* was evident in astrocytes and oligodendrocytes alike, again highlighting the importance of cell type-resolved analyses.

Intriguingly, the GWAS risk variant enrichment analysis revealed enrichments only in astrocyte-specific chromatin peaks. Microglial-driven alterations in genes participating in protein homeostasis, which are commonly believed to be a hallmark of AD [13, 22, 56], seemed to be confined to PSP in our analysis (Fig. 3b), consistent with the pronounced microglial transcriptional networks observed by Allen et al. [1]. The lack of risk variant enrichment as well as the significant GA increase in genes associated with UPS and CMA suggest that microglial activation in PSP is rather unlikely determined by sequence alterations as defined in GWAS. Unlike other tauopathies such as AD or Pick's Disease, the pTau-laden astrocytic phenotype is considered a hallmark of PSP and CBD, where loss of synapse support and concurrent inflammation can exert deleterious effects [4, 6, 37]. Our results therefore suggest that future experiments should prioritize the investigation of astrocytes over microglia in PSP and CBD.

In summary, comparing these two 4R tauopathies from an epigenetic perspective demonstrates broad overlap in terms of disease-associated regulatory processes. Nevertheless, our analysis also suggests distinct pathogenetic properties, particularly with regard to the phenotype of astrocytes. The proposed tauopathy signatures should be contextualized with different data sets and more diverse disease populations to define their specificity as well as overlapping features with related disease entities. Future research might also benefit from integrating our data in multi-omic projects or when studying pathomechanisms and causal relationships in suitable disease models.

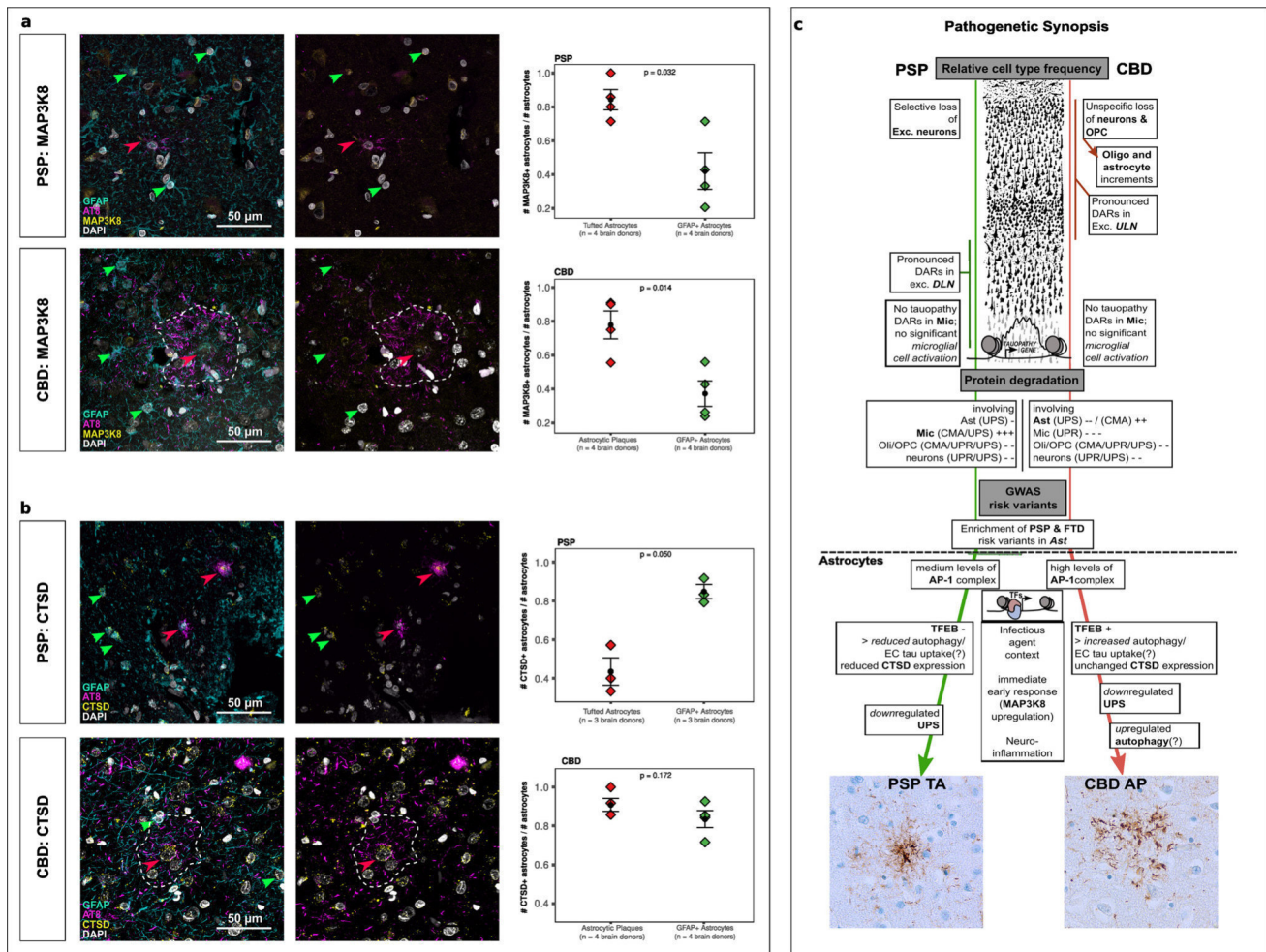


Fig. 7 TF target gene validation and synopsis of pathogenesis. **a** Immunofluorescent staining analysis showing 4-channels merge (GFAP, AT8, MAP3K8, DAPI) and 3-channels merge (AT8, MAP3K8, DAPI) of PSP (upper row) and CBD (lower row) MFG. Arrowheads mark GFAP+ (green) and AT8+ (red) astrocytes. Boxplots depicting fractions of GFAP+MAP3K8+astrocytes over GFAP+astrocytes compared with the fractions of AT8+MAP3K8+astrocytes over AT8+astrocytes. Statistics were calculated using a two-tailed *paired t*-test with *p* values as indicated. **b** Immunofluorescent staining analysis showing 4-channels merge (GFAP, AT8, CTSD, DAPI) and 3-channels merge (AT8, CTSD, DAPI) of PSP (upper row) and CBD (lower row) MFG. Arrowheads mark GFAP+ (green) and AT8+ (red) astrocytes. Boxplots depicting fractions of GFAP+CTSD+astrocytes over GFAP+astrocytes compared with the fractions of AT8+CTSD+astrocytes over AT8+astrocytes. Plot structure equal to a. **c** Concept of epigenetic contribution to the pathogenesis in the primary 4R tauopathies PSP and CBD. The upper half summarizes global findings of this study, while the lower half focuses on changes assigned to astrocytes. Dif-

ferences in neuronal cell loss were observed and mirrored by prominent DAR-patterns in different neuronal subclusters. Protein degradation was induced in Mic in PSP, while Ast served this role in CBD. PSP and FTD-associated risk variants were exclusively enriched in Ast. Focusing on the latter glia type, disease-specific molecular patterns comprising regulators of the immediate early response, autophagy, and UPS delineate differential pathogenetic signatures. The histological illustration of the neocortex was modified from https://commons.wikimedia.org/wiki/File:Cajal_cortex_drawings.png. AP astrocytic plaque, CMA chaperon-mediated autophagy, CTSD Cathepsin D, DAR differentially accessible region, *Dis.Ent.* disease entity, EC extracellular, Exc. DLN excitatory deep-layer neurons, Exc. ULN excitatory upper-layer neurons, FDR false discovery rate, GO gene ontology, MAP3K8 Mitogen-activated protein 3 kinase 8, Mic microglia, ML machine learning, Oli oligodendrocytes, OPC oligodendrocytic precursor cells, TA-RAP tufted astrocyte-associated regulon activity profile, TF(ME) transcription factor (motif enrichment), UPS ubiquitin-proteasome-system, UPR unfolded-protein-response

Acknowledgements We would like to address thanks to the patients and their families for making this research possible. Beyond that, we thank the associates of the *Neurobiobank Munich* for their structural support. Moreover, we thank Dr. E. Beltran, Dr. J. Fischer-Sternjak, and Prof. Dr. Kerschensteiner for granting access to the Chromium controller and laboratory facilities. We thank Dr. N. Buresch for providing

technical support and Dr. E. Bauerschmidt for proof reading. Finally, we are grateful for Prof. Dr. A. Daneke's and Prof. Dr. J. Levin's professional input as clinical professionals.

Author contributions Neuropathological evaluation was conducted by SR and supported by TA and JH. Cases were selected by SR, OW, and

supported by TA and JH. Material preparation and data collection was performed by NB and VCR. Biological quality control was performed by VCR and JM. NB conducted the bioinformatical analysis with help from FLS and input from MMD. Immunofluorescence staining and imaging was conducted by FLS, KP, and JW. The manuscript was written by NB and FLS with significant input from VCR, OW, TA, and JH; FLS, VCR, and JH supervised all aspects of the work. All authors have read and approved the final and revised manuscript.

Funding Open Access funding enabled and organized by Projekt DEAL. Funding of this project was realized by the Munich Cluster of Systems Neurology (SyNergy), LMU Munich, Munich, Germany. N.B. holds a scholarship from the German Academic Scholarship Foundation, F.L.S.'s research is supported by European Union Marie-Curie Actions (H2020-MSCA-IF-2017: NOJUNKDNA; 792832). K.P. receives funding by the Marie Skłodowska-Curie actions grant, ITN SynDegen (721802). This work was funded by Studienstiftung des Deutschen Volkes and Deutsche Forschungsgemeinschaft (Grant nos. STR 1573/3-1, EXC 2145).

Data availability All scripts for pre-processing and analyzing the snATAC-seq data from PSP/CBD frontal cortex and the Allen et al. bulkRNA-seq data from PSP/CTX are available on GitHub (https://github.com/nes-b/snATAC-seq_psp_cbd). Raw data that support the findings of this study are available in the European Bioinformatics Institute—European Nucleotide Archive (EBI-ENA) under the accession: PRJEB54978.

Declarations

Conflict of interest The authors declare that they have no competing interests.

Ethics approval Human brain tissue samples were collected and provided by the Neurobiobank Munich (NBM) in accordance with Institutional Review Board protocols approved by the Ethics Committee of the LMU Munich (#345-13). Written informed consent was obtained from the donors or their next of kin. Ethical approval for this particular study was also granted by the Ethics Committee of the LMU Munich (#19-442). All procedures were performed in line with the 1964 Helsinki declaration and its later amendments or comparable ethical standards.

Open Access This article is licensed under a Creative Commons Attribution 4.0 International License, which permits use, sharing, adaptation, distribution and reproduction in any medium or format, as long as you give appropriate credit to the original author(s) and the source, provide a link to the Creative Commons licence, and indicate if changes were made. The images or other third party material in this article are included in the article's Creative Commons licence, unless indicated otherwise in a credit line to the material. If material is not included in the article's Creative Commons licence and your intended use is not permitted by statutory regulation or exceeds the permitted use, you will need to obtain permission directly from the copyright holder. To view a copy of this licence, visit <http://creativecommons.org/licenses/by/4.0/>.

References

- Allen M, Wang X, Serie DJ, Strickland SL, Burgess JD, Koga S et al (2018) Divergent brain gene expression patterns associate with distinct cell-specific tau neuropathology traits in progressive supranuclear palsy. *Acta Neuropathol* 136:709–727. <https://doi.org/10.1007/s00401-018-1900-5>
- Armstrong MJ, Litvan I, Lang AE, Bak TH, Bhatia KP, Borroni B et al (2013) Criteria for the diagnosis of corticobasal degeneration. *Neurology* 80:496–503. <https://doi.org/10.1212/WNL.0b013e31827f0fd1>
- Van den Berge K, Roux de Bézieux H, Street K, Saelens W, Cannoodt R, Saeys Y et al (2020) Trajectory-based differential expression analysis for single-cell sequencing data. *Nat Commun* 11:1–13. <https://doi.org/10.1038/s41467-020-14766-3>
- Bigio EH, Vono MB, Satumira S, Adamson J, Sontag E, Hyman LS et al (2001) Cortical synapse loss in progressive supranuclear palsy. *J Neuropathol Exp Neurol* 60:403–410. <https://doi.org/10.1093/jnen/60.5.403>
- Binder JL, Chander P, Deretic V, Weick JP, Bhaskar K (2020) Optical induction of autophagy via transcription factor EB (TFEB) reduces pathological tau in neurons. *PLoS ONE* 15:e0230026. <https://doi.org/10.1371/journal.pone.0230026>
- Briel N, Pratsch K, Roerber S, Arzberger T, Herms J (2020) Contribution of the astrocytic tau pathology to synapse loss in progressive supranuclear palsy and corticobasal degeneration. *Brain Pathol.* <https://doi.org/10.1111/bpa.12914>
- Bryois J, Skene NG, Sullivan PF et al (2020) Genetic identification of cell types underlying brain complex traits yields insights into the etiology of Parkinson's disease. *Nat Genet* 52:482–493. <https://doi.org/10.1038/s41588-020-0610-9>
- Buenrostro JD, Giresi PG, Zaba LC, Chang HY, Greenleaf WJ (2013) Transposition of native chromatin for fast and sensitive epigenomic profiling of open chromatin, DNA-binding proteins and nucleosome position. *Nat Methods* 10:1213–1218. <https://doi.org/10.1038/nmeth.2688>
- Castro MAA, De Santiago I, Campbell TM, Vaughn C, Hickey TE, Ross E et al (2015) Regulators of genetic risk of breast cancer identified by integrative network analysis. *Nat Genet* 48:12–21. <https://doi.org/10.1038/ng.3458>
- Cohen J (1960) A coefficient of agreement for nominal scales. *Educ Psychol Meas* 20:37–46. <https://doi.org/10.1177/001316446002000104>
- Dickson DW, Bergeron C, Chin SS, Duyckaerts C, Horoupian D, Ikeda K et al (2002) Office of rare diseases neuropathologic criteria for corticobasal degeneration. *J Neuropathol Exp Neurol* 61:935–946. <https://doi.org/10.1093/jnen/61.11.935>
- Dunham I, Kundaje A, Lochovsky L et al (2012) An integrated encyclopedia of DNA elements in the human genome. *Nature* 489:57–74. <https://doi.org/10.1038/nature11247>
- Eckenweber F, Medina-Luque J, Blume T, Sacher C, Biechele G, Wind K et al (2020) Longitudinal TSPO expression in tau transgenic P301S mice predicts increased tau accumulation and deteriorated spatial learning. *J Neuroinflamm.* <https://doi.org/10.1186/s12974-020-01883-5>
- Fang R, Preissl S, Li Y, Hou X, Lucero J, Wang X et al (2021) Comprehensive analysis of single cell ATAC-seq data with SnapATAC. *Nat Commun* 12:1–15. <https://doi.org/10.1038/s41467-021-21583-9>
- Ferrer I (2017) Diversity of astroglial responses across human neurodegenerative disorders and brain aging. *Brain Pathol* 27:645–674. <https://doi.org/10.1111/bpa.12538>
- Ferrer I, Ferrer I (2018) Astroglial pathology in tauopathies. *Neuroglia* 1:126–150. <https://doi.org/10.3390/neuroglia1010010>
- Filipcik P, Cente M, Zilka N, Smolek T, Hanes J, Kucerak J et al (2015) Intraneuronal accumulation of misfolded tau protein induces overexpression of Hsp27 in activated astrocytes. *Biochim Biophys Acta Mol Basis Dis* 1852:1219–1229. <https://doi.org/10.1016/j.bbadis.2015.03.003>

18. Forrest SL, Kril JJ, Halliday GM (2019) Cellular and regional vulnerability in frontotemporal tauopathies. *Acta Neuropathol* 138:705–727
19. Frost B, Hemberg M, Lewis J, Feany MB (2014) Tau promotes neurodegeneration through global chromatin relaxation. *Nat Neurosci* 17:357–366. <https://doi.org/10.1038/nn.3639>
20. Gerrits E, Brouwer N, Kooistra SM, Woodbury ME, Vermeiren Y, Lambourne M et al (2021) Distinct amyloid- β and tau-associated microglia profiles in Alzheimer's disease. *Acta Neuropathol* 141:681–696. <https://doi.org/10.1007/S00401-021-02263-W/FIGURES/4>
21. Goedert M (2016) The ordered assembly of tau is the gain-of-toxic function that causes human tauopathies. *Alzheimer's Dement* 12:1040–1050. <https://doi.org/10.1016/J.JALZ.2016.09.001>
22. Grubman A, Chew G, Ouyang JF, Sun G, Choo XY, McLean C et al (2019) A single-cell atlas of entorhinal cortex from individuals with Alzheimer's disease reveals cell-type-specific gene expression regulation. *Nat Neurosci* 22:2087–2097. <https://doi.org/10.1038/s41593-019-0539-4>
23. Hampel H, Ewers M, Bürger K, Annas P, Mörtberg A, Bogstedt A et al (2009) Lithium trial in Alzheimer's disease: A randomized, single-blind, placebo-controlled, multicenter 10-week study. *J Clin Psychiatry* 70:922–931. <https://doi.org/10.4088/JCP.08m04606>
24. Höglinger GU, Melhem NM, Dickson DW, Sleiman PMA, Wang L-S, Klei L et al (2011) Identification of common variants influencing risk of the tauopathy progressive supranuclear palsy. *Nat Genet* 43:699–705. <https://doi.org/10.1038/ng.859>
25. Höglinger GU, Respondek G, Kovacs GG (2018) New classification of tauopathies. *Rev Neurol (Paris)* 174:664–668. <https://doi.org/10.1016/j.neurol.2018.07.001>
26. Huang LK, Chao SP, Hu CJ (2020) Clinical trials of new drugs for Alzheimer disease. *J Biomed Sci* 27:18–18
27. Jabbari E, Koga S et al (2021) Genetic determinants of survival in progressive supranuclear palsy: a genome-wide association study. *Lancet Neurol* 20:107–116. [https://doi.org/10.1016/S1474-4422\(20\)30394-X](https://doi.org/10.1016/S1474-4422(20)30394-X)
28. Jc U, Ca L, El B, Ls L, Mh G (2019) Interrogation of human hematopoiesis at single-cell and single-variant resolution. *Nat Genet* 51:683–693. <https://doi.org/10.1038/S41588-019-0362-6>
29. Jiang S, Bhaskar K (2020) Degradation and transmission of tau by autophagic-endolysosomal networks and potential therapeutic targets for tauopathy. *Front Mol Neurosci* 13:199
30. Kang SG, Eskandari-Sedighi G, Hromadkova L, Safar JG, Westaway D (2020) Cellular biology of tau diversity and pathogenic conformers. *Front Neurol* 11:2
31. Kelley DR, Snoek J, Rinn JL (2016) Basset: Learning the regulatory code of the accessible genome with deep convolutional neural networks. *Genome Res* 26:990–999. <https://doi.org/10.1101/gr.200535.115>
32. Kim S, Choi KJ, Cho SJ, Yun SM, Jeon JP, Koh YH et al (2016) Fisetin stimulates autophagic degradation of phosphorylated tau via the activation of TFEB and Nrf2 transcription factors. *Sci Rep*. <https://doi.org/10.1038/srep24933>
33. Klemm SL, Shipony Z, Greenleaf WJ (2019) Chromatin accessibility and the regulatory epigenome. *Nat Rev Genet* 20:207–220
34. Kouri N, Ross OA, Dickson DW et al (2015) Genome-wide association study of corticobasal degeneration identifies risk variants shared with progressive supranuclear palsy. *Nat Commun* 6:1–7. <https://doi.org/10.1038/ncomms8247>
35. Lake BB, Ai R, Kaeser GE, Salathia NS, Yung YC, Liu R et al (2016) Neuronal subtypes and diversity revealed by single-nucleus RNA sequencing of the human brain. *Science* 352:1586–1590. <https://doi.org/10.1126/science.aaf1204>
36. Leclair-Visonneau L, Rouaud T, Debilly B, Durif F, Houeto JL, Kreisler A et al (2016) Randomized placebo-controlled trial of sodium valproate in progressive supranuclear palsy. *Clin Neurol Neurosurg* 146:35–39. <https://doi.org/10.1016/j.clineuro.2016.04.021>
37. Lipton AM, Munro Cullum C, Satumtira S, Sontag E, Hyman LS, White CL et al (2001) Contribution of asymmetric synapse loss to lateralizing clinical deficits in frontotemporal dementias. *Arch Neurol* 58:1233–1239. <https://doi.org/10.1001/archneur.58.8.1233>
38. Litvan I, Hauw JJ, Bartko JJ, Lantos PL, Daniel SE, Horoupian DS et al (1996) Validity and reliability of the preliminary NINDS neuropathologic criteria for progressive supranuclear palsy and related disorders. *J Neuropathol Exp Neurol* 55:97–105. <https://doi.org/10.1097/00005072-199601000-00010>
39. Martini-Stoica H, Cole AL, Swartzlander DB, Chen F, Wan Y-W, Bajaj L et al (2018) TFEB enhances astroglial uptake of extracellular tau species and reduces tau spreading. *J Exp Med* 215:2355–2377. <https://doi.org/10.1084/jem.20172158>
40. Mathys H, Davila-Velderrain J, Peng Z, Gao F, Mohammadi S, Young JZ et al (2019) Single-cell transcriptomic analysis of Alzheimer's disease. *Nature* 570:332–337. <https://doi.org/10.1038/s41586-019-1195-2>
41. McKenzie AT, Wang M, Hauberg ME, Fullard JF, Kozlenkov A, Keenan A et al (2018) Brain cell type specific gene expression and co-expression network architectures. *Sci Rep* 8:8868. <https://doi.org/10.1038/s41598-018-27293-5>
42. Mukherjee S, Klaus C, Pricop-Jeckstadt M, Miller JA, Struebing FL (2019) A microglial signature directing human aging and neurodegeneration-related gene networks. *Front Neurosci* 13:2. <https://doi.org/10.3389/fnins.2019.00002>
43. Myers RM, Stamatoyannopoulos J, Risk B et al (2011) A User's Guide to the encyclopedia of DNA elements (ENCODE). *PLOS Biol* 9:e1001046. <https://doi.org/10.1371/JOURNAL.PBIO.1001046>
44. Nieto-Bodelón M, Santpere G, Torrejón-Escribano B, Puig B, Ferrer I (2006) Expression of transcription factors c-Fos, c-Jun, CREB-1 and ATF-2, and caspase-3 in relation with abnormal tau deposits in Pick's disease. *Acta Neuropathol* 111:341–350. <https://doi.org/10.1007/s00401-005-0013-0>
45. Nott A, Holtman IR, Coufal NG, Schlachetzki JCM, Yu M, Hu R et al (2019) Brain cell type-specific enhancer–promoter interactome maps and disease-risk association. *Science* 366:1134–1139. <https://doi.org/10.1126/science.aay0793>
46. Olah M, Menon V, Habib N, Taga MF, Ma Y, Yung CJ et al (2020) Single cell RNA sequencing of human microglia uncovers a subset associated with Alzheimer's disease. *Nat Commun* 11:1–18. <https://doi.org/10.1038/s41467-020-19737-2>
47. Piñero J, Ramírez-Anguaita JM, Saüch-Pitarch J, Ronzano F, Centeno E, Sanz F et al (2020) The DisGeNET knowledge platform for disease genomics: 2019 update. *Nucleic Acids Res* 48:D845–D855. <https://doi.org/10.1093/nar/gkz1021>
48. Piras A, Collin L, Grüniger F, Graff C, Rönnbäck A (2016) Autophagic and lysosomal defects in human tauopathies: analysis of post-mortem brain from patients with familial Alzheimer disease, corticobasal degeneration and progressive supranuclear palsy. *Acta Neuropathol Commun* 4:22. <https://doi.org/10.1186/s40478-016-0292-9>
49. Pliner HA, Packer JS, McFaline-Figueroa JL, Cusanovich DA, Daza RM, Aghamirzaie D et al (2018) Cicero predicts cis-regulatory DNA interactions from single-cell chromatin accessibility data. *Mol Cell* 71:858–871.e8. <https://doi.org/10.1016/J.MOLCEL.2018.06.044>
50. Raivich G, Bohatschek M, Da Costa C, Iwata O, Galiano M, Hristova M et al (2004) The AP-1 transcription factor c-Jun is required for efficient axonal regeneration. *Neuron* 43:57–67. <https://doi.org/10.1016/j.neuron.2004.06.005>
51. Reynolds CH, Betts JC, Blackstock WP, Nebreda R, Anderson BH (2000) Phosphorylation sites on tau identified by

- nano electrospray mass spectrometry: differences in vitro between the mitogen-activated protein kinases ERK2, c-Jun N-terminal kinase and P38, and glycogen synthase kinase-3
52. Ribeiro MT, Singh S, Guestrin C (2016) “Why should i trust you?” Explaining the predictions of any classifier. In: Proceedings of the ACM SIGKDD International Conference on Knowledge Discovery and Data Mining. Association for Computing Machinery, pp 1135–1144
 53. Rojo AI, Pajares M, Rada P, Nuñez A, Nevado-Holgado AJ, Killik R et al (2017) NRF2 deficiency replicates transcriptomic changes in Alzheimer’s patients and worsens APP and TAU pathology. *Redox Biol* 13:444–451. <https://doi.org/10.1016/j.REDOX.2017.07.006>
 54. Schwartzentruber J, Cooper S, Liu JZ, Barrio-Hernandez I, Bello E, Kumasaka N et al (2021) Genome-wide meta-analysis, fine-mapping and integrative prioritization implicate new Alzheimer’s disease risk genes. *Nat Genet* 53:392–402. <https://doi.org/10.1038/s41588-020-00776-w>
 55. Sidoryk-Wegrzynowicz M, Gerber YN, Ries M, Sastre M, Tolkovsky AM, Spillantini MG (2017) Astrocytes in mouse models of tauopathies acquire early deficits and lose neurosupportive functions. *Acta Neuropathol Commun* 5:89. <https://doi.org/10.1186/s40478-017-0478-9>
 56. Spangenberg EE, Green KN (2017) Inflammation in Alzheimer’s disease: Lessons learned from microglia-depletion models. *Brain Behav Immun* 61:1–11. <https://doi.org/10.1016/j.bbi.2016.07.003>
 57. Thurman RE, Rynes E, Stamatoyannopoulos JA et al (2012) (2012) The accessible chromatin landscape of the human genome. *Nat* 489:75–82. <https://doi.org/10.1038/nature11232>
 58. Tiwari N, Pataskar A, Pé S, Ló Pez-Mascaraque L, Tiwari VK, Correspondence BB (2018) Stage-specific transcription factors drive astroglialogenesis by remodeling gene regulatory landscapes. *Stem Cell* 23:557–571.e8. <https://doi.org/10.1016/j.stem.2018.09.008>
 59. Tolosa E, Litvan I, Ven Gerpen J et al (2014) A phase 2 trial of the GSK-3 inhibitor tideglusib in progressive supranuclear palsy. *Mov Disord* 29:470–478. <https://doi.org/10.1002/mds.25824>
 60. Vaquerizas JM, Kummerfeld SK, Teichmann SA, Luscombe NM (2009) A census of human transcription factors: function, expression and evolution. *Nat Rev Genet* 10:252–263. <https://doi.org/10.1038/nrg2538>
 61. Vukic V, Callaghan D, Walker D, Lue LF, Liu QY, Couraud PO et al (2009) Expression of inflammatory genes induced by beta-amyloid peptides in human brain endothelial cells and in Alzheimer’s brain is mediated by the JNK-AP1 signaling pathway. *Neurobiol Dis* 34:95–106. <https://doi.org/10.1016/j.nbd.2008.12.007>
 62. Wang C, Xiong M, Gratuzze M, Bao X, Shi Y, Andhey PS et al (2021) Selective removal of astrocytic APOE4 strongly protects against tau-mediated neurodegeneration and decreases synaptic phagocytosis by microglia. *Neuron*. <https://doi.org/10.1016/j.neuron.2021.03.024>
 63. Xiao Y, Jin J, Chang M, Nakaya M, Hu H, Zou Q et al (2014) TPL2 mediates autoimmune inflammation through activation of the TAK1 axis of IL-17 signaling. *J Exp Med* 211:1689–1702. <https://doi.org/10.1084/jem.20132640>
 64. Yoshida M (2014) Astrocytic inclusions in progressive supranuclear palsy and corticobasal degeneration. *Neuropathology* 34:555–570. <https://doi.org/10.1111/neup.12143>
 65. Zarrin AA, Bao K, Lupardus P (2020) Vucic D (2020) Kinase inhibition in autoimmunity and inflammation. *Nat Rev Drug Discov* 20(20):39–63. <https://doi.org/10.1038/s41573-020-0082-8>
 66. Zhou YY, Li Y, Jiang WQ, Zhou LF (2015) MAPK/JNK signalling: a potential autophagy regulation pathway. *Biosci Rep* 35:1–10. <https://doi.org/10.1042/BSR20140141>

Publisher’s Note Springer Nature remains neutral with regard to jurisdictional claims in published maps and institutional affiliations.

Bibliography

1. Alexander SK, Rittman T, Xuereb JH, Bak TH, Hodges JR, Rowe JB (2014) Validation of the new consensus criteria for the diagnosis of corticobasal degeneration. *J Neurol Neurosurg Psychiatry* 85:923–927. doi: 10.1136/jnnp-2013-307035
2. Allen M, Carrasquillo MM, Funk C, Heavner BD, Zou F, Younkin CS, Burgess JD, Chai H-S, Crook J, Eddy JA, Li H, Logsdon B, Peters MA, Dang KK, Wang X, Serie D, Wang C, Nguyen T, Lincoln S, Malphrus K, Bisceglia G, Li M, Golde TE, Mangravite LM, Asmann Y, Price ND, Petersen RC, Graff-Radford NR, Dickson DW, Younkin SG, Ertekin-Taner N (2016) Human whole genome genotype and transcriptome data for Alzheimer's and other neurodegenerative diseases. *Sci Data* 3:160089. doi: 10.1038/sdata.2016.89
3. Allen M, Wang X, Serie DJ, Strickland SL, Burgess JD, Koga S, Younkin CS, Nguyen TT, Malphrus KG, Lincoln SJ, Alamprese M, Zhu K, Chang R, Carrasquillo MM, Kouri N, Murray ME, Reddy JS, Funk C, Price ND, Golde TE, Younkin SG, Asmann YW, Crook JE, Dickson DW, Ertekin-Taner N (2018) Divergent brain gene expression patterns associate with distinct cell-specific tau neuropathology traits in progressive supranuclear palsy. *Acta Neuropathol* 136:709–727. doi: 10.1007/s00401-018-1900-5
4. Alonso ADC, Zaidi T, Novak M, Grundke-Iqbal I, Iqbal K (2001) Hyperphosphorylation induces self-assembly of τ into tangles of paired helical filaments/straight filaments. *Proc Natl Acad Sci U S A* 98:6923–6928. doi: 10.1073/PNAS.121119298
5. Alzheimer's Association (2017) 2017 Alzheimer's disease facts and figures. *Alzheimer's & Dementia* 13:325–373. doi: 10.1016/J.JALZ.2017.02.001
6. Anastacio H, Matosin N, Ooi L (2022) Neuronal hyperexcitability in Alzheimer's disease: what are the drivers behind this aberrant phenotype? *Transl Psychiatry* 12. doi: 10.1038/s41398-022-02024-7
7. Apetauerova D, Scala SA, Robert Hamill CW, Simon DK, Pathak S, Robin Ruthazer M, David Standaert MG, Yacoubian TA (2016) CoQ10 in progressive supranuclear palsy. doi: 10.1212/NXI.0000000000000266
8. Araque A, Carmignoto G, Haydon PG (2001) Dynamic Signaling Between Astrocytes and Neurons. doi: 10.1146/annurev.physiol.63.1.795
9. Armstrong MJ, Litvan I, Lang AE, Bak TH, Bhatia KP, Borroni B, Boxer AL, Dickson DW, Grossman M, Hallett M, Josephs KA, Kertesz A, Lee SE, Miller BL, Reich SG, Riley DE, Tolosa E, Tröster AI, Vidailhet M, Weiner WJ (2013) Criteria for the diagnosis of corticobasal degeneration. *Neurology* 80:496–503. doi: 10.1212/WNL.0b013e31827f0fd1
10. Ashton NJ, Puig-Pijoan A, Milà-Alomà M, Fernández-Lebrero A, García-Escobar G, González-Ortiz F, Kac PR, Brum WS, Benedet AL, Lantero-Rodríguez J, Day TA, Vanbrabant J, Stoops E, Vanmechelen E, Triana-Baltzer G, Moughadam S, Kolb H, Ortiz-Romero P, Karikari TK, Minguillon C, Hernández Sánchez JJ, Navalpotro-Gómez I, Grau-Rivera O, María Manero R, Puente-Periz V, de la Torre R, Roquer J, Dage JL, Zetterberg H, Blennow K, Suárez-Calvet M (2022) Plasma and CSF biomarkers in a memory clinic: Head-to-head comparison of phosphorylated tau immunoassays. *Alzheimer's & Dementia*. doi: 10.1002/alz.12841
11. Astillero-Lopez V, Gonzalez-Rodriguez M, Villar-Conde S, Flores-Cuadrado A, Martinez-Marcos A, Ubeda-Banon I, Saiz-Sanchez D (2022) Neurodegeneration and astrogliosis in the entorhinal cortex in Alzheimer's disease: Stereological layer-specific assessment and proteomic analysis. *Alzheimer's and Dementia*. doi: 10.1002/ALZ.12580
12. Bayoumy S, Verberk IMW, den Dulk B, Hussainali Z, Zwan M, van der Flier WM, Ashton NJ, Zetterberg H, Blennow K, Vanbrabant J, Stoops E, Vanmechelen E, Dage JL, Teunissen CE (2021) Clinical and analytical comparison of six Simoa assays for plasma P-tau isoforms P-tau181, P-tau217, and P-tau231. *Alzheimers Res Ther* 13:1–15. doi: 10.1186/S13195-021-00939-9

13. Bazargani N, Attwell D (2016) Astrocyte calcium signaling: The third wave. *Nat Neurosci* 19:182–189
14. Beck G, Yamashita R, Kido K, Ikenaka K, Chiba T, Yonenobu Y, Saito Y, Morii E, Hasegawa M, Murayama S, Mochizuki H (2023) An autopsy case of progressive supranuclear palsy treated with monoclonal antibody against tau. *Neuropathology*. doi: 10.1111/NEUP.12890
15. Bensimon G, Ludolph A, Bastin L, et al. (2009) Riluzole treatment, survival and diagnostic criteria in Parkinson plus disorders: The NNIPPS Study. *Brain* 132:156–171. doi: 10.1093/BRAIN/AWN291
16. Benussi A, Karikari TK, Ashton N, Gazzina S, Premi E, Benussi L, Ghidoni R, Rodriguez JL, Emeršič A, Simrén J, Binetti G, Fostinelli S, Giunta M, Gasparotti R, Zetterberg H, Blennow K, Borroni B (2020) Diagnostic and prognostic value of serum NfL and p-Tau 181 in frontotemporal lobar degeneration. *J Neurol Neurosurg Psychiatry* 91:960–967. doi: 10.1136/jnnp-2020-323487
17. Bigio EH, Vono MB, Satumtira S, Adamson J, Sontag E, Hyman LS, White CL, Baker M, Hutton M (2001) Cortical Synapse Loss in progressive Supranuclear palsy. *J Neuropathol Exp Neurol* 60:403–410. doi: 10.1093/jnen/60.5.403
18. Binder JL, Chander P, Deretic V, Weick JP, Bhaskar K (2020) Optical induction of autophagy via Transcription factor EB (TFEB) reduces pathological tau in neurons. *PLoS One* 15:e0230026. doi: 10.1371/journal.pone.0230026
19. Bluett B, Pantelyat AY, Litvan I, Ali F, Apetauerova D, Bega D, Bloom L, Bower J, Boxer AL, Dale ML, Dhall R, Duquette A, Fernandez HH, Fleisher JE, Grossman M, Howell M, Kerwin DR, Leegwater-Kim J, Lepage C, Ljubenkov PA, Mancini M, McFarland NR, Moretti P, Myrick E, Patel P, Plummer LS, Rodriguez-Porcel F, Rojas J, Sidiropoulos C, Sklerov M, Sokol LL, Tuite PJ, VandeVrede L, Wilhelm J, Wills AMA, Xie T, Golbe LI (2021) Best Practices in the Clinical Management of Progressive Supranuclear Palsy and Corticobasal Syndrome: A Consensus Statement of the CurePSP Centers of Care. *Front Neurol* 12:1123. doi: 10.3389/FNEUR.2021.694872
20. Boxer AL, Lang AE, Grossman M, Knopman DS, Miller BL, Schneider LS, Doody RS, Lees A, Golbe LI, Williams DR, Corvol JC, Ludolph A, Burn D, Lorenzi S, Litvan I, Roberson ED, Höglinger GU, Koestler M, Jack CR, van Deerlin V, Randolph C, Lobach I v., Heuer HW, Gozes I, Parker L, Whitaker S, Hirman J, Stewart AJ, Gold M, Morimoto BH (2014) Davunetide in patients with progressive supranuclear palsy: a randomised, double-blind, placebo-controlled phase 2/3 trial. *Lancet Neurol* 13:676–685. doi: 10.1016/S1474-4422(14)70088-2
21. Brendel M, Barthel H, van Eimeren T, Marek K, Beyer L, Song M, Palleis C, Gehmeyr M, Fietzek U, Respondek G, Sauerbeck J, Nitschmann A, Zach C, Hammes J, Barbe MT, Onur O, Jessen F, Saur D, Schroeter ML, Rumpf JJ, Rullmann M, Schildan A, Patt M, Neumaier B, Barret O, Madonia J, Russell DS, Stephens A, Roeber S, Herms J, Bötzel K, Classen J, Bartenstein P, Villemagne V, Levin J, Höglinger GU, Drzezga A, Seibyl J, Sabri O (2020) Assessment of 18F-PI-2620 as a Biomarker in Progressive Supranuclear Palsy. *JAMA Neurol* 77:1408–1419. doi: 10.1001/JAMANEUROL.2020.2526
22. Brunet De Courssou J-B, Durr A, Adams D, Corvol J-C, Mariani L-L Antisense therapies in neurological diseases. doi: 10.1093/brain/awab423
23. Butovsky O, Weiner HL (2018) Microglial signatures and their role in health and disease. *Nat Rev Neurosci* 19:622–635
24. Camporesi E, Nilsson J, Brinkmalm A, Becker B, Ashton NJ, Blennow K, Zetterberg H (2020) Fluid Biomarkers for Synaptic Dysfunction and Loss. *Biomark Insights* 15. doi: 10.1177/1177271920950319
25. Congdon EE, Sigurdsson EM (2018) Tau-targeting therapies for Alzheimer disease. *Nat Rev Neurol* 14:399–415
26. Conrad C, Andreadis A, Trojanowski JQ, Dickson DW, Kang D, Chen X, Wiederholt W, Hansen L, Masliah E, Thal LJ, Katzman R, Xia Y, Saitoh T (1997) Genetic evidence for the involvement of τ in progressive supranuclear palsy. *Ann Neurol* 41:277–281. doi: 10.1002/ANA.410410222

27. Constantinides VC, Paraskevas GP, Paraskevas PG, Stefanis L, Kapaki E (2019) Corticobasal degeneration and corticobasal syndrome: A review. *Clin Park Relat Disord* 1:66–71. doi: 10.1016/J.PRDOA.2019.08.005
28. Courade JP, Angers R, Mairet-Coello G, Pacico N, Tyson K, Lightwood D, Munro R, McMillan D, Griffin R, Baker T, Starkie D, Nan R, Westwood M, Mushikiwabo ML, Jung S, Odede G, Sweeney B, Popplewell A, Burgess G, Downey P, Citron M (2018) Epitope determines efficacy of therapeutic anti-Tau antibodies in a functional assay with human Alzheimer Tau. *Acta Neuropathol* 136:729. doi: 10.1007/S00401-018-1911-2
29. Coyle-Gilchrist ITS, Dick KM, Patterson K, Rodríguez PV, Wehmann E, Wilcox A, Lansdall CJ, Dawson KE, Wiggins J, Mead S, Brayne C, Rowe JB (2016) Prevalence, characteristics, and survival of frontotemporal lobar degeneration syndromes. *Neurology* 86:1736–1743. doi: 10.1212/WNL.0000000000002638
30. Cummings J, Lee G, Nahed P, Kamar MEZN, Zhong K, Fonseca J, Taghva K (2022) Alzheimer's disease drug development pipeline: 2022. *Alzheimer's & Dementia: Translational Research & Clinical Interventions* 8. doi: 10.1002/trc2.12295
31. Dabir D v., Robinson MB, Swanson E, Zhang B, Trojanowski JQ, Lee VMY, Forman MS (2006) Impaired Glutamate Transport in a Mouse Model of Tau Pathology in Astrocytes. *Journal of Neuroscience* 26:644–654. doi: 10.1523/JNEUROSCI.3861-05.2006
32. Dejanovic B, Huntley MA, de Mazière A, Meilandt WJ, Wu T, Srinivasan K, Jiang Z, Gandham V, Friedman BA, Ngu H, Foreman O, Carano RAD, Chih B, Klumperman J, Bakalarski C, Hanson JE, Sheng M (2018) Changes in the Synaptic Proteome in Tauopathy and Rescue of Tau-Induced Synapse Loss by C1q Antibodies. *Neuron* 100:1322-1336.e7. doi: 10.1016/j.neuron.2018.10.014
33. Deutsch MB, Mendez MF, Teng E (2015) Interactions between Traumatic Brain Injury and Frontotemporal Degeneration. *Dement Geriatr Cogn Disord* 39:143–153. doi: 10.1159/000369787
34. DeVos SL, Miller RL, Schoch KM, Holmes BB, Kebodeaux CS, Wegener AJ, Chen G, Shen T, Tran H, Nichols B, Zanardi TA, Kordasiewicz HB, Swayze EE, Bennett CF, Diamond MI, Miller TM (2017) Tau Reduction Prevents Neuronal Loss and Reverses Pathological Tau Deposition and Seeding in Mice with Tauopathy. *Sci Transl Med* 9. doi: 10.1126/SCITRANSLMED.AAG0481
35. Dickson DW (1999) Neuropathologic differentiation of progressive supranuclear palsy and corticobasal degeneration. *Journal of Neurology, Supplement* 246:6–15. doi: 10.1007/bf03161076
36. Dickson DW, Bergeron C, Chin SS, Duyckaerts C, Horoupian D, Ikeda K, Jellinger K, Lantos PL, Lippa CF, Mirra SS, Tabaton M, Vonsattel JP, Wakabayashi K, Litvan I (2002) Office of Rare Diseases Neuropathologic Criteria for Corticobasal Degeneration. *J Neuropathol Exp Neurol* 61:935–946. doi: 10.1093/jnen/61.11.935
37. Dickson DW, Kouri N, Murray ME, Josephs KA (2011) Neuropathology of Frontotemporal Lobar Degeneration-Tau (FTLD-Tau). *Journal of Molecular Neuroscience* 45:384–389. doi: 10.1007/s12031-011-9589-0
38. Diniz LP, Almeida JC, Tortelli V, Lopes CV, Setti-Perdigão P, Stipursky J, Kahn SA, Romão LF, de Miranda J, Alves-Leon SV, de Souza JM, Castro NG, Panizzutti R, Gomes FCA (2012) Astrocyte-induced synaptogenesis is mediated by transforming growth factor β signaling through modulation of d-serine levels in cerebral cortex neurons. *Journal of Biological Chemistry* 287:41432–41445. doi: 10.1074/jbc.M112.380824
39. Douglas PM, Dillin A (2010) Protein homeostasis and aging in neurodegeneration. *Journal of Cell Biology* 190:719–729
40. Erkinen MG, Kim MO, Geschwind MD (2018) Clinical neurology and epidemiology of the major neurodegenerative diseases. *Cold Spring Harb Perspect Biol* 10. doi: 10.1101/cshperspect.a033118

41. Escartin C, Galea E, Verkhatsky A, et al. (2021) Reactive astrocyte nomenclature, definitions, and future directions. *Nature Neuroscience* 2021 24:3 24:312–325. doi: 10.1038/s41593-020-00783-4
42. Ezerskiy LA, Schoch KM, Sato C, Beltcheva M, Horie K, Rigo F, Martynowicz R, Karch CM, Bateman RJ, Miller TM (2022) Astrocytic 4R tau expression drives astrocyte reactivity and dysfunction. *JCI Insight* 7. doi: 10.1172/JCI.INSIGHT.152012
43. Ferrer I, López-González I, Carmona M, Arregui L, Dalfó E, Torrejón-Escribano B, Diehl R, Kovacs GG (2014) Glial and Neuronal Tau Pathology in Tauopathies. *J Neuropathol Exp Neurol* 73:81–97. doi: 10.1097/NEN.0000000000000030
44. Fleury V, Brindel P, Nicastro N, Burkhard PR (2018) Descriptive epidemiology of parkinsonism in the Canton of Geneva, Switzerland. *Parkinsonism Relat Disord* 54:30–39. doi: 10.1016/j.parkreldis.2018.03.030
45. Fontaine SN, Sabbagh JJ, Baker J, Martinez-Licha CR, Darling A, Dickey CA (2015) Cellular factors modulating the mechanism of tau protein aggregation. *Cellular and Molecular Life Sciences* 72:1863–1879. doi: 10.1007/S00018-015-1839-9
46. Foster NL, Wilhelmsen K, Sima AAF, Jones MZ, D’Amato CJ, Gilman S (1997) Frontotemporal dementia and parkinsonism linked to chromosome 17: A consensus conference. *Ann Neurol* 41:706–715. doi: 10.1002/ANA.410410606
47. Franzmeier N, Brendel M, Ewers M, et al. (2022) Tau deposition patterns are associated with functional connectivity in primary tauopathies. *Nature Communications* 2022 13:1 13:1–18. doi: 10.1038/s41467-022-28896-3
48. Goedert M (2016) The ordered assembly of tau is the gain-of-toxic function that causes human tauopathies. *Alzheimer’s & Dementia* 12:1040–1050. doi: 10.1016/J.JALZ.2016.09.001
49. Goedert M, Eisenberg DS, Crowther RA (2017) Propagation of Tau Aggregates and Neurodegeneration. *Annu Rev Neurosci* 40:189–210. doi: 10.1146/annurev-neuro-072116-031153
50. Golbe L (1988) Prevalence and natural history of progressive supranuclear palsy. doi: doi.org/10.1212/WNL.38.7.1031
51. Gooch CL, Pracht E, Borenstein AR (2017) The burden of neurological disease in the United States: A summary report and call to action. *Ann Neurol* 81:479–484
52. Grubman A, Chew G, Ouyang JF, Sun G, Choo XY, McLean C, Simmons RK, Buckberry S, Vargas-Landin DB, Poppe D, Pflueger J, Lister R, Rackham OJL, Petretto E, Polo JM (2019) A single-cell atlas of entorhinal cortex from individuals with Alzheimer’s disease reveals cell-type-specific gene expression regulation. *Nat Neurosci* 22:2087–2097. doi: 10.1038/s41593-019-0539-4
53. Guo C, Jeong HH, Hsieh YC, Klein HU, Bennett DA, de Jager PL, Liu Z, Shulman JM (2018) Tau Activates Transposable Elements in Alzheimer’s Disease. *Cell Rep* 23:2874–2880. doi: 10.1016/J.CELREP.2018.05.004
54. Haase C, Stieler JT, Arendt T, Holzer M (2004) Pseudophosphorylation of tau protein alters its ability for self-aggregation. *J Neurochem* 88:1509–1520. doi: 10.1046/J.1471-4159.2003.02287.X
55. Halassa MM, Fellin T, Haydon PG (2007) The tripartite synapse: roles for gliotransmission in health and disease. *Trends Mol Med* 13:54–63. doi: 10.1016/J.MOLMED.2006.12.005
56. Hassan A, Whitwell JL, Boeve BF, Jack CR, Parisi JE, Dickson DW, Josephs KA (2010) Symmetric corticobasal degeneration (S-CBD). *Parkinsonism Relat Disord* 16:208–214. doi: 10.1016/J.PARKRELDIS.2009.11.013
57. Hauw JJ, Daniel SE, Dickson D, Horoupian DS, Jellinger K, Lantos PL, Mc Kee A, Tabaton M, Litvan I (1994) Preliminary NINDS Neuropathologic Criteria for Steele-Richardson-Olszewski Syndrome (Progressive Supranuclear Palsy). *Neurology* 44:2015–2019

58. Höglinger GU (2018) Is it Useful to Classify Progressive Supranuclear Palsy and Corticobasal Degeneration as Different Disorders? *No. Mov Disord Clin Pract* 5:141–144. doi: 10.1002/MDC3.12582
59. Höglinger GU, Melhem NM, Dickson DW, Sleiman PMA, Wang L-S, Klei L, Rademakers R, de Silva R, Litvan I, Riley DE, van Swieten JC, Heutink P, Wszolek ZK, Uitti RJ, Vandrovcova J, Hurtig HI, Gross RG, Maetzler W, Goldwurm S, Tolosa E, Borroni B, Pastor P, Cantwell LB, Han MR, Dillman A, van der Brug MP, Gibbs JR, Cookson MR, Hernandez DG, Singleton AB, Farrer MJ, Yu C-E, Golbe LI, Revesz T, Hardy J, Lees AJ, Devlin B, Hakonarson H, Müller U, Schellenberg GD (2011) Identification of common variants influencing risk of the tauopathy progressive supranuclear palsy. *Nat Genet* 43:699–705. doi: 10.1038/ng.859
60. Höglinger GU, Respondek G, Stamelou M, Kurz C, Josephs KA, Lang AE, Mollenhauer B, Müller U, Nilsson C, Whitwell JL, Arzberger T, Englund E, Gelpi E, Giese A, Irwin DJ, Meissner WG, Pantelyat A, Rajput A, van Swieten JC, Troakes C, Antonini A, Bhatia KP, Bordelon Y, Compta Y, Corvol J-C, Colosimo C, Dickson DW, Dodel R, Ferguson L, Grossman M, Kassubek J, Krismer F, Levin J, Lorenzl S, Morris HR, Nestor P, Oertel WH, Poewe W, Rabinovici G, Rowe JB, Schellenberg GD, Seppi K, van Eimeren T, Wenning GK, Boxer AL, Golbe LI, Litvan I (2017) Clinical diagnosis of progressive supranuclear palsy: The movement disorder society criteria. *Movement Disorders* 32:853–864. doi: 10.1002/mds.26987
61. Holland N, Jones PS, Savulich G, Wiggins JK, Hong YT, Fryer TD, Manavaki R, Sephton SM, Boros I, Malpetti M, Hezemans FH, Aigbirhio FI, Coles JP, O'Brien J, Rowe JB (2020) Synaptic Loss in Primary Tauopathies Revealed by [11C]UCB-J Positron Emission Tomography. *Movement Disorders* 35:1834–1842. doi: 10.1002/MDS.28188
62. Hong S, Beja-Glasser VF, Nfonoyim BM, Frouin A, Li S, Ramakrishnan S, Merry KM, Shi Q, Rosenthal A, Barres BA, Lemere CA, Selkoe DJ, Stevens B (2016) Complement and microglia mediate early synapse loss in Alzheimer mouse models. *Science* (1979) 352:712–716. doi: 10.1126/science.aad8373
63. Horie K, Barthélemy NR, Spina S, VandeVrede L, He Y, Paterson RW, Wright BA, Day GS, Davis AA, Karch CM, Seeley WW, Perrin RJ, Koppiseti RK, Shaikh F, Lago AL, Heuer HW, Ghoshal N, Gabelle A, Miller BL, Boxer AL, Bateman RJ, Sato C (2022) CSF tau microtubule-binding region identifies pathological changes in primary tauopathies. *Nature Medicine* 2022 1–8. doi: 10.1038/s41591-022-02075-9
64. Hou Y, Dan X, Babbar M, Wei Y, Hasselbalch SG, Croteau DL, Bohr VA (2019) Ageing as a risk factor for neurodegenerative disease. *Nat Rev Neurol* 15:565–581
65. Houlden H, Baker M, Morris HR, MacDonald N, Pickering-Brown S, Adamson J, Lees AJ, Rossor MN, Quinn NP, Kertesz A, Khan MN, Hardy J, Lantos PL, St. George-Hyslop P, Munoz DG, Mann D, Lang AE, Bergeron C, Bigio EH, Litvan I, Bhatia KP, Dickson D, Wood NW, Hutton M (2001) Corticobasal degeneration and progressive supranuclear palsy share a common tau haplotype. *Neurology* 56:1702–1706. doi: 10.1212/WNL.56.12.1702
66. Huang AYS, Woo J, Sardar D, Lozzi B, Bosquez Huerta NA, Lin CCJ, Felice D, Jain A, Paulucci-Holthausen A, Deneen B (2020) Region-Specific Transcriptional Control of Astrocyte Function Oversees Local Circuit Activities. *Neuron* 106:992-1008.e9. doi: 10.1016/J.NEURON.2020.03.025
67. Iwasaki Y, Yoshida M, Hattori M, Goto A, Aiba I, Hashizume Y, Sobue G (2004) Distribution of tuft-shaped astrocytes in the cerebral cortex in progressive supranuclear palsy. *Acta Neuropathol* 108:399–405. doi: 10.1007/s00401-004-0904-5
68. Jabbari E, Holland N, Chelban V, Jones ; P Simon, Lamb R, Rawlinson C, Guo T, Costantini AA, Tan MMX, Heslegrave AJ, Roncaroli F, Klein JC, Ansoorge O, Kieren ;, Allinson SJ, Jaunmuktane Z, Holton JL, Revesz T, Warner TT, Lees AJ, Zetterberg H, Russell LL, Bocchetta M, Rohrer JD, Williams NM, Grosset DG, Burn DJ, Pavese N, Gerhard A, Kobilecki C, Leigh ; P Nigel, Church A, Hu MTM, Woodside J, Houlden H, Rowe JB, Morris HR Diagnosis Across the Spectrum of Progressive Supranuclear Palsy and Corticobasal Syndrome. doi: 10.1001/jamaneurol.2019.4347

69. Jabbari E, Koga S, T.M. Hu M, et al. (2021) Genetic determinants of survival in progressive supranuclear palsy: a genome-wide association study. *Lancet Neurol* 20:107–116. doi: 10.1016/S1474-4422(20)30394-X
70. Jiang S, Bhaskar K (2020) Degradation and Transmission of Tau by Autophagic-Endolysosomal Networks and Potential Therapeutic Targets for Tauopathy. *Front Mol Neurosci* 13:199
71. Kahlson MA, Colodner KJ (2015) Glial Tau Pathology in Tauopathies: Functional Consequences. *J Exp Neurosci* 9:43–50. doi: 10.4137/JEN.S25515
72. Kavanagh T, Halder A, Drummond E (2022) Tau interactome and RNA binding proteins in neurodegenerative diseases. *Molecular Neurodegeneration* 2022 17:1 17:1–17. doi: 10.1186/S13024-022-00572-6
73. Kawashima M, Miyake M, Kusumi M, Adachi Y, Nakashima K (2004) Prevalence of progressive supranuclear palsy in Yonago, Japan. *Movement Disorders* 19:1239–1240. doi: 10.1002/mds.20149
74. Kim B, Mikytuck B, Suh E, Gibbons GS, van Deerlin VM, Vaishnavi SN, Spindler MA, Massimo L, Grossman M, Trojanowski JQ, Irwin DJ, Lee EB (2021) Tau immunotherapy is associated with glial responses in FTLD-tau. *Acta Neuropathol* 142:243–257. doi: 10.1007/S00401-021-02318-Y
75. Kim S, Choi KJ, Cho SJ, Yun SM, Jeon JP, Koh YH, Song J, Johnson GVW, Jo C (2016) Fisetin stimulates autophagic degradation of phosphorylated tau via the activation of TFEB and Nrf2 transcription factors. *Sci Rep* 6. doi: 10.1038/srep24933
76. Kim SK, Nabekura J, Koizumi S (2017) Astrocyte-mediated synapse remodeling in the pathological brain. *Glia* 65:1719–1727. doi: 10.1002/glia.23169
77. Koga S, Ghayal NB, Dickson DW (2021) Deep Learning-Based Image Classification in Differentiating Tufted Astrocytes, Astrocytic Plaques, and Neuritic Plaques. *J Neuropathol Exp Neurol* 80:306–312. doi: 10.1093/JNEN/NLAB005
78. Koga S, Zhou X, Dickson DW (2021) Machine learning-based decision tree classifier for the diagnosis of progressive supranuclear palsy and corticobasal degeneration. *Neuropathol Appl Neurobiol*. doi: 10.1111/NAN.12710
79. Kouri N, Ross OA, Dickson DW, et al. (2015) Genome-wide association study of corticobasal degeneration identifies risk variants shared with progressive supranuclear palsy. *Nat Commun* 6:1–7. doi: 10.1038/ncomms8247
80. Lampe L, Huppertz HJ, Anderl-Straub S, Albrecht F, Ballarini T, Bisenius S, Mueller K, Niehaus S, Fassbender K, Fliessbach K, Jahn H, Kornhuber J, Lauer M, Prudlo J, Schneider A, Synofzik M, Kassubek J, Danek A, Villringer A, Diehl-Schmid J, Otto M, Schroeter ML (2023) Multiclass prediction of different dementia syndromes based on multi-centric volumetric MRI imaging. *Neuroimage Clin* 37. doi: 10.1016/J.NICL.2023.103320
81. Lampe L, Niehaus S, Huppertz H-J, Merola A, Reinelt J, Mueller K, Anderl-Straub S, Fassbender K, Fliessbach K, Jahn H, Kornhuber J, Lauer M, Prudlo J, Schneider A, Synofzik M, Danek A, Diehl-Schmid J, Otto M, Germany F-C, Villringer A, Egger K, Hattingen E, Hilker-Roggendorf R, Schnitzler A, Südmeyer M, Oertel W, Atypical G, Consortium P, Group S, Kassubek J, Höglinger G, Schroeter ML (2021) Comparative analysis of machine learning algorithms for multi-syndrome classification of neurodegenerative syndromes. *Alzheimers Res Ther*. doi: 10.1186/s13195-022-00983-z
82. Leclair-Visonneau L, Rouaud T, Debilly B, Durif F, Houeto J-L, Kreisler A, Defebvre L, Lamy E, Volteau C, Nguyen J-M, Dily S le, Damier P, Boutoleau-Brettonnière C, Lejeune P, Derkinderen P (2016) Randomized placebo-controlled trial of sodium valproate in progressive supranuclear palsy. *Clin Neurol Neurosurg* 146:35–39. doi: 10.1016/j.clineuro.2016.04.021
83. Levin J, Kurz A, Arzberger T, Giese A, Höglinger GU (2016) The Differential Diagnosis and Treatment of Atypical Parkinsonism. *Dtsch Arztebl Int* 113:61–9. doi: 10.3238/arztebl.2016.0061

84. Leyns CEG, Holtzman DM Glial contributions to neurodegeneration in tauopathies. doi: 10.1186/s13024-017-0192-x
85. Liddelow S, Guttenplan K, Clarke LE, Bennett F, Bohlen C, Schirmer L, Bennett ML, Münch AE, Chung W-S, Peterson T, Wilton DK, Frouin A, Napier B, Stevens B, Barres B (2017) Neurotoxic reactive astrocytes are induced by activated microglia. *Nature Publishing Group* 541:17. doi: 10.1038/nature21029
86. Ling H, Macerollo A (2018) Is it Useful to Classify PSP and CBD as Different Disorders? Yes. *Mov Disord Clin Pract* 5:145. doi: 10.1002/MDC3.12581
87. Lipton AM, Munro Cullum C, Satumtira S, Sontag E, Hynan LS, White CL, Bigio EH (2001) Contribution of asymmetric synapse loss to lateralizing clinical deficits in frontotemporal dementias. *Arch Neurol* 58:1233–1239. doi: 10.1001/archneur.58.8.1233
88. Litvan I, Agid Y, Calne D, Campbell G, Dubois B, Duvoisin RC, Goetz CG, Golbe LI, Grafman J, Growdon JH, Hallett M, Jankovic J, Quinn NP, Tolosa E, Zee DS (1996) Clinical research criteria for the diagnosis of progressive supranuclear palsy (Steele-Richardson-Olszewski syndrome): Report of the NINDS-SPSP International Workshop. *Neurology* 47:1–9
89. Litvan I, Agid Y, Jankovic J, Goetz C, Brandel JP, Lai EG, Wenning G, D’Olhaberriague L, Verny M, Chaudhuri KR, McKee A, Jellinger K, Bartko JJ, Mangone CA, Pearce RKB (1996) Accuracy of clinical criteria for the diagnosis of progressive supranuclear palsy (Steele-Richardson-Olszewski syndrome). *Neurology* 46:922–930. doi: 10.1212/WNL.46.4.922
90. Litvan I, Hauw JJ, Bartko JJ, Lantos PL, Daniel SE, Horoupian DS, McKee A, Dickson D, Baner C, Tabaton M, Jellinger K, Anderson DW (1996) Validity and Reliability of the Preliminary NINDS Neuropathologic Criteria for Progressive Supranuclear Palsy and Related Disorders. *J Neuropathol Exp Neurol* 55:97–105. doi: 10.1097/00005072-199601000-00010
91. Livingston G, Huntley J, Sommerlad A, Ames D, Ballard C, Banerjee S, Brayne C, Burns A, Cohen-Mansfield J, Cooper C, Costafreda SG, Dias A, Fox N, Gitlin LN, Howard R, Kales HC, Kivimäki M, Larson EB, Ogunniyi A, Orgeta V, Ritchie K, Rockwood K, Sampson EL, Samus Q, Schneider LS, Selbaek G, Teri L, Mukadam N, Livingston G, Huntley J, Sommerlad A, Cooper C (2020) The Lancet Commissions Dementia prevention, intervention, and care: 2020 report of the Lancet Commission The Lancet Commissions. *thelancet.com* 396:413–459. doi: 10.1016/S0140-6736(20)30367-6
92. Lopes K de P, Snijders GJL, Humphrey J, Allan A, Sneeboer MAM, Navarro E, Schilder BM, Vialle RA, Parks M, Missall R, van Zuiden W, Gigase FAJ, Kübler R, van Berlekom AB, Hicks EM, Böttcher C, Priller J, Kahn RS, de Witte LD, Raj T (2022) Genetic analysis of the human microglial transcriptome across brain regions, aging and disease pathologies. *Nat Genet* 54:4–17. doi: 10.1038/s41588-021-00976-y
93. Malarte M-L, Gillberg P-G, Kumar A, Bogdanovic N, Lemoine L, Nordberg A (2022) Discriminative binding of tau PET tracers PI2620, MK6240 and RO948 in Alzheimer’s disease, corticobasal degeneration and progressive supranuclear palsy brains. *Mol Psychiatry*. doi: 10.1038/s41380-022-01875-2
94. Maphis N, Xu G, Kokiko-Cochran ON, Jiang S, Cardona A, Ransohoff RM, Lamb BT, Bhaskar K (2015) Reactive microglia drive tau pathology and contribute to the spreading of pathological tau in the brain. *Brain* 138:1738–1755. doi: 10.1093/BRAIN/AWV081
95. Martini-Stoica H, Cole AL, Swartzlander DB, Chen F, Wan Y-W, Bajaj L, Bader DA, Lee VMY, Trojanowski JQ, Liu Z, Sardiello M, Zheng H (2018) TFEB enhances astroglial uptake of extracellular tau species and reduces tau spreading. *J Exp Med* 215:2355–2377. doi: 10.1084/jem.20172158
96. Mukherjee S, Klaus C, Pricop-Jeckstadt M, Miller JA, Struebing FL (2019) A microglial signature directing human aging and neurodegeneration-related gene networks. *Front Neurosci* 13:2. doi: 10.3389/fnins.2019.00002
97. Murai KK, Pasquale EB (2011) Eph receptors and ephrins in neuron-astrocyte communication at synapses. *Glia* 59:1567–1578. doi: 10.1002/glia.21226

98. Narasimhan S, Guo JL, Changolkar L, Stieber A, McBride JD, Silva L v., He Z, Zhang B, Gathagan RJ, Trojanowski JQ, Lee VMY (2017) Pathological Tau Strains from Human Brains Recapitulate the Diversity of Tauopathies in Nontransgenic Mouse Brain. *The Journal of Neuroscience* 37:11406–11423. doi: 10.1523/JNEUROSCI.1230-17.2017
99. Nath U, Ben-Shlomo Y, Thomson RG, Lees AJ, Burn DJ (2003) Clinical features and natural history of progressive supranuclear palsy: A clinical cohort study. *Neurology* 60:910–916. doi: 10.1212/01.WNL.0000052991.70149.68
100. Nath U, Ben-Shlomo Y, Thomson RG, Morris HR, Wood NW, Lees AJ, Burn DJ (2001) The prevalence of progressive supranuclear palsy (Steele–Richardson–Olszewski syndrome) in the UK. *Brain* 124:1438–1449. doi: 10.1093/BRAIN/124.7.1438
101. Nilsson J, Constantinescu J, Nellgård B, Jakobsson P, Brum WS, Gobom J, Forsgren L, Dalla K, Constantinescu R, Zetterberg H, Hansson O, Blennow K, Bäckström D, Brinkmalm A (2022) Cerebrospinal Fluid Biomarkers of Synaptic Dysfunction Are Altered in Parkinson’s Disease and Related Disorders. *Movement Disorders*. doi: 10.1002/MDS.29287
102. Ochoa E, Ramirez P, Gonzalez E, de Mange J, Ray WJ, Bieniek KF, Frost B (2023) Pathogenic tau-induced transposable element-derived dsRNA drives neuroinflammation. *Sci Adv* 9:eabq5423. doi: 10.1126/SCIADV.ABQ5423
103. Olfati N, Shoeibi A, Litvan I (2022) Clinical Spectrum of Tauopathies. *Front Neurol* 13
104. Osaki Y, Morita Y, Kuwahara T, Miyano I, Doi Y (2011) Prevalence of Parkinson’s disease and atypical parkinsonian syndromes in a rural Japanese district. *Acta Neurol Scand* 124:182–187. doi: 10.1111/J.1600-0404.2010.01442.X
105. Palleis C, Sauerbeck J, Beyer L, Harris S, Schmitt J, Morenas-Rodriguez E, Finze A, Nitschmann A, Ruch-Rubinstein F, Eckenweber F, Biechele G, Blume T, Shi Y, Weidinger E, Prix C, Bötzel K, Danek A, Rauchmann BS, Stöcklein S, Lindner S, Unterrainer M, Albert NL, Wetzel C, Rupprecht R, Rominger A, Bartenstein P, Herms J, Perneckzy R, Haass C, Levin J, Höglinger GU, Brendel M (2021) In Vivo Assessment of Neuroinflammation in 4-Repeat Tauopathies. *Movement Disorders* 36:883–894. doi: 10.1002/MDS.28395
106. Palmqvist S, Tideman P, Cullen N, Zetterberg H, Blennow K, Dage JL, Stomrud E, Janelidze S, Mattsson-Carlgren N, Hansson O (2021) Prediction of future Alzheimer’s disease dementia using plasma phospho-tau combined with other accessible measures. *Nat Med* 1–9. doi: 10.1038/s41591-021-01348-z
107. Panatier A, Robitaille R (2016) Astrocytic mGluR5 and the tripartite synapse. *Neuroscience* 323:29–34. doi: 10.1016/J.NEUROSCIENCE.2015.03.063
108. Pardo L, Valor LM, Eraso-Pichot A, Barco A, Golbano A, Hardingham GE, Masgrau R, Galea E (2017) CREB Regulates Distinct Adaptive Transcriptional Programs in Astrocytes and Neurons. *Scientific Reports* 2017 7:1 7:1–14. doi: 10.1038/s41598-017-06231-x
109. Paslawski W, Bergström S, Zhang X, Remnestål J, He Y, Boxer A, Månberg A, Nilsson P, Svenningsson P (2021) Cerebrospinal Fluid Proteins Altered in Corticobasal Degeneration. *Movement Disorders* 36:1278–1280
110. Pastor P (2001) Significant association between the tau gene A0/A0 genotype and Parkinson’s disease
111. Peplow P v., Martinez B, Gennarelli TA (2022) Prevalence, Needs, Strategies, and Risk Factors for Neurodegenerative Diseases. *NeuroMethods* 173:3–8. doi: 10.1007/978-1-0716-1712-0_1
112. Perea JR, López E, Díez-Ballesteros JC, Ávila J, Hernández F, Bolós M (2019) Extracellular Monomeric Tau Is Internalized by Astrocytes. *Front Neurosci* 13:442. doi: 10.3389/fnins.2019.00442
113. Piacentini R, Li Puma DD, Mainardi M, Lazzarino G, Tavazzi B, Arancio O, Grassi C (2017) Reduced gliotransmitter release from astrocytes mediates tau-induced synaptic dysfunction in cultured hippocampal neurons. *Glia* 65:1302–1316. doi: 10.1002/glia.23163

114. Pickett EK, Henstridge CM, Allison E, Pitstick R, Pooler A, Wegmann S, Carlson G, Hyman BT, Spires-Jones TL (2017) Spread of tau down neural circuits precedes synapse and neuronal loss in the rTgTauEC mouse model of early Alzheimer's disease. *Synapse* 71:1–8. doi: 10.1002/syn.21965
115. Piras A, Collin L, Grüniger F, Graff C, Rönnbäck A (2016) Autophagic and lysosomal defects in human tauopathies: analysis of post-mortem brain from patients with familial Alzheimer disease, corticobasal degeneration and progressive supranuclear palsy. *Acta Neuropathol Commun* 4:22. doi: 10.1186/s40478-016-0292-9
116. Rauch JN, Luna G, Guzman E, Audouard M, Challis C, Sibih YE, Leshuk C, Hernandez I, Wegmann S, Hyman BT, Gradinaru V, Kampmann M, Kosik KS (2020) LRP1 is a master regulator of tau uptake and spread. *Nature* 580:381. doi: 10.1038/s41586-020-2156-5
117. Rebeiz JJ, Kolodny EH, Richardson EP (1968) Corticodentatonigral Degeneration with Neuronal Achromasia. *Arch Neurol* 18:20–33. doi: 10.1001/archneur.1968.00470310034003
118. Respondek G, Grimm MJ, Piot I, Arzberger T, Compta Y, Englund E, Ferguson LW, Gelpi E, Roeber S, Giese A, Grossman M, Irwin DJ, Meissner WG, Nilsson C, Pantelyat A, Rajput A, van Swieten JC, Troakes C, Höglinger GU, Aiba I, Antonini A, Barone P, Bhatia KP, Boxer AK, Colosimo C, Corvol JC, Dickson DW, Golbe LI, Hopfner F, Josephs KA, Kassubek J, Kovacs GG, Lang AE, Levin J, Litvan I, Höllerhage M, McFarland N, Morris HR, Müller U, Oertel WH, Rowe JB, Sakakibara R, Schellenberg G, Stamelou M, van Eimeren T, Wenning GK, Whitwell JL (2020) Validation of the Movement Disorder Society Criteria for the Diagnosis of 4-Repeat Tauopathies. *Movement Disorders* 35:171–176. doi: 10.1002/MDS.27872
119. Respondek G, Krey L, Huber M, Pflugrad H, Wegner F, Höglinger GU (2021) Neuroprotective treatment of tauopathies. *Nervenarzt* 92:1227–1238. doi: 10.1007/S00115-021-01210-0
120. Richetin K, Steullet P, Pachoud M, Perbet R, Parietti E, Maheswaran M, Eddarkaoui S, Bégard S, Pythoud C, Rey M, Caillierez R, Q Do K, Halliez S, Bezzi P, Buée L, Leuba G, Colin M, Toni N, Déglon N (2020) Tau accumulation in astrocytes of the dentate gyrus induces neuronal dysfunction and memory deficits in Alzheimer's disease. *Nature Neuroscience* 2020 23:12 23:1567–1579. doi: 10.1038/s41593-020-00728-x
121. Rickner HD, Jiang L, Hong R, O'Neill NK, Mojica CA, Snyder BJ, Zhang L, Shaw D, Medalla M, Wolozin B, Cheng CS (2022) Single cell transcriptomic profiling of a neuron-astrocyte assembloid tauopathy model. *Nature Communications* 2022 13:1 13:1–22. doi: 10.1038/s41467-022-34005-1
122. Roberts M, Sevastou I, Imaizumi Y, Mistry K, Talma S, Dey M, Gartlon J, Ochiai H, Zhou Z, Akasofu S, Tokuhara N, Ogo M, Aoyama M, Aoyagi H, Strand K, Sajedi E, Agarwala KL, Spidel J, Albone E, Horie K, Staddon JM, de Silva R (2020) Pre-clinical characterisation of E2814, a high-affinity antibody targeting the microtubule-binding repeat domain of tau for passive immunotherapy in Alzheimer's disease. *Acta Neuropathol Commun* 8. doi: 10.1186/S40478-020-0884-2
123. Robinson JL, Yan N, Caswell C, Xie SX, Suh E, van Deerlin VM, Gibbons G, Irwin DJ, Grossman M, Lee EB, Lee VMY, Miller B, Trojanowski JQ (2020) Primary Tau Pathology, Not Copathology, Correlates with Clinical Symptoms in PSP and CBD. *J Neuropathol Exp Neurol* 79:296–304. doi: 10.1093/JNEN/NLZ141
124. Roemer SF, Grinberg LT, Crary JF, Seeley WW, McKee AC, Kovacs GG, Beach TG, Duyckaerts C, Ferrer IA, Gelpi E, Lee EB, Revesz T, White CL, Yoshida M, Pereira FL, Whitney K, Ghayal NB, Dickson DW (2022) Rainwater Charitable Foundation criteria for the neuropathologic diagnosis of progressive supranuclear palsy. *Acta Neuropathol* 144:603–614. doi: 10.1007/S00401-022-02479-4
125. Roos-Mattjus P, Sistonen L (2004) The ubiquitin-proteasome pathway. *Ann Med* 36:285–295. doi: 10.1080/07853890310016324
126. Rösler TW, Costa M, Höglinger GU (2020) Disease-modifying strategies in primary tauopathies. *Neuropharmacology* 167. doi: 10.1016/j.neuropharm.2019.107842
127. Sardiello M, Palmieri M, di Ronza A, Ballabio A (2009) A Gene Network Regulating Lysosomal Biogenesis and Function. *Science* (1979) 325. doi: 10.1126/science.1174447

128. Schrag A, Ben-Shlomo Y, Quinn NP (1999) Prevalence of progressive supranuclear palsy and multiple system atrophy: a cross-sectional study. *The Lancet* 354:1771–1775. doi: 10.1016/S0140-6736(99)04137-9
129. Sha S, Hou C, Viskontas I v., Miller BL (2006) Are frontotemporal lobar degeneration, progressive supranuclear palsy and corticobasal degeneration distinct diseases? *Nat Clin Pract Neurol* 2:658–665
130. Sidoryk-Wegrzynowicz M, Gerber YN, Ries M, Sastre M, Tolkovsky AM, Spillantini MG (2017) Astrocytes in mouse models of tauopathies acquire early deficits and lose neurosupportive functions. *Acta Neuropathol Commun* 5:89. doi: 10.1186/s40478-017-0478-9
131. Sirkis DW, Solsberg CW, Johnson TP, Bonham LW, Sturm VE, Lee SE, Rankin KP, Rosen HJ, Boxer AL, Seeley WW, Miller BL, Geier EG, Yokoyama JS (2022) Single-cell RNA-seq reveals alterations in peripheral CX3CR1 and nonclassical monocytes in familial tauopathy. *bioRxiv* 2022.10.28.514304. doi: 10.1101/2022.10.28.514304
132. Smethurst P, Franklin H, Clarke BE, Sidle K, Patani R The role of astrocytes in prion-like mechanisms of neurodegeneration. doi: 10.1093/brain/awab366
133. Smith AM, Davey K, Tsartsalis S, Khozoe C, Fancy N, Tang SS, Liaptsi E, Weinert M, McGarry A, Muirhead RCJ, Gentleman S, Owen DR, Matthews PM (2022) Diverse human astrocyte and microglial transcriptional responses to Alzheimer's pathology. *Acta Neuropathol* 143:75–91. doi: 10.1007/s00401-021-02372-6
134. Soppela H, Katisko K, Gadola Y, Krüger J, Hartikainen P, Alberici A, Benussi A, Koivisto A, Haapasalo A, Remes AM, Borroni B, Solje E (2022) Modifiable potential risk factors in familial and sporadic frontotemporal dementia. *Ann Clin Transl Neurol* 9:1195–1205. doi: 10.1002/acn3.51619
135. Stamelou M, Respondek G, Giagkou N, Whitwell JL, Kovacs GG, Höglinger GU (2021) Evolving concepts in progressive supranuclear palsy and other 4-repeat tauopathies. *Nat Rev Neurol* 17:601–620. doi: 10.1038/S41582-021-00541-5
136. Stamelou M, Reuss A, Pilatus U, Magerkurth J, Niklowitz P, Eggert KM, Krisp A, Menke T, Schade-Brittinger C, Oertel WH, Höglinger GU (2008) Short-term effects of coenzyme Q10 in progressive supranuclear palsy: a randomized, placebo-controlled trial. *Mov Disord* 23:942–949. doi: 10.1002/MDS.22023
137. Steele JC, Clifford Richardson J, Olszewski J (1964) Progressive Supranuclear Palsy a Heterogeneous Degeneration Involving the Brain Stem, Basal Ganglia and Cerebellum with Vertical Gaze and Pseudo-bulbar Palsy, Nuchal Dystonia and Dementia. *Arch Neurol* 10:333–359. doi: 10.1001/archneur.1964.00460160003001
138. Sung K, Jimenez-Sanchez M (2020) Autophagy in Astrocytes and its Implications in Neurodegeneration. *J Mol Biol* 432:2605–2621. doi: 10.1016/j.jmb.2019.12.041
139. Swallow DMA, Zheng CS, Counsell CE (2022) Systematic Review of Prevalence Studies of Progressive Supranuclear Palsy and Corticobasal Syndrome. *Mov Disord Clin Pract* 9:604–613. doi: 10.1002/mdc3.13489
140. Takigawa H, Ikeuchi T, Aiba I, Morita M, Onodera O, Shimohata T, Tokuda T, Murayama S, Nakashima K (2016) Japanese Longitudinal Biomarker Study in PSP and CBD (JALPAC): A prospective multicenter PSP/CBD cohort study in Japan. *Parkinsonism Relat Disord* 22:e120–e121. doi: 10.1016/j.parkreldis.2015.10.282
141. Tang Y, Le W (2015) Differential Roles of M1 and M2 Microglia in Neurodegenerative Diseases. *Molecular Neurobiology* 2015 53:2 53:1181–1194. doi: 10.1007/S12035-014-9070-5
142. Tolosa E, Litvan I, Ven Gerpen J, et al. (2014) A phase 2 trial of the GSK-3 inhibitor tideglusib in progressive supranuclear palsy. *Movement Disorders* 29:470–478. doi: 10.1002/mds.25824
143. Trabzuni D, Wray S, Vandrovцова J, Ramasamy A, Walker R, Smith C, Luk C, Gibbs JR, Dillman A, Hernandez DG, Arepalli S, Singleton AB, Cookson MR, Pittman AM, de Silva R, Weale ME, Hardy J,

- Ryten M (2012) MAPT expression and splicing is differentially regulated by brain region: relation to genotype and implication for tauopathies. *Hum Mol Genet* 21:4094–4103. doi: 10.1093/hmg/dds238
144. Tsai RM, Miller Z, Koestler M, Rojas JC, Ljubenkova PA, Rosen HJ, Rabinovici GD, Fagan AM, Cobigo Y, Brown JA, Jung JI, Hare E, Geldmacher DS, Natelson-Love M, McKinley EC, Luong PN, Chuu EL, Powers R, Mumford P, Wolf A, Wang P, Shamloo M, Miller BL, Roberson ED, Boxer AL (2020) Reactions to Multiple Ascending Doses of the Microtubule Stabilizer TPI-287 in Patients With Alzheimer Disease, Progressive Supranuclear Palsy, and Corticobasal Syndrome: A Randomized Clinical Trial. *JAMA Neurol* 77:215–224. doi: 10.1001/JAMANEUROL.2019.3812
 145. Vasile F, Dossi E, Rouach N (2017) Human astrocytes: structure and functions in the healthy brain. *Brain Struct Funct* 222:2017–2029. doi: 10.1007/s00429-017-1383-5
 146. Vellodi A (2005) Lysosomal storage disorders. *Br J Haematol* 128:413–431. doi: 10.1111/J.1365-2141.2004.05293.X
 147. Vogels T, Murgoci A-N, Hromádka T (2019) Intersection of pathological tau and microglia at the synapse. *Acta Neuropathol Commun* 7:109. doi: 10.1186/s40478-019-0754-y
 148. van de Vrede L, Ljubenkova PA, Rojas JC, Welch AE, Boxer AL (2020) Four-Repeat Tauopathies: Current Management and Future Treatments. *Neurotherapeutics* 2020 17:4 17:1563–1581. doi: 10.1007/S13311-020-00888-5
 149. Weickert S, Wawrzyniuk M, John LH, Rüdiger SGD, Drescher M (2020) The mechanism of Hsp90-induced oligomerization of Tau. *Sci Adv* 6. doi: 10.1126/SCIADV.AAX6999
 150. Wermuth L (1990) High prevalence of Parkinson's disease in the Faroe Islands
 151. Wermuth L, Bech S, Petersen MS, Joensen P, Weihe P, Grandjean P (2008) Prevalence and incidence of Parkinson's disease in The Faroe Islands. *Acta Neurol Scand* 118:126–131. doi: 10.1111/j.1600-0404.2007.00991.x
 152. Yan MM, Ni JD, Song D, Ding M, Huang J (2015) Interplay between unfolded protein response and autophagy promotes tumor drug resistance. *Oncol Lett* 10:1959. doi: 10.3892/OL.2015.3508
 153. Yokoyama JS, Karch CM, Fan CC, Bonham LW, Kouri N, Ross OA, Rademakers R, Kim J, Wang Y, Höglinger GU, Müller U, Ferrari R, Hardy J, Momeni P, Sugrue LP, Hess CP, James Barkovich A, Boxer AL, Seeley WW, Rabinovici GD, Rosen HJ, Miller BL, Schmansky NJ, Fischl B, Hyman BT, Dickson DW, Schellenberg GD, Andreassen OA, Dale AM, Desikan RS (2017) Shared genetic risk between corticobasal degeneration, progressive supranuclear palsy, and frontotemporal dementia. *Acta Neuropathol* 133:825–837. doi: 10.1007/S00401-017-1693-Y
 154. Yoshida M (2014) Astrocytic inclusions in progressive supranuclear palsy and corticobasal degeneration. *Neuropathology* 34:555–570. doi: 10.1111/neup.12143
 155. Yoshiyama Y, Higuchi M, Zhang B, Huang SM, Iwata N, Saito TCC, Maeda J, Suhara T, Trojanowski JQ, Lee VMY (2007) Synapse Loss and Microglial Activation Precede Tangles in a P301S Tauopathy Mouse Model. *Neuron* 53:337–351. doi: 10.1016/j.neuron.2007.01.010
 156. Zhang Y, Wu KM, Yang L, Dong Q, Yu JT (2022) Tauopathies: new perspectives and challenges. *Mol Neurodegener* 17
 157. Chronic traumatic encephalopathy - Symptoms and causes - Mayo Clinic. <https://www.mayoclinic.org/diseases-conditions/chronic-traumatic-encephalopathy/symptoms-causes/syc-20370921>. Accessed 19 Dec 2022
 158. CELLxGENE | Gene Expression. <https://cellxgene.cziscience.com/gene-expression>. Accessed 24 Jan 2023

Appendix A:

Not included.

Appendix B:

Appendix Table 1. Overview of select publications reporting epidemiological data from clinical and pathologically validated PSP and CBD/CBS cohorts. Weighted means incorporating study sample sizes.

Abbreviations: clin, clinical diagnosis; NA, not applicable; n.r., not relevant for calculation; path, pathological diagnosis; SD, standard deviation; *, only median values for “Age at Onset” and/or “Age at Death” reported in original article; #, total sum.

Diagnosis	First author	Year	DOI URL	Crude Prevalence rate per 100,000	N	Mean Age at Onset	Range Age at Onset	Mean Disease Duration	Range Disease Duration	Mean Age at Death	Range Age at Death	Validation
CBS	Wermuth	2008	https://doi.org/10.1111/j.1600-0404.2007.00991.x	0	n.r.	NA	NA	NA	NA	NA	NA	clin
CBS	Osaki	2011	https://doi.org/10.1111/j.1600-0404.2010.01442.x	9	6	71	SD 9	4	NA	NA	NA	clin
CBS	Coyle-Gilchrist	2016	https://doi.org/10.1212/WNL.0000000000002638	2.2	48	66	SD 8.5	NA	NA	NA	NA	clin
CBS	Fleury	2018	https://doi.org/10.1016/j.parkreldis.2018.03.030	3	n.r.	NA	NA	NA	NA	NA	NA	clin
CBD	Yoshida	2014	https://doi.org/10.1111/neup.12143	NA	27	63	51:79	6	03:13	69	54:86	path
CBD	Jabbari, p.m.-validated cohort	2019	https://doi.org/10.1001/jamaneurol.2019.4347	NA	8	64	SD 7.2	NA	NA	NA	NA	path
CBD	Respondek	2020	https://doi.org/10.1002/mds.27872	NA	55	63.8	42:81	6.7	01:12	70.4	51:85	path
Weighted mean (All)				3.55	144#	64.69		6.30		69.94		clin/path
Weighted mean (Validated)					90#	63.58		6.47		69.94		path
PSP	Golbe	1988	https://doi.org/10.1212/WNL.38.7.1031	1.4	50	62.9	SD 6.4, 44:75	6.9	SD 3.9, 2:17	69.8	NA	clin
PSP	Wermuth	1997	https://doi.org/10.1212/WNL.49.2.426	4.6	n.r.	NA	NA	NA	NA	NA	NA	clin
PSP	Schrag	1999	https://doi.org/10.1016/S0140-6736(99)04137-9	4.9	5	67.5	53:84	4.4	01:10	71.9	NA	clin
PSP	Nath, national cohort	2001*	https://doi.org/10.1093/brain/124.7.1438	1	187	66	41:83	5	QU 1:17	NA	NA	clin
PSP	Nath	2003	https://doi.org/10.1212/01.WNL.0000052991.70149.68	NA	75	67.6	NA	5.7	NA	73.3	NA	clin
PSP	Kawashima	2004	https://doi.org/10.1002/mds.20149	5.8	8	71	SD 6.6	NA	NA	NA	NA	clin
PSP	Wermuth	2008	https://doi.org/10.1111/j.1600-0404.2007.00991.x	4.1	n.r.	NA	NA	NA	NA	NA	NA	clin
PSP	Osaki	2011	https://doi.org/10.1111/j.1600-0404.2010.01442.x	18.1	12	76	SD 7	5	NA	NA	NA	clin
PSP	Coyle-Gilchrist	2016	https://doi.org/10.1212/WNL.0000000000002638	2.8	48	67	SD 7.8	NA	NA	NA	NA	clin
PSP	Takigawa	2016	https://doi.org/10.1016/j.parkreldis.2015.10.282	17.9	n.r.	NA	NA	NA	NA	NA	NA	clin
PSP	Fleury	2018	https://doi.org/10.1016/j.parkreldis.2018.03.030	8.3	n.r.	NA	NA	NA	NA	NA	NA	clin
PSP	Yoshida	2014	https://doi.org/10.1111/neup.12143	NA	70	67	39:92	8	01:28	75	49:106	path
PSP	Jabbari, p.m.-validated cohort	2019	https://doi.org/10.1001/jamaneurol.2019.4347	NA	23	66	SD 7.4	NA	NA	NA	NA	path
PSP	Respondek	2020	https://doi.org/10.1002/mds.27872	NA	195	66.3	41:91	7.7	00:27	74.1	54-94	path
PSP	Geut	2020	https://doi.org/10.1186/s40478-020-00914-9	NA	45	66	51:84	8	03:23	74	57:90	path
PSP	Roemer	2022*	https://doi.org/10.1007/s00401-022-02479-4	NA	1680	68	NA	7	QU 5:9	75	QU 70:81	path
Weighted mean (All)				6.89	2398#	67.53		6.89		74.71		clin/path
Weighted mean (Validated)					2013#	67.73		7.13		74.89		path

Appendix Table 2: Clinical trials in Alzheimer Disease.Modified from Cummings et al. 2022 [30] based on clinicaltrials.gov. Retrieved 7th January 2023.**Abbreviations:** ASO, antisense oligonucleotide; HP, human probands; MCI, mild cognitive impairment; MTBR, microtubule binding domain

ALZHEIMER DISEASE TRIALS								
TRIAL PHASE: INDICATION	Agent	CADRO mecha- nism class	Mechanism of action	Status (CT.gov ID)	Sponsor	Start date	End date	
I: AD	Trehalose	Cell death	Induces autophagy and promotes clearance of aggregated proteins	Unknown, results pending: (NCT04663854)	Mashhad University of Medical Sciences	Aug-20	Aug-22	
I: HP	BEY2153	Proteostasis/proteinopathies	A β and tau aggregation inhibitor; inhibits neuronal death	Unknown, results pending: (NCT04476303)	BeyondBio	Aug-20	Oct-21	
I: MCI/AD	BDPP	Proteostasis/proteinopathies	Prevents A β and tau aggregation	Completed, results pending: (NCT02502253)	Johns Hopkins University, Mount Sinai School of Medicine	Jun-15	Jun-22	
I: MCI/AD	Contraloid acetate	Proteostasis/proteinopathies	Aggregation inhibitor	Completed, results pending: (NCT04711486)	Charite University, Berlin, Germany	Dec-20	Nov-21	
I: HP	REM0046127	Synaptic Plasticity/Neuroprotection	Regulates calcium dyshomeostasis; tau and A β reduction	Completed, results pending: (NCT04672135)	reMYND, NeuroScios GmbH	Nov-20	May-22	
I: AD	ASN51	Tau	O-GlycNAcase Inhibitor	Recruiting: (NCT04759365)	Asceneuron	Jun-21	Jan-22	
I: AD	Lu AF87908	Tau	Monoclonal antibody to reduce tau	Recruiting: (NCT04149860)	Lundbeck	Sep-19	Jul-22	
I: MCI/AD	NIO752	Tau	ASO against <i>MAPT</i> /Tau transcript	Not yet recruiting: (NCT05469360)	Novartis Pharmaceuticals	Sep-22	Nov-23	
I: HP	TB006	Tau	Anti-tau monoclonal antibody	Recruiting: (NCT04920786)	TrueBinding, Inc.	Jun-21	Jan-23	
II: AD	Grapeseed extract	Proteostasis/proteinopathies	Polyphenolic compound; antioxidant; prevent aggregation of A β and tau	Unknown, results pending: (NCT02033941)	Mount Sinai School of Medicine, NCCIH	Nov-14	Dec-21	
II: MCI/AD	Rapamycin (sirolimus)	Proteostasis/proteinopathies	mTOR inhibitor; ameliorate metabolic and vascular effects of aging, derepress autophagy	Recruiting: (NCT04629495)	The University of Texas Health Science Center at San Antonio	Aug-21	Aug-24	
II: AD	Neflamapimod (VX-745)	Synaptic plasticity/neuroprotection	p38 MAPK- α inhibitor; enhance endolysosomal function to reduce synaptic dysfunction	Recruiting, results pending: (NCT03435861)	EIP Pharma	Oct-18	Jun-21	
II: MCI/AD	BPN14770	Synaptic plasticity/neuroprotection/MODIF: autophagy	PDE-4 inhibitor; prolongs cAMP activity and improves neuronal plasticity	Unknown, results pending: (NCT03817684)	Tetra discovery partners	Apr-19	Feb-20	
II: AD	JNJ-63733657	Tau	Monoclonal antibody targeting soluble P-tau (N-terminus)	Recruiting: (NCT04619420)	Janssen	Jan-21	Nov-25	
II: AD	LY3372689	Tau	O-GlycNAcase inhibitor; promote tau glycosylation, prevent tau aggregation	Active, not recruiting: (NCT05063539)	Eli Lilly	Sep-21	Jun-24	
II: AD	PU-AD	Tau	Heat shock protein 90 inhibitor; to prevent aggregation and hyperphosphorylation of tau	Terminated, results pending: (NCT04311515)	Samus therapeutics	Jun-20	Nov-22	

TRIAL PHASE: INDICATION	Agent	CADRO mecha- nism class	Mechanism of action	Status (CT.gov ID)	Sponsor	Start date	End date
II: AD	Semori- nemab (RO710570 5)	Tau	Monoclonal antibody to remove extracellular tau (N-terminal)	Active, not re- cruiting; (NCT03828747)	AC Immune SA, Genen- tech, Hoffmann-La Ro- che	Jan-19	Aug-23
II: MCI/AD	ACI-35	Tau	Active immunotherapy targeting tau	Active, not re- cruiting; (NCT04445831)	AC Immune, Janssen	Jul-19	Oct-23
II: MCI/AD	UCB 0107/ Be- pranemab	Tau	Anti-tau monoclonal antibody (near MTBR)	Active, not re- cruiting; (NCT04867616)	UCB Biopharma	Jun-21	Nov-25
II: MCI/AD	IONIS MAP- TRx (BII8080)	Tau	Antisense oligonucleotide target- ing tau expression; <i>MAPT</i> RNA in- hibitor	Recruiting; (NCT05399888)	Ionis Pharmaceuticals	Aug-22	Dec-26
II: MCI/AD	Nicotina- mide	Tau	HDAC inhibitor; to reduce tau-in- duced microtubule depolymeri- zation and tau phosphorylation	Completed, results pending; (NCT03061474)	University of California, Irvine	Jul-17	Dec-22
II: MCI/DIAD	E2814	Tau	Anti-tau monoclonal antibody (MTBR)	Active, not re- cruiting; (NCT04971733)	Eisai	Jun-21	Apr-24
III: AD	Nilotinib BE	Proteostasis/Pro- teinopathies	Tyrosine kinase inhibitor; autoph- agy enhancer; promotes clear- ance of A β and tau	Not yet recruiting; (NCT05143528)	KeifeRx	Feb-22	Jun-26
III: MCI/AD	TRx0237/L MTX	Tau	Tau protein aggregation inhibitor	Active, not recruit- ing; (NCT03446001)	TauRx Therapeutics	Jan-18	Mar-23

Acknowledgements

This thesis marks the end of a four-year journey. It was my closest friends and relatives who motivated me, and my colleagues who supported me. Only with both, I stayed tuned and had the chance to develop new ideas and skills.

First, I would like to thank my mentor and supervisor, Jochen Herms. From my first day at the ZNP, I could count on your support, so I could work on such exciting projects, attend meetings and receive valuable personal advice. Professor Danek and Professor Levin, my expert examiners, thank you for providing valuable contributions from clinical and translational perspectives.

Felix, you have been a great co-supervisor, and you spurred my motivation to develop my bioinformatic skills. I appreciate your professional advice, also regarding the Summer School in Systems Genetics, the time you spent discussing our research concepts (even though you caught a heavy cold) and your patience when I overloaded the server's RAM. Viktoria, your guidance, along with the wet-lab experiments, was extremely well organized. I do particularly appreciate you sharing your opinions on neuroscientific trends and your valuable scientific comments. Katrin, José, Katharina and Tanja, you were the first friends in the lab. I definitely enjoyed your stories, your advice from "real" doctoral candidates' perspectives, and the bouldering sessions with you. Sigrun and Thomas Arzberger, you have both taught me lessons about the neuropathology of tauopathies. I especially appreciate the time you spent exploring slides and theories about astrocytic pathology with me.

I would also like to thank all other DZNE lab members (Carmelo, Paul, Yuan, Mochen, Fanfan, Lars, Carolin and Carsten), the ZNP members (Manu, Otto, Jeannine, Norbert Buresch, Ben, Janina, Vanessa, Michael Schmidt, Michael Rüter, Daniel, Felix, Peer, Sonja, Melanie, Alex and Mourad), the Kerschensteiner lab members (Eduardo and Judith) and Dewachter lab members at UHasselt (Ilse and Cosmin) for your instant conceptual and technical support, and your willingness to respond to my curious questions. Matthias Brendel's group members and associates (Florian, Johannes, Xianyuan, Letizia and Laura), it's been a pleasure working with such a highly motivated and ambitious team. For the early lab education at UUlm I would like to express special thanks to Professor Britsch, Svenja and Christoph.

To my friends, especially Julian, Dimitri, Moritz, and Marc, I appreciate your interest in my research and the vivid night-science discussions. My family, who always supported me on my way to where I am, thank you for the good times we had in between and the strong backing. Elli, you could comprehend my passion for this research and lent a listening ear whenever I had a new insight. You inspired me with discussions, new viewpoints, and delicate questioning. Your steady cheering kept me motivated.